

ISSN 1916-9698

**INTERNATIONAL  
JOURNAL OF  
CHEMISTRY**

**Vol. 1, No. 1  
February 2009**



**Canadian Center of Science and Education**



## Contents

Effect of Biosorption Parameters Kinetics Isotherm and Thermodynamics for Acid Green Dye Biosorption from Aqueous Solution by Brewery Waste <i>V.Jaikumar &amp; V Ramamurthi</i>	2
Preparation of LaFeO <sub>3</sub> Porous Hollow Nanofibers by Electrospinning <i>Xiangting Dong, Jinxian Wang, Qizheng Cui, Guixia Liu &amp; Wensheng Yu</i>	13
Preparation of Nano-ZnO and Its Application to the Textile on Antistatic Finishing <i>Fan Zhang &amp; Junling Yang</i>	18
Lead Removal from Aqueous Solution Using Silica Ceramic: Adsorption Kinetics and Equilibrium Studies <i>Md. Salim &amp; Yukihiko Munekage</i>	23
Synthesis, Characterization and Application of O, O-diethyl Acrylamide Phosphate <i>Aibing Jiang, Bowen Cheng, Yuanlin Ren &amp; Zhenhuan Li</i>	31
Extraction, Separation and Identification of Chemical Ingredients of <i>Elephantopus Scaber</i> L. Using Factorial Design of Experiment <i>Anees Ahmad, Abbas F. M. Alkarkhi, Sufia Hena &amp; Lim Han Khim</i>	36
Study on the Reaction Kinetics of Ultrasonic Radiation Non-homogeneous Phase Chitin Deacetylation <i>Cuirong Zhang, Yingde Cui &amp; Zhenyu Jia</i>	50
Performance Research of Polyester Fabric Treated by Nano Titanium Dioxide (Nano-TiO <sub>2</sub> ) Anti-ultraviolet Finishing <i>Haixia Li, Hua Deng &amp; Jing Zhao</i>	57
Synthesis of $\beta$ -Lactam Fused Eneidyne by Intramolecular Kinugasa Reaction: Comparison of Reactivity with Monocyclic Analogues <i>Amit Basak, Runa Pal &amp; Sanket Das</i>	63
Synthesis and Modification of Polypropylene by Radiation-induced Grafting <i>Feng Yuan, Junfu Wei, Enqi Tang, Kongyin Zhao &amp; Li Wei</i>	75
Preparation and Properties of Polyester Based Nanocomposites with Good Air-tightness <i>Fusheng Luo</i>	82
Preparation of Cation Exchange Resin Filled EVAL Hollow Fiber Membrane Adsorbent <i>Fengli Zhang</i>	87



## Effect of Biosorption Parameters Kinetics Isotherm and Thermodynamics for Acid Green Dye Biosorption from Aqueous Solution by Brewery Waste

V.Jaikumar

Department of Chemical Engineering, A.C.Tech. Campus  
Anna University Chennai, Chennai 600025, India  
Tel: 91-44-2220-3536 E-mail: jaikumar\_phd@yahoo.com

V Ramamurthi (Corresponding author)

Department of Chemical Engineering, A.C.Tech. Campus  
Anna University Chennai, Chennai 600025, India  
Tel: 91-44-2220-3523 E-mail: vramamurthi@yahoo.co.in

*The research is financed by Council of Scientific and Industrial Research (CSIR), New Delhi, India, grant number CSIR Lr. No. 9/468(371)/2007-EMR-1 dated 30.03.2007.*

### Abstract

Biosorption of Acid Green (AG 25) was investigated using Spent Brewery Grains (SBG) a brewing industry waste in a batch system with respect to initial pH, temperature, initial dye concentration, biosorbent dosage, and contact time. The biomass exhibited the highest dye uptake capacity at 303 K, initial pH value of 3, the initial dye concentration of 90mg/L, biosorbent dosage of 0.2 g and contact time of 75 min. The extent of dye removal increased with increase in time, biosorbent dosage and decreased with increase in temperature. The equilibrium sorption capacity of the biomass increased on increasing the initial dye concentration up to 90 mg/L and then started decreasing in the studied concentration up to 300 mg/L. The experimental result has shown that the acidic pH favours the biosorption. Langmuir and Freundlich adsorption model is used for the mathematical description of the biosorption equilibrium and isotherm constants are evaluated. Equilibrium data fitted very well to the Langmuir model. The pseudo first- and second-order kinetic models were also applied to the experimental data. The results indicated that the dye uptake process followed the pseudo second-order rate expression and biosorption rate constants increased with increasing concentration.

**Keywords:** Biosorption, Acid green, Spent brewery grains, Isotherm, Kinetics, Thermodynamics

### 1. Introduction

Worldwide textile industries consumes very large volumes of water for wet processing of textiles such as scouring, bleaching, mercerizing, dyeing, printing and final finishing. These operations contribute to significant quantities of effluents and their pollution loads are considerable. Dyeing and printing is the most complex of the wet processes and includes hundreds of dyes and auxiliary chemicals which contribute to major pollution load of the receiving water bodies and ground water aquifers. Over 100,000 commercially available dyes exist and more than  $7 \times 10^5$  tonnes per year are produced annually (Zollinger, 1987). Innumerable dyes are employed in the textile and dyeing industries. They are classified according to their chemical composition. However in textile processing dyes are classified based on their applications. Some prominent types of dyes used in India and other parts of the world are acid dyes, basic dyes, direct dyes, mordant dyes, pre-metallized dyes, reactive dyes, sulfur dyes and vat dyes. The major constituent that causes difficulties in the treatment of dye house effluents is the colour. Color is the first contaminant to be recognized in wastewater and the presence of very small amounts of dyes in water is highly visible and undesirable (Robinson et al., 2001).

Dye wastewater is usually treated by physical or chemical treatment processes. These include chemical coagulation/flocculation, precipitation, ozonation, adsorption, oxidation, irradiation, ion exchange and photo

degradation. Some of these techniques have shown to be effective, although they have limitations. Among these are: excess amount of chemical usage, or accumulation of concentrated sludge with disposal problems; expensive plant requirements and operational costs; lack of effective color reduction; and sensitivity to a variable wastewater input (Robinson *et al.*, 2001).

The use of biomaterials as biosorbents for the treatment of wastewaters will provide as a potential alternate to the conventional treatment methods. The process of uptake of solute using biomaterials including microbial cells, whether dead or alive, is known as biosorption. The main advantages of biosorption are high selectivity, cost effectiveness and good removal performance. World wide numerous low cost bio materials have been tried for biosorption of dyes (McKay *et al.*, 1983); Silica (McKay, 1984); the hardwood sawdust (Asfour *et al.*, 1985); Bagasse pith (McKay *et al.*, 1987); Fly ash (Khare *et al.*, 1987); Paddy straw (Deo, 1993); Rice husk (Lee & Low, 1997); Palm fruit bunch (Nasser, 1997). In the present investigation, the biomass SBG a brewery industry waste was used as biosorbent and its capacity to remove acid green an anionic dye was evaluated. A survey of literature showed that no work has been done so far on dye removal process using SBG as biosorbent for the removal of acid green dye stuffs from their aqueous solutions. Few studies have been conducted on spent grains as biosorbent of heavy metals Cadmium, lead (Low, 2000) and Copper (Lu & Gibb, 2008). Acid green has wider applications, which include paper industry, leather industry, dyeing and textile industries etc.

In the brewing process, barley is initially steeped, germinated, kilned and then sent for mash conversion and lautertun, the grain obtained from lautertun is the spent grain used in the present study. Spent grains are normally utilized as feed for cow, cattle and like animals, but due to absence of this activity in industrialized and urbanized countries it is difficult to dispose it, since large amounts are produced annually and also difficult to store it due to formation of microorganism and fly on it. Also due to prosperous market of the alcohol industry in India, the production of alcohol has steadily increased in the last years from 1654 million liters in 1999-2000 to 2300 million liters in 2007-2008.

The aim of this present work is to explore the possibility of utilizing SBG for the biosorptive removal of AG 25 dye from aqueous solution. The effect of factors such as initial pH, temperature, initial dye concentration, biosorbent dosage, and contact time was investigated. The kinetics of AG 25 biosorption onto SBG was analyzed by fitting to kinetics models. Experimental equilibrium data were fitted to Langmuir and Freundlich isotherm equation. Thermodynamics parameters Gibb's free energy changes ( $\Delta G$ ), enthalpy changes ( $\Delta H$ ) and entropy changes ( $\Delta S$ ) were estimated for the biosorption of acid green onto SBG.

## 2. Materials and methods

### 2.1 Biosorbent

Spent Brewery Grains, taken from Mohan breweries and distilleries Limited, Chennai, India, was suspended in 0.13M Sulphuric acid solution (12g of SBG per 100mL of acid solution) for one hour. Then it was filtered and the acid solution was discarded. The biomass was washed with distilled water many times until it is completely free from the acid and dried at 60°C for 24 hours. The dried biomass was ground, sieved and stored for further use in the experiments. SBG with a particle of 0.25mm was used in the experiments.

### 2.2 Adsorbate

The adsorbate AG 25 dye (C.I. number = 61570, C.I. name = AG 25, Chemical formula =  $C_{28}H_{20}N_2Na_2O_8S_2$ , F W = 622.58, Commercial name = Alizarin cyanin green G, Chemical class = anthraquinone, nature = acid ) was supplied by Sigma-Aldrich Chemicals Ltd., India. The structure of AG 25 is given in Fig. 1. An accurately weighed quantity (1 g) of AG 25 was dissolved in double distilled water to prepare stock solution of 1000 mg/L. Experimental solutions of the desired concentrations were prepared by dilution of stock solution with double-distilled water.

### 2.3 Analytical measurements

The concentration of the dye AG 25 were determined using a UV-vis spectrophotometer (HITACHI U 2000, spectrophotometer) at a wavelength corresponding to the maximum absorbance of the dye ( $\lambda_{max} = 642$  nm). Calibration curves were plotted between absorbance and concentration of the dye solution.

### 2.4 Batch experiments

Batch experiments were conducted using 250 mL Erlenmeyer flasks to which 50 mL of dye containing waste water and biomass were added. These flasks were agitated in a temperature –controlled orbital shaker at a constant speed of 150 rpm to study the effect of important parameters like pH, adsorbent dosage, initial dye concentration, contact time and temperature. Samples were withdrawn at appropriate time intervals and these samples were centrifuged (Research centrifuge Remi scientific work, India) at 4000 rpm. The supernatant was used for analysis of the residual dye concentration. The effect of pH on dye removal was studied over a pH range of 2-12. pH was adjusted by addition of dilute aqueous solutions of 0.1N HCl or 0.1N NaOH. For the optimum amount of adsorbent per unit mass of adsorbate, a 50mL dye solution was contacted with different amounts of SBG till equilibrium was attained. The kinetics of

adsorption was determined by analyzing adsorptive uptake of the dye from the aqueous solution at different time intervals. The adsorption isotherm was found by agitating AG 25 solution of different concentrations with the known amount of SBG till the equilibrium was achieved. The effect of temperature on the sorption characteristics was investigated at 303,313,323 K. Initial dye concentration varied from 30 to 300 mg/L.

### 3. Results and discussion

#### 3.1 Effect of pH

pH affects not only the biosorption capacity, but also the color of the dye solution and the solubility of some dyes (Fu & Viraraghavan, 2001). Therefore, the pH value of the solution was an important controlling factor in the biosorption process (Waranusantigul *et al.*, 2003). The effect of initial pH on AG 25 biosorption by SBG is shown in the Fig. 2. The maximum dye sorption occurred at pH 3 and the removal decreased thereafter. This may be due to high electrostatic attraction between the positively charged surface of the SBG and anionic dye AG 25. Acid dyes are also called as anionic dyes because of the negative electrical structure of the chromophore group. As the initial pH increases, the number of negatively charged sites on the biosorbent surfaces increases and the number of positively charged sites decreases. A negative surface charge does not favor the biosorption of dye anions due to electrostatic repulsion (Namasivayam & Kavitha, 2002). In general, the acidic dye uptakes are much higher in acidic solutions than those in neutral and alkaline conditions (Chiou & Li, 2002).

#### 3.2 Effect of temperature

Investigation of temperature effect on the biosorption of acidic dyes is very important in the real application of biosorption as various textile and other dye effluents are produced at relatively high temperatures. The biosorption of AG 25 on SBG was investigated as a function of temperature and maximum uptake value was obtained at 303 K as can be seen from Fig. 3. biosorption decreased with further increase in temperature due to the decreased surface activity suggesting that biosorption between AG 25 and SBG was an exothermic process and the mechanism was mainly physical adsorption enhanced by a chemical effect (Aksu & Tezer, 2005).

#### 3.3 Effect of biosorbent dosage

The effect of biosorbent dosage on the removal of AG 25 by SBG at  $C_0 = 100$  mg/L is shown in the Fig. 4. It can be seen that the AG 25 removal increases up to a certain limit and then it remains constant. The increase in the biosorption with the biosorbent dosage can be attributed to greater surface area and the availability of more biosorption sites (Mane *et al.*, 2007). At biosorbent dosage greater than 0.2 g the surface AG 25 concentration and the solution AG 25 concentration come to equilibrium with each other. However the biosorption capacity (mg/g) decreased with increase in SBG dosage and this may be attributed to overlapping or aggregation of biosorbent sites resulting in decrease in total biosorbent surface area available to dye and an increase in diffusion path length.

#### 3.4 Effect of initial dye concentration

The effect of initial dye concentration on the biosorption of dye was investigated and shown in Fig. 5. It provides an important driving force to overcome all mass transfer resistances of the dye between the aqueous and solid phases, thus increases the uptake. The equilibrium uptake values increased from 7.05 to 65.17 mg/g with increasing initial dye concentration from 30 to 300 mg/L as a result of the increase in the driving force. However, AG 25 removal yield increased from 94 to 98 % from 30 to 90 mg/L concentration, and then started to decrease from 97 to 86 % for initial dye concentration of 120 to 300 mg/L. At lower dye concentrations solute concentrations to biosorbent sites ratio is higher, which cause an increase in color removal (Ozer *et al.*, 2005). At higher concentrations, lower adsorption yield is due to the saturation of adsorption sites (Ozer *et al.*, 2005).

#### 3.5 Effect of contact time

The effect of contact time on biosorption of AG 25 by SBG at  $C_0 = 100$  mg/L for biosorbent dosage 0.2 g was studied. It was observed that rapid biosorption of dye has taken place in the first 15 minutes and thereafter, the rate of biosorption decreased gradually and reached equilibrium in about 75 min. around 98 % of AG 25 removal was obtained in about 75 min. This may be due to strong attractive forces between the dye molecules and the adsorbent. Fast diffusion on the external surface was followed by fast pore diffusion into the intra particle matrix to attain rapid equilibrium (Ho & Chiang, 2001). Further increase in contact time showed that there is no significant increase in the removal of AG 25 by SBG, so further experiments were conducted for 75 min contact time only.

#### 3.6 Kinetic modelling

In order to investigate the biosorption processes of AG 25 on the SBG, pseudo-first order and pseudo-second order kinetic models were used.

##### 3.6.1 Pseudo-first-order model

The pseudo-first-order equation is given as (Lagergren, 1898):

$$dq_t / dt = k_f (q_e - q_t) \quad (1)$$

Where  $q_t$  is the amount of adsorbate adsorbed at time  $t$  (mg/g),  $q_e$  is the biosorption capacity at equilibrium (mg/g),  $k_f$  is the pseudo-first-order rate constant ( $\text{min}^{-1}$ ), and  $t$  is the contact time (min). The integration of Eq. (1) With the initial condition,  $q_t = 0$  at  $t = 0$  leads to:

$$\log(q_e - q_t) = \log q_e - \frac{k_f}{2.303} t \quad (2)$$

The values of biosorption rate constant ( $k_f$ ) for AG 25 adsorption on SBG were determined from the plot of  $\log(q_e - q_t)$  against  $t$  (not shown here).

### 3.6.2 Pseudo-second-order model

The pseudo-second-order model is given as (McKay & Ho, 1999):

$$\frac{dq}{dt} = k_s (q_e - q_t)^2 \quad (3)$$

Where  $k_s$  is the pseudo-second-order rate constant ( $\text{g/mg min}$ ),  $q_e$  is the amount of dye adsorbed at equilibrium (mg/g), and  $q_t$  is the amount of dye adsorbed at time  $t$  (mg/g). Integrating Eq. (3) for the boundary conditions  $t = 0$  to  $t = t$  and  $q_t = 0$  to  $q_t = q_t$  gives

$$q_t = \frac{q_e^2 k_s t}{1 + q_e k_s t} \quad (4)$$

Eq. (4) is the integrated rate law for a second-order reaction (Ho, 2006) and can be rearranged to obtain

$$q_t = \frac{t}{\frac{1}{k_s q_e^2} + \frac{t}{q_e}} \quad (5)$$

This has a linear form of

$$\frac{t}{q_t} = \frac{1}{k_s q_e^2} + \frac{1}{q_e} t \quad (6)$$

The initial biosorption rate,  $h$  (mg/g min) is defined as:

$$h = k_s q_e^2 \quad (7)$$

The rate parameters  $k_s$  and  $q_e$  can be directly obtained from the intercept and slope of the plot ( $t/q_t$ ) against  $t$  (Fig. 6). Values of  $k_s$ ,  $q_s$ ,  $h$  and correlation coefficient  $R^2$  are listed in Table 1. The Table 1 indicates that the pseudo second order model rate constant  $k$  values and initial biosorption rate  $h$  values increased with increasing the initial dye concentrations. It suggests that  $k$  and  $h$  values are affected by the initial dye concentrations. The calculated correlation coefficients are closer to unity for pseudo-second-order kinetics than that for the pseudo-first-order kinetic model. Therefore, the sorption can be approximated more appropriately by the pseudo-second-order kinetic model for the biosorption of AG 25 by SBG.

### 3.7 Equilibrium modelling

The equilibrium sorption isotherm is fundamentally important in the design of biosorption system. Equilibrium studies in biosorption gives the capacity of the sorbent. Equilibrium relationships between sorbent and sorbate are described by adsorption isotherms, usually the ratio between the quantity sorbed and that remaining in the solution at a fixed temperature at equilibrium (Ho et al., 2002). Langmuir and Freundlich isotherm constants were determined from the plots of  $C_e/q_e$  versus  $C_e$  (Fig. 7) and  $\ln q_e$  versus  $\ln C_e$  (Fig. 8) respectively. It was found that the Langmuir isotherm best represents the equilibrium adsorption of AG 25 on SBG. The isotherm constants and the correlation coefficient,  $R^2$  with the experimental data is given in Table 2.

### 3.7.1 Langmuir isotherm

The Langmuir isotherm is often used to describe the sorption of solute from solution as

$$\frac{q_e}{q_m} = \frac{bc_e}{1 + bc_e} \quad (8)$$

This relation can be written in linearized form as

$$\frac{C_e}{q_e} = \frac{1}{bq_m} + \frac{C_e}{q_m} \quad (9)$$

Where  $q_e$  is the amount of adsorbate adsorbed at equilibrium (mg/g),  $b$  is the Langmuir constant related to the energy of biosorption (L/mg),  $q_m$  is the maximum sorption capacity corresponding to complete monolayer coverage (mg/g), and  $C_e$  is the equilibrium solute concentration (mg/L).

The Langmuir isotherm is applicable to monolayer sorption of adsorbate onto SBG, as shown in Fig. 7. The correlation coefficient,  $R^2$ , was 0.905. According to Eq. (9), the maximum sorption capacity,  $q_m$  was calculated to be 212.76 mg/g, and the equilibrium constant,  $b$ , 0.03566 L/mg. A large value of  $b$  implies strong bonding of AG 25 dye to SBG at this temperature.

The favourable nature of adsorption can be expressed in terms of dimensionless separation factor of equilibrium parameter, which is defined by Eq. (10)

$$R_L = \frac{1}{1 + bC_o} \quad (10)$$

Where  $b$  is the Langmuir constant and  $C_o$  is the initial concentration of the adsorbate in solution.

The values of  $R_L$  indicates the type of isotherm to be irreversible ( $R_L = 0$ ), favourable ( $0 < R_L < 1$ ), linear ( $R_L = 1$ ) or unfavourable ( $R_L > 1$ ).  $R_L$  values for acid green adsorption onto SBG were less than 1 and greater than zero indicating favourable adsorption (Table 2).

### 3.8 Estimation of thermodynamic parameters

The thermodynamics parameters Gibb's free energy changes ( $\Delta G$ ), are calculated using the following equations (Wang et al., 2008)

$$\Delta G = -RT \ln K_c \quad (11)$$

$$K_c = \frac{C_{Ae}}{C_e} \quad (12)$$

Where  $K_c$  is the equilibrium constant,  $C_{Ae}$  is the amount of dye adsorbed on the biosorbent per liter of the solution at equilibrium (mg/L),  $C_e$  is the equilibrium concentration of the dye in the solution (mg/L),  $T$  is absolute temperature and  $R$  is the universal gas constant (8.314 J/mol K). Also, enthalpy changes ( $\Delta H$ ) and entropy changes ( $\Delta S$ ) can be estimated by the following equations, respectively (Jain et al., 2004)

$$\Delta H = -R \left( \frac{T_2 T_1}{T_2 - T_1} \right) \ln \frac{K_2}{K_1} \quad (13)$$

$$\Delta S = \frac{\Delta H - \Delta G}{T} \quad (14)$$

Where,  $K_1$  and  $K_2$  are the values of the equilibrium constant at temperatures  $T_1$  and  $T_2$ , respectively. The free energy of biosorption ( $\Delta G$ ), enthalpy ( $\Delta H$ ) and entropy ( $\Delta S$ ) changes were estimated by using Eq. (11)-(14) for the system AG 25/SBG. Table 3 shows negative values of  $\Delta G$  and  $\Delta H$  indicates that biosorption is spontaneous and exothermic in nature. The positive value of entropy reflects the affinity of the biosorbent for AG 25 dye.

$\Delta H$  for physical adsorption ranges from -4 to -40 kJ/mol, compared to that of chemical adsorption ranging from -40 to -800 kJ/mol. (Crini & Badot, 2008) As shown in Table 3, the  $\Delta H$  values suggest that the adsorption process might be considered as physical adsorption in nature enhanced by a chemical effect.

### 3.9 Evaluation of spent brewery grain as biosorbent

Table 4 shows the comparison of the maximum monolayer adsorption capacities of various adsorbents for AG 25 dye. The value of  $q_{\max}$  in this study (212.76 mg/g) is larger than those in most of previous studies except that of chitosan based biosorbents. More over the SBG used in this study does not require any pretreatment or processing such as chemical modification or activation making it as low cost biosorbent obtained from industrial waste. Furthermore, the industrial waste, SBG, used in this work could be easily obtained as low cost in India and other parts of the developing and developed countries where there is no activity of cattle farming. The results showed that SBG is effective for AG25 dye and could be an alternative for more costly biosorbents used for dye removal in waste water treatment processes.

## 4. Conclusions

The capability of the use of spent brewery grains for the removal of Acid Green dye was examined, including equilibrium and kinetic studies. Experiments were performed as a function of initial solution pH, temperature, initial dye concentration, biosorbent dosage and contact time. The solution pH, temperature and initial dye concentration played a significant role in affecting the capacity of biosorbent. The further increase in pH over 5.0, temperature over 303 K and initial dye concentration of 120 mg/L led to a reduction of the biosorption capacity of the biomass. Optimum biosorbent dosage was 0.2 g/L of solution. The equilibrium between the adsorbate in the solution and on the biosorbent surface was practically achieved in 75 min. Biosorption kinetics was found to follow pseudo-second-order rate expression. Equilibrium biosorption data for AG 25 on SBG were best represented by Langmuir isotherm. The typical dependence of dye uptake on temperature and kinetic studies indicated the biosorption process of AG 25 onto SBG to be physical adsorption enhanced with chemical effect and diffusion controlled. Thermodynamics parameters were estimated for the biosorption of acid green onto SBG. Negative values of  $\Delta G$  and  $\Delta H$  indicate that biosorption is spontaneous and exothermic in nature. The positive value of  $\Delta S$  reflects the affinity of the biosorbent for AG 25 dye.

The present study concludes that spent brewery grains could be employed as a low-cost and ecofriendly biosorbent as an alternative to the current expensive methods of removing dyes from textile effluents. The scope of the further study is to try the feasibility of using SBG as biosorbent for the treatment of industrial effluents containing other dyes and mixture of dyes.

## Acknowledgements

The financial support for this investigation given by Council of Scientific and Industrial Research (CSIR), Ministry of Human Resources Development, New Delhi, India under the grant CSIR Lr. No. 9/468(371)/2007-EMR-1 dated 30.03.2007 is gratefully acknowledged.

## References

- Aksu, Z., & Tezer, S. (2005). Biosorption of reactive dyes on the green alga *Chlorella vulgaris*. *Process Biochemistry*, 40, 1347-1361.
- Asfour, H.M., Fadel, O.A., Nasser, M.M., & El-Geundi, M.S. (1985). Colour removal from textile effluents using hardwood sawdust as adsorbent. *J. Chem. Technol. Biotechnol.* 35, 21-27.
- Aydin, H., & Baysal, G. (2006). Adsorption of acid dyes in aqueous solutions by shells of bittim (*Pistacia khinjuk* Stocks). *Desalination*, 196, 248-259.
- Cheung, W.H., Szeto, Y.S., & McKay, G. (2007). Intraparticle diffusion processes during acid dye adsorption onto chitosan. *Bioresour. Technol.* 98, 2897-2904.
- Chiou, M.S., & Li, H.Y. (2002). Equilibrium and kinetic modeling of adsorption of reactive dye on cross-linked chitosan beads *J. Hazardous Matter*, B 93, 233-248.
- Crini, G., & Badot, P.M. (2008). Application of chitosan, a natural aminopolysaccharide, for dye removal from aqueous solutions by adsorption processes using batch studies: A review of recent literature. *Prog. Polym. Sci.* 33, 399-447.
- Deo, N., & Ali, M. (1993). Adsorption by a new low cost material Congo red 2. *Ind. J. Environ. Protect.* 13, 496-508.
- Fu, Y., & Viraraghavan, T. (2001) Fungal decolorization of dye wastewaters: a review.. *Bioresour. Technol.* 79, 251-262.
- Gibbs, G., Tobin, J.M. & Guibal, E. (2003). Sorption of Acid Green 25 on chitosan: Influence of experimental parameters on uptake kinetics and sorption isotherms. *J. Appli. Polym. Sci.* 90, 1073-1080.
- Hameed, B.H. & Hakimi, H. (2008). Utilization of durian (*Durio zibethinus* Murray) peel as low cost sorbent for the

- removal of acid dye from aqueous solutions. *Biochemical Engg. Journal*. 39, 338-343.
- Hameed, B.H., Ahmad, A.A., & Aziz, N. (2007). Isotherms, kinetics and thermodynamics of acid dye adsorption on activated palm ash. *Chemical Engg. Journal*. 133, 195-203.
- Ho, Y.S., & Chiang, C.C. (2001). Sorption studies of acid dye by mixed sorbents. *Adsorption-Journal of the International Adsorption Society*. 7, 139-147.
- Ho, Y.S. (2006). Review of second-order models for adsorption systems. *J.Hazardous Mater*. 136, 681-689.
- Ho, Y.S., Huang, C.T., & Huang, H.W. (2002). Equilibrium sorption isotherm for metal ions on tree fern. *Process Biochem*. 37 (12), 1421-1430.
- Jain, A.K., Gupta, V.K., Jain, Shubhi & Suhas. (2004). Removal of chlorophenols using industrial wastes. *Environ. Sci. Technol*. 38, 1195-2000.
- Khare, S.K., Panday, K., Srivastava, R.M., & Singh, V.N. (1987). Removal of victoria blue from aqueous solution by fly ash. *J. Chem. Technol. Biotechnol*. 38, 99-104.
- Lagergren, S. (1898). *Kungliga Svenska Vetenskapsakademiens: Handlingar*. 24(4), 1-39.
- Lee, C.K., & Low, K.S. (1997). Quaternized rice husk as sorbent for reactive dyes. *Bioresour. Technol*. 61, 121-125.
- Low, K.S., Lee, C.K., & Liew, S.C. (2000). Sorption of cadmium and lead from aqueous solutions by spent grain. *Process Biochemistry*. 36, 59-64.
- Lu, S., & Gibb, S.W. (2008). Copper removal from wastewater using spent-grain as biosorbent. *Bioresour. Technol*. 99, 1509-1517.
- Mane, V.S., Mall, I.D., & Srivastava, V.C. (2007). Use of Bagasse Fly Ash as an Adsorbent for the Removal of Brilliant Green Dye from Aqueous Solution. *Dyes and Pigments*, 73, 269-278.
- McKay, G., Blair, H.S., & Gardner, J.S. (1983). Rate studies for the adsorption of dyestuffs on chitin. *J. Colloid Interface Sci*. 95, 108-119.
- McKay, G. (1984). Analytical solution using a pore diffusion model for a pseudo irreversible isotherm for the adsorption of basic dye on silica. *J.AIChE*. 30, 692-697.
- McKay, G., Geundi, E.I., & Nasser, M.M. (1987). Equilibrium studies during the removal of dyestuff's from aqueous solutions using bagasse pith. *Water Resour*. 21, 1513-1520.
- McKay, G., & Ho, Y.S. (1999). Pseudo-second order model for sorption processes. *Process Biochem*. 34, 451-465.
- Nassar, M.M. (1999). Interparticle diffusion of basic red and basic yellow dyes on palm fruit bunch. *Water Sci. Technol*. 40, 133-139.
- Namasivayam, C., & Kavitha, D. (2002). Removal of Congo Red from water by adsorption on to activated carbon prepared from coir pith, an agricultural solid waste. *Dyes and pigments*. 54, 47-58.
- Ozer, A., Akkaya, G., & Turabik, M. (2005). The biosorption of Acid Red 337 and Acid Blue 324 on *Enteromorpha prolifera*: The application of nonlinear regression analysis to dye biosorption. *Chem. Eng. J*. 112, 181-190.
- Robinson, T., McMullan, G., Marchant, R. & Nigam, P. (2001). Remediation of dyes in textile effluent: a critical review on current treatment technologies with a proposed alternative. *Bioresour. Technol*. 77, 247-255.
- Wang, B.E., Hu, Y.Y., Xie, L., & Peng, K. (2008). Biosorption behavior of azo dye by inactive CMC immobilized *Aspergillus fumigatus* beads. *Bioresour. Technol*. 99(4), 794-800.
- Waranusantigul, P., Pokethitiyook, P., Kruatrachue, M. & Upatham, E.S. (2003). Kinetics of basic dye (methylene blue) biosorption by giant duckweed (*Spirodela polyrrhiza*). *Environ. Pollut*. 125, 385-392.
- Zollinger, H. (1987). *Colour Chemistry – synthesis properties and applications of organic dyes and pigments*. New York: VCH publishers. pp. 92 - 100.

Table 1. Kinetic parameters for the removal of AG 25 by SBG, Pseudo-second-order model

$C_o$ (mg/L)	$q_e$ (mg/g)	$k_s$ (g/mg min)	$h$ (mg/g min)	$R^2$
60	14.7058	0.034715	7.5075	0.9999
90	22.2222	0.036096	17.8253	1
120	29.6735	0.036873	32.4675	1
150	37.1747	0.037299	72.2118	1
200	49.7512	0.037408	92.5925	1
250	62.1118	0.038119	147.0588	1
300	74.6268	0.038204	212.766	1

Table 2. Langmuir and Freundlich isotherm constants of AG 25 biosorption on SBG

Langmuir constants			Freundlich constants			
$q_m$ (mg/g)	$b$ (L/mg)	$R^2$	$R_L$	$K_F$ (mg/g)(L/mg) <sup>n</sup>	$n$	$R^2$
212.76	0.03566	0.905	0.2190	11.29	1.58	0.901

Table 3. Thermodynamics parameters for AG 25 dye biosorption onto SBG

Temperature (K)	$\Delta G$ (kJ/mol)	$\Delta H$ (J/mol K)	$\Delta S$ (J/mol K)
303	-8.84	-54.87	29.0
313	-10.95		
323	-12.32		

Table 4. Comparison of biosorption capacities of various biosorbents for AG 25 dye

Biosorbent	$q_{max}$ (mg/g)	Reference
Spent brewery grains	212.76	This study
Shells of bittim	16.0	(Aydın & Baysal 2006)
Durian peel	63.29	(Hameed & Hakimi 2008)
Activated palm ash	123.4	(Hameed et al., 2007)
Chitosan	525.0	(Gibbs et al., 2003)
Crab shell	645.1	(Cheung et al., 2007)

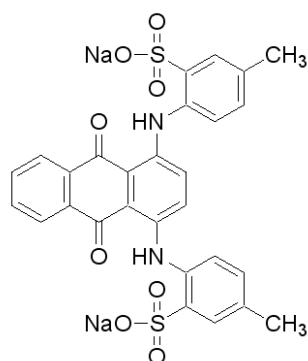


Figure 1. Chemical structure of AG 25

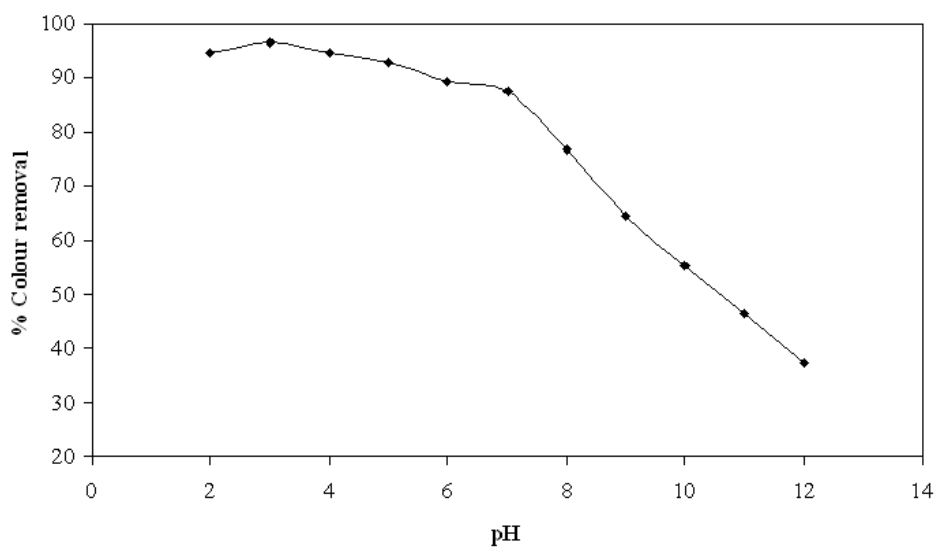


Figure 2. The effect of initial pH of dye solution

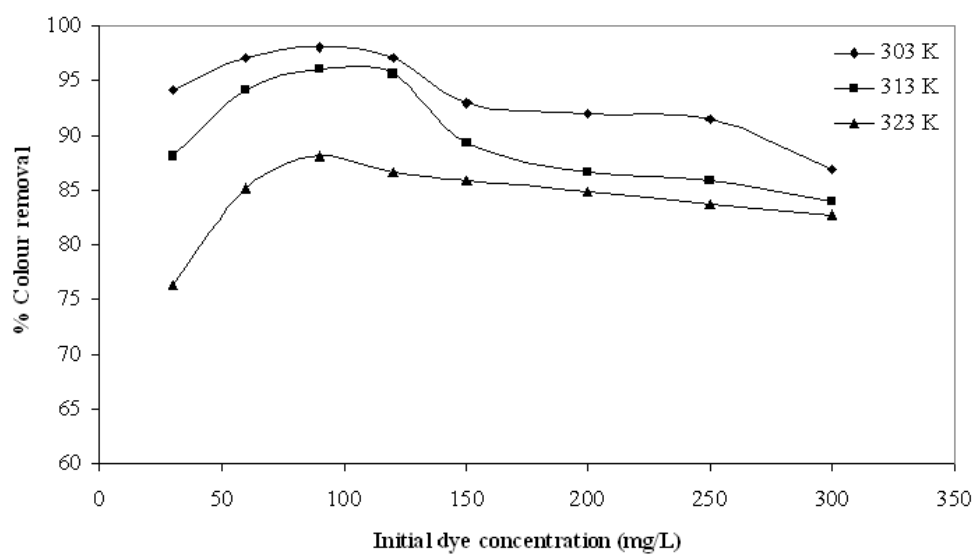


Figure 3. The effect of temperature

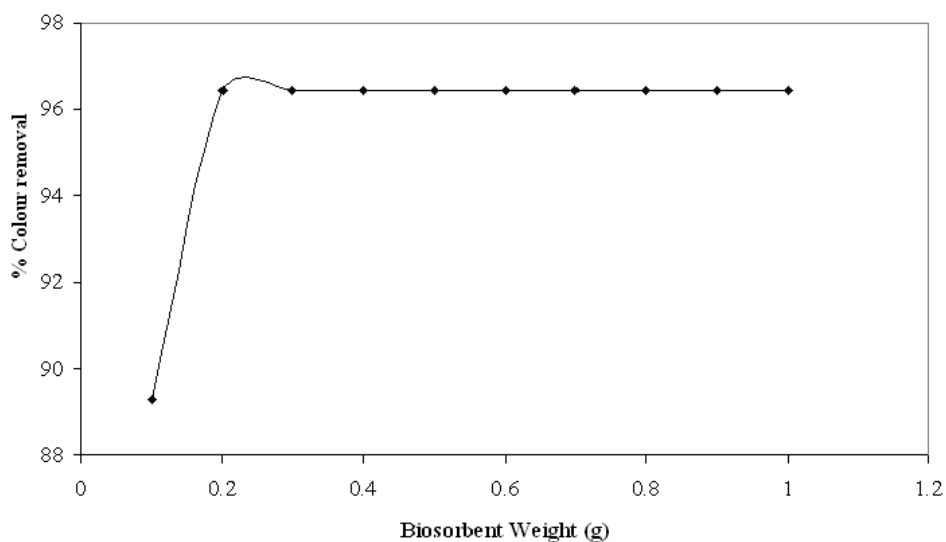


Figure 4. Effect of biosorbent dosage

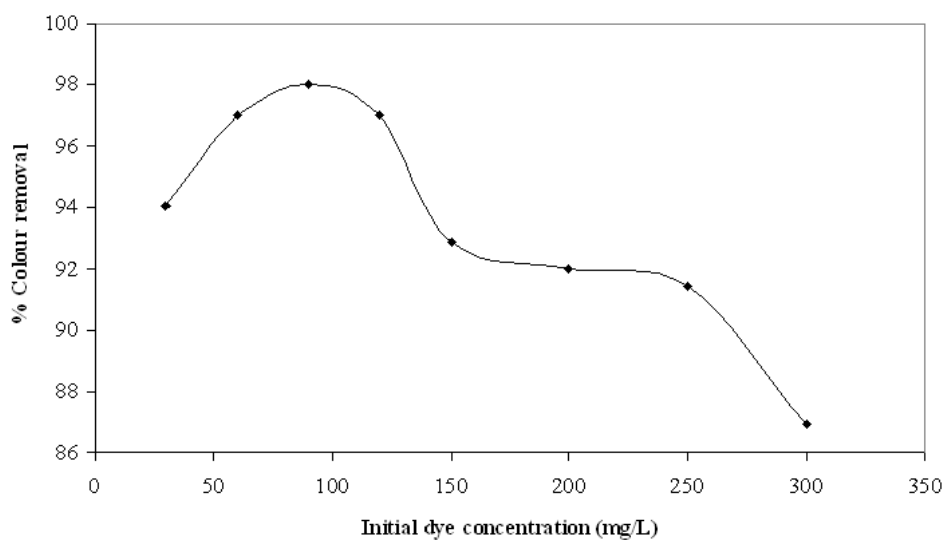


Figure 5. Effect of initial dye concentration

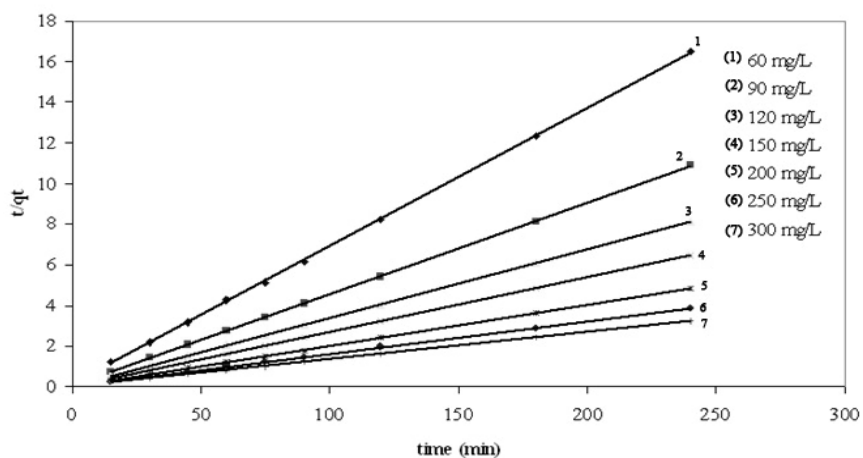


Figure 6. Pseudo-second-order kinetic plots for the removal of AG 25

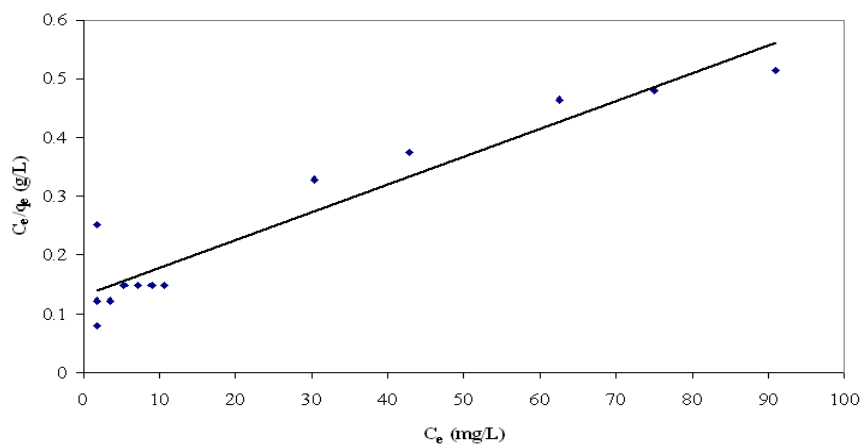


Figure 7. Langmuir isotherm

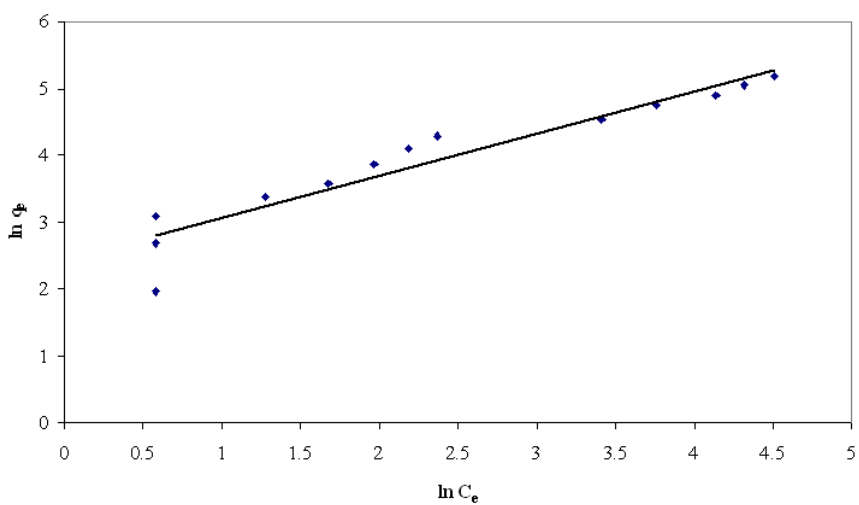


Figure 8. Freundlich isotherm



## Preparation of LaFeO<sub>3</sub> Porous Hollow Nanofibers by Electrospinning

Xiangting Dong (Corresponding author), Jinxian Wang, Qizheng Cui, Guixia Liu & Wensheng Yu

School of Chemistry and Environmental Engineering

Changchun University of Science and Technology

Changchun, Jilin 130022, China

Tel: 86-431-8558-2574 E-mail: dongxiangting888@yahoo.com.cn

*This work was financially supported by the Science and Technology Development Planning Project of Jilin Province (Grant Nos. 20040125, 20060504, 20070402), the Scientific Research Planning Project of the Education Department of Jilin Province (Under grant Nos. 200224, 2005109, 2007-45)*

### Abstract

Polyvinyl Pyrrolidone (PVP)/[La(NO<sub>3</sub>)<sub>3</sub>+Fe(NO<sub>3</sub>)<sub>3</sub>] composite nanofibers were fabricated by electrospinning. SEM micrographs indicated that the surface of the prepared composite fibers was smooth, and the diameters of the nanofibers were in the range of 1-3 μm. XRD analysis revealed that the composite nanofibers were amorphous in structure. LaFeO<sub>3</sub> nanofibers were fabricated by calcination of the PVP/[La(NO<sub>3</sub>)<sub>3</sub>+Fe(NO<sub>3</sub>)<sub>3</sub>] composite fibers. The diameters of LaFeO<sub>3</sub> nanofibers were smaller than those of the relevant composite fibers. The surface of the LaFeO<sub>3</sub> nanofibers became coarse with the increase of calcination temperatures. LaFeO<sub>3</sub> hollow-centered and porous nanofibers formed by nanoparticles were acquired when firing temperature was 600-800°C. SEM images indicated that the diameters of the synthesized LaFeO<sub>3</sub> nanofibers ranged from 500 to 800nm, and their lengths were greater than 100 μm. XRD analysis revealed that LaFeO<sub>3</sub> nanofibers were orthorhombic in structure with space group Pn<sup>\*</sup>a. Possible formation mechanism for LaFeO<sub>3</sub> nanofibers was preliminarily proposed.

**Keywords:** La, LaFeO<sub>3</sub>, Nanofibers, Electrospinning

### 1. Introduction

The science and technology of nanostructured materials is advancing at a rapid pace (Mohapatra, 2008 & Zhang, 2007). Over the past decade, the preparation and functionalization of one-dimensional nanostructured materials has become one of the most highly energized research fields (Hu, 2008 & Kar, 2006). One-dimensional nanostructured materials, such as nanowires, nanorods, nanowhiskers and nanofibers, have stimulated great interest due to their importance in basic scientific research and potential technological applications (Huynh, 2002 & Duan, 2003). They are expected to play an important role as both interconnects and functional components in the fabrication of nanoscale electronic and optoelectronic devices. In order to obtain these materials, various preparation methods have been developed including arc discharge, laser ablation, template, precursor thermal decomposition, and other methods (Iijima, 1991, Morales, 1998, Shi, 2001 & Pan, 2001). Electrospinning technique is widely applied to prepare polymer nanofibers (Li, 2004, 1151-1170). Recently, some inorganic compounds nanofibers have been prepared by electrospinning technique using electrospun fibers of polymer/inorganic composite as the precursor (Li, 2004, Zhang, 2008 & Shao, 2004). This processing involved the following three steps: (1) Preparation of a gel with suitable inorganic precursor and proper polymer, and achieving the right rheology for electrospinning process; (2) Electrospinning of the gel to obtain fibers of polymer/inorganic precursors composite; (3) Calcinations of the composite fibers to obtain final oxide fibers. It is important; however, to control all of the above three steps in order to obtain high quality fibers with the desired final properties. LaFeO<sub>3</sub> has attracted much interest recently due to their specific electrical, and catalytic properties (Dong, 1994 & Yang, 2003). A few methods on the preparation of LaFeO<sub>3</sub> nanocrystalline materials were reported (Wang, 2006, Yang, 2005, Wang, 2006, Qi, 2003 & Yang, 2006). However, to the best of our knowledge, there have been no reports on the preparation of LaFeO<sub>3</sub> nanofibers by electrospinning. In this paper, LaFeO<sub>3</sub> nanofibers were fabricated by calcination of the electrospun fibers of PVP/(lanthanum nitrate and iron nitrate) composite, and some new results were obtained.

## 2. Experimental section

### 2.1 Chemicals

Polyvinyl pyrrolidone (PVP)( $M_r \approx 10000$ ) and iron nitrate enneahydrate [ $\text{Fe}(\text{NO}_3)_3 \cdot 9\text{H}_2\text{O}$ ] were purchased from Tianjin Kermel Chemical Reagents Development Center. Lanthanum nitrate hexahydrate [ $\text{La}(\text{NO}_3)_3 \cdot 6\text{H}_2\text{O}$ ] was obtained from Tianjin Guangfu Institute of Fine Chemicals. All chemicals were analytically pure and directly used as received without further purification. Distilled water was used as solvent.

### 2.2 Preparation of PVP/[ $\text{La}(\text{NO}_3)_3$ and $\text{Fe}(\text{NO}_3)_3$ ] composite gel

PVP/[ $\text{La}(\text{NO}_3)_3$  and  $\text{Fe}(\text{NO}_3)_3$ ] composite solution was prepared by dissolving 12.3699g of PVP powders, 2.0536g of  $\text{La}(\text{NO}_3)_3 \cdot 6\text{H}_2\text{O}$  and 1.9160g of  $\text{Fe}(\text{NO}_3)_3 \cdot 9\text{H}_2\text{O}$  in 10.55g of distilled water, and stirring for 10h, then remaining motionlessly for 2h. Thus, a viscous gel of PVP/[ $\text{La}(\text{NO}_3)_3$ +  $\text{Fe}(\text{NO}_3)_3$ ] composite containing 46%(wt%) PVP, 10% (wt%) metallic nitrate, 44%(wt%)  $\text{H}_2\text{O}$ , and the molar ratio 1:1 of  $\text{La}^{3+}$  to  $\text{Fe}^{3+}$  were obtained for electrospinning processing.

### 2.3 Fabrication of PVP/[ $\text{La}(\text{NO}_3)_3$ and $\text{Fe}(\text{NO}_3)_3$ ] composite fibers and $\text{LaFeO}_3$ nanofibers

The setup used for electrospinning was indicated in Fig. 1. The above composite gel of PVP,  $\text{La}(\text{NO}_3)_3$ ,  $\text{Fe}(\text{NO}_3)_3$  and  $\text{H}_2\text{O}$  mixture was contained in a plastic syringe with a stainless steel needle on its top. A copper wire connected to a DC high-voltage generator was placed in the gel, and the gel was kept in the syringe by adjusting the angle between syringe and the fixing bar. A grounded aluminum foil served as counter electrode and collector plate. A voltage of 18 kV was applied to the composite gel and a sprayed dense web of fibers was collected on the aluminum foil. The collected fibers were PVP/[ $\text{La}(\text{NO}_3)_3$  and  $\text{Fe}(\text{NO}_3)_3$ ] composite fibers. The prepared composite fibers were dried initially at  $70^\circ\text{C}$  for 12h under vacuum, and then calcined at a heating rate of  $120^\circ\text{C}/\text{h}$  and remained for 10h at  $300^\circ\text{C}$ ,  $600^\circ\text{C}$  and  $800^\circ\text{C}$ , respectively. Thus,  $\text{LaFeO}_3$  nanofibers were obtained when calcinations temperature is  $600\text{--}800^\circ\text{C}$ .

### 2.4 Characterization methods

XRD analysis was performed with a Holland Philips Analytical PW1710 BASED X-ray diffractometer using  $\text{Cu K}\alpha_1$  radiation, the working current and voltage were 30mA and 40kV, respectively. Scans were made from  $10^\circ$  to  $80^\circ$  at the speed of  $3^\circ/\text{min}$ , and step was  $0.05^\circ$ . The morphology and size of the fibers were observed with a S-4200 scanning electron microscope made by Japanese Hitachi company. FTIR spectra of the samples were recorded on BRUKER Vertex 70 Fourier transform infrared spectrophotometer made by Germany Bruker company, and the specimen for the measurement was prepared by mixing the sample with KBr powders and then the mixture was pressed into pellets, the spectrum was acquired in a wave number range from  $4000\text{cm}^{-1}$  to  $400\text{cm}^{-1}$  with a resolution of  $4\text{ cm}^{-1}$ .

## 3. Results and discussion

### 3.1 XRD patterns

In order to investigate the lowest crystallizing temperature and the variety of phases, the PVP/[ $\text{La}(\text{NO}_3)_3$  and  $\text{Fe}(\text{NO}_3)_3$ ] composite fibers and samples obtained by calcining the composite fibers at different temperatures for 10h were characterized by XRD, as indicated in Fig. 2. The results showed that the PVP/[ $\text{La}(\text{NO}_3)_3$ + $\text{Fe}(\text{NO}_3)_3$ ] composite fibers were amorphous in structure, only a broad peak was located around  $20^\circ$ , it was the typical peak of the amorphous polymer, indicating that the composite fibers were amorphous in structure. The sample was also amorphous at  $300^\circ\text{C}$ , and no obvious diffraction peaks could be observed. The polycrystalline  $\text{LaFeO}_3$  nanofibers with single phase were synthesized when calcination temperature was in the range of  $600\text{--}800^\circ\text{C}$ , the  $d$ (spacing between crystallographic plane) values and relative intensities of  $\text{LaFeO}_3$  are consistent with those of JCPDS standard card(37-1493), and the crystal structure of the prepared  $\text{LaFeO}_3$  was orthorhombic system with space group  $\text{Pn}^*a$ .

### 3.2 SEM images

In order to study the morphology and size of the as-synthesized fibers, the prepared fibers were investigated by SEM, as shown in Fig. 3. As seen from Fig. 3, the morphology and size of the fibers varied strongly with the increase of calcination temperatures. The surface of the PVP/[ $\text{La}(\text{NO}_3)_3$ +  $\text{Fe}(\text{NO}_3)_3$ ] composite fibers was very smooth, and the diameter of the composite fibers was in the range of  $1\mu\text{m}\text{--}3\mu\text{m}$ . The morphology and size of the fibers at  $300^\circ\text{C}$  were almost the same as those of the composite fibers. The surface morphology of  $\text{LaFeO}_3$  nanofibers became coarse with the increase of calcination temperatures.  $\text{LaFeO}_3$  porous hollow nanofibers formed by nanoparticles were acquired at  $600^\circ\text{C}\text{--}800^\circ\text{C}$ . SEM analysis indicated that the diameters of the synthesized  $\text{LaFeO}_3$  nanofibers were in the range of  $500\text{nm}\text{--}800\text{nm}$ , and their lengths were greater than  $100\mu\text{m}$ . The diameters of  $\text{LaFeO}_3$  nanofibers were smaller than those of the PVP/[ $\text{La}(\text{NO}_3)_3$ + $\text{Fe}(\text{NO}_3)_3$ ] composite fibers owing to the decomposition and evaporation of PVP and  $\text{NO}_3^-$ .

### 3.3 FTIR spectra analysis

Pure PVP, PVP/[ $\text{La}(\text{NO}_3)_3$ + $\text{Fe}(\text{NO}_3)_3$ ] composite fibers and  $\text{LaFeO}_3$  nanofibers (obtained by calcination of the PVP/[ $\text{La}(\text{NO}_3)_3$ + $\text{Fe}(\text{NO}_3)_3$ ] composite fibers at  $800^\circ\text{C}$  for 10h) were analyzed by FTIR, as shown in Fig. 4. As seen

from Fig. 4, PVP(Fig. 4a) and PVP/[La(NO<sub>3</sub>)<sub>3</sub>+Fe(NO<sub>3</sub>)<sub>3</sub>] composite fibers(Fig. 4b) had the identical spectra, but absorption peaks intensity of spectrum for PVP/[La(NO<sub>3</sub>)<sub>3</sub>+Fe(NO<sub>3</sub>)<sub>3</sub>] composite fibers was lower than those of spectrum for pure PVP. This resulted from the lower content of PVP in the PVP/[La(NO<sub>3</sub>)<sub>3</sub>+Fe(NO<sub>3</sub>)<sub>3</sub>] composite fibers. All absorption peaks were attributed to PVP at 3436cm<sup>-1</sup>, 2956cm<sup>-1</sup>, 1663cm<sup>-1</sup>, 1424cm<sup>-1</sup>, and 1290cm<sup>-1</sup>, corresponding to the stretching vibrations of hydroxyl group( $\nu_{O-H}$ ), C-H bond( $\nu_{C-H}$ ), carbonyl group( $\nu_{C=O}$ ), C-H bond( $\nu_{C-H}$ ), and C-N bond or C-O bond( $\nu_{C-N}$  or  $\nu_{C-O}$ ), respectively. It was seen from Fig. 4c that all peaks of PVP disappeared, and at low wave number range, new absorption peak at 561cm<sup>-1</sup> appeared. The new absorption peak was ascribed to the vibration of metal-oxygen bond, indicating that LaFeO<sub>3</sub> was formed. The results of FTIR analysis were in good agreement with XRD results.

### 3.4 Possible formation mechanism of LaFeO<sub>3</sub> porous hollow nanofibers

Possible formation mechanism of LaFeO<sub>3</sub> porous and hollow nanofibers was described as follows. La(NO<sub>3</sub>)<sub>3</sub>·6H<sub>2</sub>O, Fe(NO<sub>3</sub>)<sub>3</sub>·9H<sub>2</sub>O and PVP were mixed with distilled water to form gel with certain viscosity. PVP acted as template during the formation processing of LaFeO<sub>3</sub> nanofibers. La<sup>3+</sup>, Fe<sup>3+</sup> and NO<sub>3</sub><sup>-</sup> were mixed with or absorbed onto PVP molecules to fabricate PVP/[La(NO<sub>3</sub>)<sub>3</sub>+Fe(NO<sub>3</sub>)<sub>3</sub>] composite fibers under electrospinning. During calcination treatment of the composite fibers, solvent water containing La<sup>3+</sup>, Fe<sup>3+</sup>, and NO<sub>3</sub><sup>-</sup> ions in the composite fibers would remove to the surface of the PVP/[La(NO<sub>3</sub>)<sub>3</sub>+Fe(NO<sub>3</sub>)<sub>3</sub>] composite fibers and eventually evaporated from the composite fibers. Thus, La<sup>3+</sup>, Fe<sup>3+</sup>, and NO<sub>3</sub><sup>-</sup> ions also remove to the surface of the composite fibers brought by removed water. With the increasing in calcination temperature, PVP, and NO<sub>3</sub><sup>-</sup> would oxidize and volatilize rapidly, La<sup>3+</sup> and Fe<sup>3+</sup> were oxidized into LaFeO<sub>3</sub> crystallites, and many crystallites were combined to form small LaFeO<sub>3</sub> nanoparticles, and these nanoparticles were mutually connected to generate hollow-centered and porous LaFeO<sub>3</sub> nanofibers. It was found from experiments that the average molecular weight of PVP and PVP content in the starting mixed gel had important impact on the formation of LaFeO<sub>3</sub> porous hollow nanofibers. Further work is under way.

## 4. Conclusions

### 4.1

PVP/[La(NO<sub>3</sub>)<sub>3</sub>+Fe(NO<sub>3</sub>)<sub>3</sub>] composite fibers were fabricated by electrospinning. Polycrystalline LaFeO<sub>3</sub> nanofibers were synthesized by calcining the relevant composite fibers at 600-800°C.

### 4.2

XRD analysis revealed that the composite fibers were amorphous in structure. The crystal structure of LaFeO<sub>3</sub> nanofibers was orthorhombic system with space group Pn\**a*.

### 4.3

SEM micrographs indicated that the surface of the prepared composite fibres was smooth, and the diameters of the composite fibres were in the range of 1-3µm. The diameters of LaFeO<sub>3</sub> nanofibers were smaller than those of the composite fibers. The surface of the LaFeO<sub>3</sub> nanofibers became coarse with the increase of calcination temperatures. LaFeO<sub>3</sub> porous and hollow nanofibers formed by nanoparticles were acquired when calcining temperature was 600-800°C. The diameters of LaFeO<sub>3</sub> nanofibers were in the range of 500nm-800nm, and their lengths were greater than 100µm.

## References

- Dong, X. T., Guo, Y. Z., Yu, D. C., et al. (1994). Study of synthesis and electrical properties of LaFeO<sub>3</sub> ultrafine powders. *Mater. Sci. & Technol.*, 2(1), 11-14.
- Duan, X. F., Huang, Y., Agarwal, R., Lieber, C. M. (2003). Single-nanowire electrically driven lasers. *Nature*, 421, 241-245.
- Hu, X. K., Qian, Y. T., Song, Z. T., et al. (2008). Comparative study on MoO<sub>3</sub> and H<sub>x</sub>MoO<sub>3</sub> nanobelts: structure and electric transport. *J. Chem Mater*, 20(4), 1527-1533.
- Huynh, W. U., Dittmer, J. J., Alivisatos, A. P. (2002). Hybrid nanorod-polymer solar cells. *Science*, 295, 2425-2427.
- Iijima, S. (1991). Helical microtubules of graphitic carbon. *Nature*, 354, 56-58.
- Kar, S., Chaudhuri, S. (2006). Shape selective growth of CdS one-dimensional nano-structures by a thermal evaporation process. *J. Phys. Chem. B*, 110(10), 4542-4547.
- Li, D., Xia, Y. N. (2004). Direct fabrication of composite and ceramic hollow nanofibers by electrospinning. *Nano Lett.*, 4(5), 933-938.
- Li, D., Xia, Y. N. (2004). Electrospinning of Nanofibers: Reinventing the Wheel. *Adv. Mater.*, 16(14), 1151-1170.
- Mohapatra, S. K., Misra, M., Mahajan, V. K., et al. (2008). Synthesis of Y-branched TiO<sub>2</sub> nanotubes. *Materials Letters*, 62, 1772-1774.

Morales, A. M., Lieber, C. M. (1998). A laser ablation method for the synthesis of crystalline semiconductor nanowires. *Science*, 279, 208-211.

Pan, Z. W., Dai, Z. R., Wang, E.L. (2001). Nanobelts of semiconducting oxides. *Science*, 291, 1947-1949.

Qi, X. W., Zhou, J., Yue, Z. X., et al. (2003). A simple way to prepare nanosized  $\text{LaFeO}_3$  powders at room temperature. *Ceramic International*, 29(3), 347-349.

Shao, C. L., Guan, H. Y., Liu, Y. C., et al. (2004). A novel method for making  $\text{ZrO}_2$  nanofibres via an electrospinning technique. *J. Crystal Growth*, 267, 380-384.

Shi, W. S., Zheng, Y. F., Wang, N., et al. (2001). A general synthetic route to III-V compound semiconductor nanowires. *Adv. Mater.*, 13, 591-594.

Wang, D., Chu, X. F., Gong, M. L. (2006). Single-crystalline  $\text{LaFeO}_3$  nanotubes with rough walls: synthesis and gas-sensing properties. *Nanotechnology*, 17, 5501-5505.

Wang, Y. P., Zhu, J. W., Zhang, L. L., et al. (2006). Preparation and characterization of perovskite  $\text{LaFeO}_3$  nanocrystals. *Mater. Lett.*, 60, 1767-1770.

Yang, Q. H., Fu, X. X. (2003). Analysis of photocatalytic oxidation activity of nano- $\text{LaMO}_3$  (M=Cr, Mn, Fe, Co) compounds. *J. Chin. Ceram. Soc.*, 31(3), 254-256.

Yang, Z., Huang, Y., Dong B., et al. (2006). Controlled synthesis of highly ordered  $\text{LaFeO}_3$  nanowires using a citrate-based sol-gel route. *Mater. Res. Bull.*, 41(2), 274-281.

Yang, Z., Huang, Y., Dong, B., et al. (2005). Fabrication and structural properties of  $\text{LaFeO}_3$  nanowires by an ethanol-ammonia-based sol-gel template route. *Applied physics A, Materials science & processing*, 81(3), 453-457.

Zhang, S. H., Dong, X. T., Xu, S. Z., et al. (2007). Preparation and characterization of  $\text{TiO}_2/\text{SiO}_2$  submicron-scaled coaxial cables via a static electricity spinning technique. *Acta Chimica Sinica*, 65(23), 2675-2679.

Zhang, S. H., Dong, X. T., Xu, S. Z., et al. (2008). Preparation and characterization of  $\text{TiO}_2/\text{SiO}_2$  composite hollow nanofibers via an electrospinning technique. *Acta Materiae Compositae Sinica*, 25(3), 138-143.

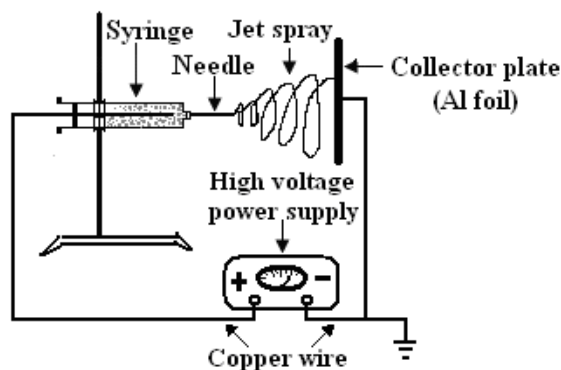


Figure 1. Schematic diagram of electrospinning setup

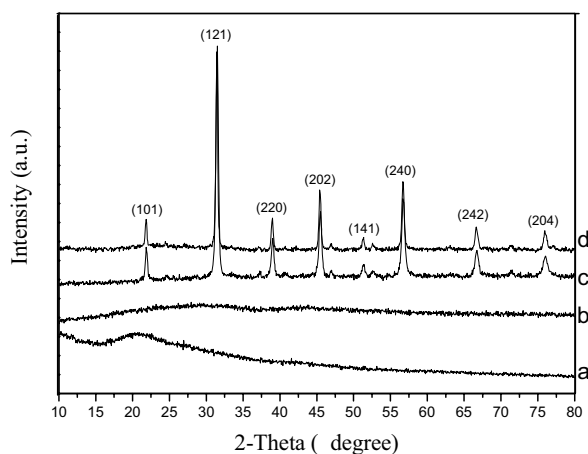


Figure 2. XRD patterns of samples

a. PVP/ $[\text{La}(\text{NO}_3)_3 + \text{Fe}(\text{NO}_3)_3]$  composite fibers b. 300°C c. 600°C d. 800°C

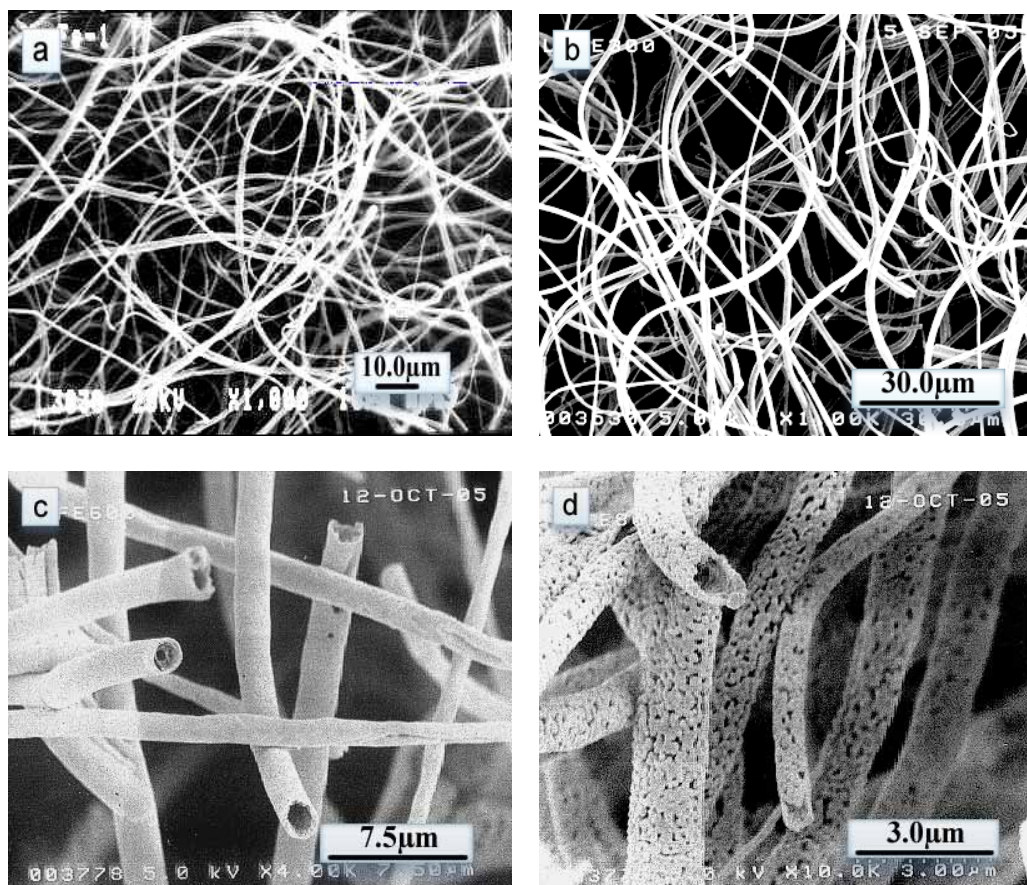


Figure 3. SEM micrographs of the fibers obtained at different temperatures  
 a. PVP/[La(NO<sub>3</sub>)<sub>3</sub>+Fe(NO<sub>3</sub>)<sub>3</sub>] composite fibers b. 300°C c. 600°C d. 800°C

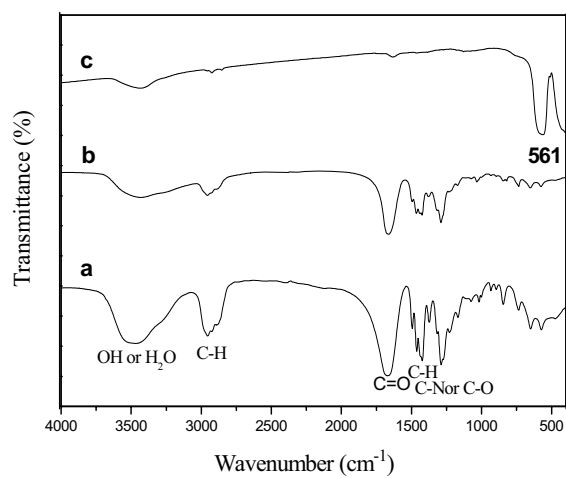


Figure 4. FTIR spectra of the samples  
 a. PVP b. PVP/[La(NO<sub>3</sub>)<sub>3</sub>+Fe(NO<sub>3</sub>)<sub>3</sub>] composite fibers c. LaFeO<sub>3</sub> nanofibers



## Preparation of Nano-ZnO and Its Application to the Textile on Antistatic Finishing

Fan Zhang & Junling Yang (Corresponding author)

School of Material Science and Chemical Engineer

Tianjin Polytechnic University

Tianjin 300160, China

E-mail: fftjpu@yeah.net

### Abstract

Nano-ZnO was prepared by direct precipitation method with zinc chloride and sodium carbonate anhydrous as raw materials, and its particle size and dispersion were characterized by TEM. The effects of concentration and the ratio of reactants and reaction temperature on its dispersion in aqueous solution were analyzed and the best reaction conditions were as follows: reaction temperature 60°C, ultrasonic vibration time 40 min, concentration of the reactant 0.5mol/l and molar ratio of reactants 1:2 for the preparation. The cotton fabric and the polyester fabric which were both finished by pad-dry-cure process with antistatic finishing agent, which was compounded with nano-ZnO, were tested on their antistatic property. According to the comparison between the cotton and the polyester treated fabrics on antistatic property, the results showed that the charge density of the polyester fabric was reduced to  $9.5 \times 10^{-8}$  C/m<sup>2</sup> from  $5.8 \times 10^{-6}$  C/m<sup>2</sup>, which was about 10 times as that of the cotton fabric.

**Keywords:** Nano-ZnO, Direct precipitation method, Cotton fabric, Polyester fabric, Antistatic finishing

### 1. Introduction

To protect human health and improve human living environment, many researchers have been paid attention to functional textiles in recent years (Hee, 2007, p.8020). And the rapidly developing nanotechnology become a research hotspot, because the special physical and chemical properties, which are beneficial to study on the functional products and produce many new applications, are showed when the bulk particle size is reduced to nanometer range (Herrera, 2006, p.245; Iijima, 1999, p.297; Kruis, 2001, p.39). In the metal oxides that are widely used in different areas, zinc oxide powders are important material for applications due to their unique optical, electrical, dermatological and antibacterial properties (Takahashi, 2007, p.722; Alessio, 2007). Currently, the synthesis approaches of nano-ZnO are various, which are mainly divided into three kinds: the solid, the solution and the vapor phase methods (Muccillo, 2004, p.302). In this paper, nano-ZnO were obtained through a direct precipitation reaction, which belongs to the solution phase methods, between zinc chloride and sodium carbonate anhydrous. The effects of reaction temperature, concentration and the ratio of reactants, and so on, on the deposition of nano-ZnO in aqueous solution were discussed. And nano-ZnO was used to prepare the nanometer antistatic finishing agent, which was applied to treat cotton and polyester fabrics, and then the antistatic performance of the treated textiles was evaluated through the charge density (Alessio, 2007).

### 2. Experimental

#### 2.1 Synthesis of nano-ZnO

Zinc chloride (ZnCl<sub>2</sub>, purity 98.0%), sodium carbonate anhydrous (Na<sub>2</sub>CO<sub>3</sub>, purity 99.8%) and Ethanol absolute (CH<sub>3</sub>CH<sub>2</sub>OH, purity 99.7%) were obtained from Tianjin Chemical Reagent III Co. Zinc chloride was of chemic grade, and all the other reagents were of analytical grade. surfactant and 106 binder were purchased from market. All were used as received without any further purification in the experiment.

The preparation of nano-ZnO according to the literature (Liao, 2003, pp.22-23): the nano-ZnO was prepared by direct precipitation method, ZnCl<sub>2</sub> and Na<sub>2</sub>CO<sub>3</sub> were dissolved in water respectively. And then the Na<sub>2</sub>CO<sub>3</sub> solution was dropped into ZnCl<sub>2</sub> solution, and that resulted in precipitation, then it was treated with ultrasonic vibration and aged several hours. In order to remove salt, as-burnt powders were filtered then rinsed in distilled water and ethanol. Finally, the precursor was dried in oven at 80°C for 4 h, and thermal treatment at 450°C for 3 h led to the formation of

nano-ZnO (Chen, 2006, p.435).

### 2.2 Fabric treatments

White cotton and polyester fabrics were used as received. The mass per unit surface was 104 g/m<sup>2</sup> for cotton and 150 g/m<sup>2</sup> for polyester (Alessio, 2007).

A certain concentration of nanometer antistatic finishing agent was prepared as follows: a certain amount of nano-ZnO and surfactant were added into distilled water and the mixture was mixed well with ultrasonic vibration for several minutes, and then the adhesion agent is added under stirring (Li, 2006, p.265).

The cotton and polyester samples were soaked for 5 min in the nanometer antistatic finishing agent, then the clothes were squeezed to remove the excess finishing agent by a NM—450 open-width impregnator (two dipping and rolling). The treated fabrics were dried and baked in a DK—5E curing machine, respectively, at 80 °C for 1 min and 160 °C for 3 min (Alessio, 2007).

### 2.3 Measurements

The morphologies and size of the products were characterized by a Hitachi Model H-7650 transmission electron microscope (TEM) (Tang, 2006, p.548). The charge density of the fabrics with and without finishing were measured according to a standard method (Professional Standards of the People's Republic of China ZB W 04008-89). The whiteness of the fabrics with and without finishing were performed via a WSD—3U fluorescent whiteness meter.

## 3. Results and discussion

### 3.1 The impact of reaction conditions

The size and quality of the particles have effect on particle's settling velocity in dispersion medium. The larger the particle, the higher settling velocity it is (Ni, 2006). Nanoparticles owe to the properties of small dimension, large specific surface area and high surface activity, which lead to agglomeration easily (Luo, 2003, p.27). Settlement experiment was employed to estimate the diameter and dispersion in aqueous solution of nano-ZnO through the deposition time. The results show that the deposition time is longer, the particle is smaller and the dispersion is better (Cui, 2001, p.99). In this experiment, various experimental conditions were analyzed based on the deposition time of nano-ZnO in aqueous solution.

#### 3.1.1 The impact of time of the ultrasonic vibration

Mechanical action caused by ultrasonic vibration within the submicroscopic range including mechanical mass transfer, heating effect and cavitation effect, in which, the pulverization effect produced by transient cavitation effect make the precipitation becoming homogeneous minimal particles and cavitation bubbles, which reduce the specific surface free energy of crystal nucleus, formed by steady cavitation effect inhibit the agglomeration and growth of the crystal nucleus, so the particle size of the product is reduced (Liang, 2002, p.570; Qiu, 1999, p.45; Zhang, 2002, p.82). However, heating effect will raise medium temperature, and that increases the collision probability of the particles. Which lead to a reagglomeration of the dispersed particles, forming a second-level agglomeration, so speed up the settlement of the particles and result in a declined dispersion (Qiu, 1999, p.45; Jiang, 2007, p.725; Luo, 2007, p.185). As can be seen from Fig. 1, with the increase of time of the ultrasonic vibration, the deposition time of nano-ZnO in aqueous solution increased at first and then decreased. This is because the increase of time of the ultrasonic vibration leads to fully cavitation effect, and heating effect become more and more obviously when the time went on continually. Therefore, the time of ultrasonic vibration of 40 min was chosen for experiment.

#### 3.1.2 The impact of temperature

The deposition time of nano-ZnO in aqueous solution present a trend of first increases then decrease, which is shown in Fig. 2. This is due to the temperature has an impact on supersaturation of solution, which relate with the nucleation rate in system. As the temperature rises, the faster reaction rate and the increasing of supersaturation of reaction products lead to crystal core forming rate was accelerated in the short reaction time, that means the controlling step of the reaction is transferred from grain growth to crystal nucleus formation, so the particles are smaller. With the temperatures continuing to rise, the phenomenon of "nuclear-aggregation" caused by the rapid formation of crystal nucleus is obvious that result in forming aggregate among the crystal nucleus (Wang, 2006, p.41; Kang, 2005, p.348). Therefore, 60 °C was the best temperature.

#### 3.1.3 The impact of concentration of zinc chloride

As shown in Fig. 3, the concentration of reaction has a great effect on products' diameter. With the increase of the supersaturation of the solution in response to the increasing of ion concentration in system, a great deal crystal nucleus are generated instant of the reaction, which lead to tiny crystalline grains increased. So the "the size fraction agglomeration" phenomenon becomes gradually significant, and that result in the larger particles (Kang, 2005, p.348; Wang, 2006, p.41; Ding, 2002, p.1016). The deposition time of the nano-ZnO in aqueous solution show a trend of

decreasing, which reflect a change of diameter of the products. The dispersion of nano-ZnO in aqueous solution was the best when the concentration of ZnCl<sub>2</sub> was 0.5mol/l.

### 3.1.4 The impact of ratio of the reactant

The deposition time of nano-ZnO which was prepared with different ratios in aqueous solution are 2-6 h, the results indicate that the impact of the ratio of reaction on products' dispersion is not obvious. As is shown in Fig. 3, the ratio of the reaction has a greater impact on production of precursor. This is because the nanoparticles were prepared by direct precipitation method, which use the precipitation reaction among reactants, and the precipitation-dissolution equilibrium exists in reaction system, whose direction is influenced by the common ion effect and the salt effect. With the increasing of the reactant content, the leading role of the common ion effect and the salt effect, respectively, gradually weaken and enhance. In order to ensure the precipitation-dissolution equilibrium, the directions of reaction change from deposit generation to dissolution (General chemical staff room of Tianjin University, 1983), which lead to a trend of the precursor output that first increased then decreased.

Considering the effects of ratio of the reactant on the dispersion of nano-ZnO in aqueous solution and precursor output, the best molar ratio of zinc chloride and sodium carbonate anhydrous was 1:2.

### 3.2 TEM analysis of nano-ZnO

In the process of nano-ZnO preparation by direct precipitation method, the stirring, reaction temperature, concentration and the ratio of reactants have a great impact on the size distribution and dispersion of nano-ZnO. The diameter and dispersion of the products which were prepared with the optimal reaction conditions, which were obtained by the former phase's experiment, were improved. The diameter of nano-ZnO, which can be seen from the TEM image shown in Fig. 5, was between 20 and 40 nm.

### 3.3 The functional finishing of fabric

As shown in table 1, the impact of antistatic function finishing on the fabric whiteness is not obvious. The charge density of the treated fabric decreased significantly in comparison with the original piece, show that the fabric, which finished with the antistatic finishing agent was compounded with nano-ZnO, produce antistatic performance. And low concentration of finishing agent is able to achieve better antistatic effect. However, with the increasing of the addition amount of nano-ZnO, the fabric antistatic property is decreased, that is because of the declined dispersion and increased agglomeration of nano-ZnO in finishing agent. And the increased amount of nanoparticles results in the limitation of characteristics of nano-ZnO.

Through comparison between cotton and polyester treated fabrics, the decline rate of charge density of the later is more obvious than the former, it reveals that the antistatic effect of polyester fabric finished with nanometer antistatic finishing agent is better.

## 4. Conclusions

(1) The best reaction conditions for the preparation of nano-ZnO by direct precipitation method were as follows: The time of ultrasonic vibration was 40 min, the reaction temperature was 60 °C, the concentration was 0.5 mol/l and the ratio was 1:2.

(2) The cotton and polyester fabrics treatment with nanometer antistatic finishing agent could significantly improve their antistatic properties, and low concentration of finishing agent could achieve better antistatic effect. The comparison between the two kinds of treated fabrics showed that the finishing effect of the polyester fabric was more obvious.

## References

- Alessio, B., Maximilian, D., Pierandrea, L. N., & Piero, B. (2007). Synthesis and characterization of zinc oxide nanoparticles: application to textiles as UV-absorbers. *J Nanopart Res*.
- Chen, W. F., Li, F. S., Yu, J. Y., & Li, Y. X. (2006). Novel salt-assisted combustion synthesis of high surface area ceria nanopowders by an ethylene glycol-nitrate combustion process. *Journal of Rare Earths*, 24, 434-439.
- Cui, A. L., Wang, T. J., He, H., & Jin, Y. (2001). Dispersion behavior of ultrafine titanium dioxide particles in aqueous solution. *The Chinese Journal of Process Engineering*, 99-101.
- Ding, S. W., Zhang, S. Y., Liu, S. J., Ding, Y., Kang, Q. Y., & Liu, Y. C. (2002). Synthesis and photocatalyzing property of nano-ZnO. *Chinese Journal of Inorganic Chemistry*, 1015-1019.
- Jiang, C. J., Duan, Z. W., Zhang, Z. Z., & Wang, C. (2007). Effect of surfactants on dispersing properties in alcohol solvent for silver nanopowders. *Rare Metal Materials and Engineering*, 724-727.
- Hee, Y. K., Jong, H. K., Soon, C. K., & Sung, H. J. (2007). A study on multifunctional wool textiles treated with

nano-sized silver. *J Mater Sci*, 42, 8020-8024.

Herrera, J. E., Kwak, J. H., Hu, J. Z., Wang, Y., & Peden, C. H. F. (2006). Synthesis of nanodispersed oxides of vanadium, titanium, molybdenum, and tungsten on mesoporous silica using atomic layer deposition. *Topics in Catalysis*. 245-255.

Iijima, S., Nomura, A., Mizukami, F., Shin, S., & Mizutani, F. (1999). Superparamagnetic behavior of iron oxides supported on porous silica gels. *Journal of Radioanalytical and Nuclear Chemistry*. 297-302.

General chemical staff room of Tianjin University. (1983). Inorganic chemistry. *Higher Education Press*.

Kruis, F. E., & Fissan, H. (2001). Nanoparticle charging in a twin Hewitt charger. *Journal of Nanoparticle Research*, 3, 39-50.

Kang, S. F., Liu, A. M., & Zhang, M. (2005). Aggregation of ultra-fines in chemical precipitation. *Chemical Industry and Engineering*. 346-349.

Liao, L. L., Liu, J. P., & Xu, D. Y. (2003). Studies on synthesis and effects on smoke suppression of nano-oxides. *Chinese Journal of Colloid & polymer*. 22-24.

Li, Y. H., Lin, H. M., Yu, Z. C., & Chen, W. G. (2006). Study on the application of nano-scaled antistatic finishing agent to the PET ornamental Fabric. *Journal of Zhejiang Sci-Tech University*. 264-267.

Luo, Y. X., Wang, X., Lu, L. D., Yang, X. J., & Liu, X. H. (2003). Progress of preparation and applications of nanocrystalline CuO. *Shanghai Chemical Industry*. 24-28.

Liang, X. Y., Ma, Z., Bai, Z. C., & Qin, Y. N. (2002). Properties and sonochemical preparation of nanostructured LaNiO<sub>3</sub>\*. *Acta Phys. -Chim. Sin.* 18(6),567-571.

Luo, J. H., Zhang, Z. Z., & Zhang, S. M. (2007). Study on dispersing properties of nanometer iron powder. *Foundry Technology*, 184-185.

Muccillo, E. N. S., Tadokoro, S. K., & Muccillo, R. (2004). Physical characteristics and sintering behavior of MgO-doped ZrO<sub>2</sub> nanoparticles. *Journal of Nanoparticle Research*, 6, 301-305.

Ni, X. Y., Shen, J., & Zhang, Z. H. (2006). The physicochemical properties and application of nano-materials. Beijing: *Chemical Industry Press*.

Qiu, S. Y., Yao, R. H., & Zong, M. H. (1999). Application of ultrasound to biotechnology. *Progress in Biotechnology*. 45-48.

Takahashi, N. (2007). Simple and rapid synthesis of MgO with nano-cube shape by means of a domestic microwave oven. *Solid State Sciences*. 9, 722-724.

Tang, X. L., Ren, L., Sun, L. N., Tian, W. G., Cao, M. H., & Hu, C. W. (2006). A solvothermal route to Cu<sub>2</sub>O nanocubes and Cu nanoparticles. *Chem. Res. Chinese U.* 22(5), 547-551.

Wang, Z. X., Zheng, D. M., Li, J. M., Fan, M., Liu, M., & Zhuang, Y. K. (2006). Study on producing of nanometer ZnO by direct precipitation method. *Inorganic Chemicals Industry*. 40-42.

Zhang, Y., Lin, S. Y., & Fang, Y. (2002). New developments in sonochemistry-preparation of nanomaterials by ultrasound. *Physics*. 80-83.

Table 1. Effect of nanometer antistatic finishing agent on various fabrics hunter whiteness and charge density

Specimen	Cotton	fabric	polyester	fabric
	Hunter whiteness	Charge density ( $\times 10^7$ )/(c·m <sup>-2</sup> )	Hunter whiteness	Charge density ( $\times 10^7$ )/(c·m <sup>-2</sup> )
0	93.71	36	84.56	58
1	89.63	5.7	85.35	0.95
2	90.13	6.9	86.48	7.1
3	90.40	8.4	87.45	14

0— original piece

1— the fabric was finished by 0.5% nano-ZnO, surfactant and binder

2— the fabric was finished by 1.5% nano-ZnO, surfactant and binder

3— the fabric was finished by 3% nano-ZnO, surfactant and binder

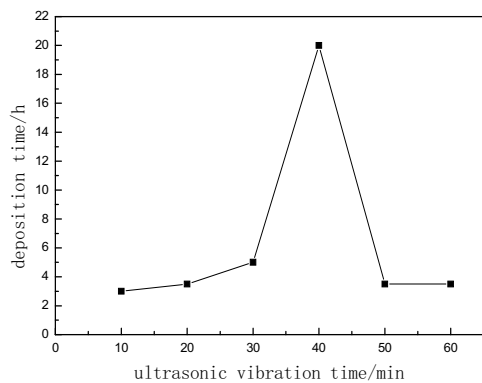


Figure 1. Effect of ultrasonic vibration time on product deposition time

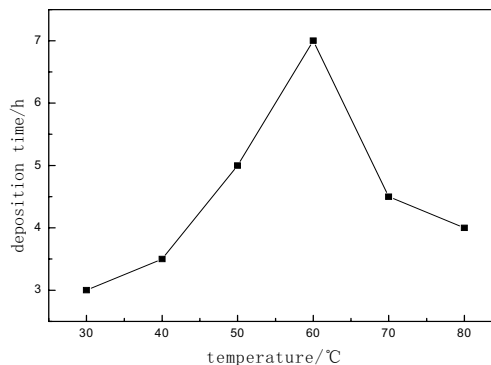


Figure 2. Effect of reaction temperature on product deposition time

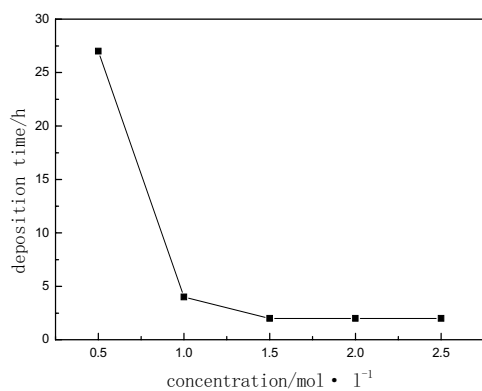


Figure 3. Effect of concentration of the zinc chloride on product deposition time

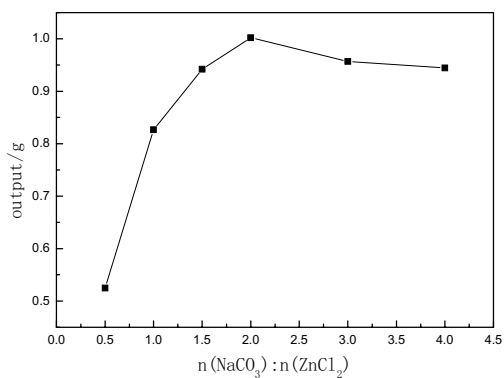


Figure 4. Effect of ratio of the reactant on precursor output

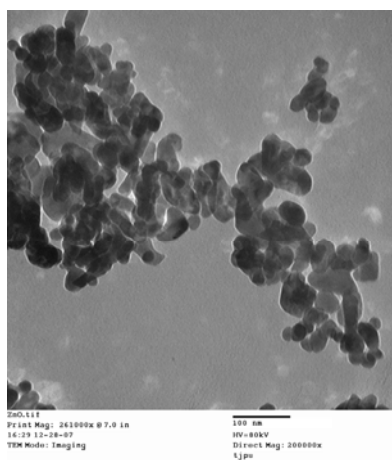


Figure 5. TEM photograph of nano-ZnO



## Lead Removal from Aqueous Solution Using Silica Ceramic: Adsorption Kinetics and Equilibrium Studies

Md. Salim (Corresponding author)

Environmental Engineering, Faculty of Agriculture

Kochi University

B200 Monobe, Nankoku, Kochi 783-8502, Japan

Bioresource Production Science

The United Graduate School of Agricultural Sciences

Ehime University, 3-5-7 Tarumi, Matsuyama, Ehime 790-8566, Japan

Tel: 81-88-864-5175 E-mail: mdsalim2@gmail.com

Yukihiro Munekage

Environmental Engineering, Faculty of Agriculture, Kochi University

B200 Monobe, Nankoku, Kochi 783-8502, Japan

Tel: 81-88-864-5175 E-mail: munekage@kochi-u.ac.jp

### Abstract

Kinetics adsorption of lead from aqueous solution using silica ceramic has been investigated in batch methods. The effect of solution pH, initial metal ion concentration, temperature and adsorbent mass on metal ion removal has been studied. The process of lead adsorption follows pseudo second-order rate expression and obeys the Langmuir's model with high correlation coefficient ( $R^2 > 0.99$ ) and better than other equations. The maximum removal achieves 2.7 mg/g. The result indicates that under the optimum conditions, the maximum adsorption value for Pb(II) comply the silica ceramic is a potential adsorbent for Pb(II).

**Keywords:** Adsorption, Kinetic, Removal, Lead, Silica ceramic

### 1. Introduction

Industrial wastewaters are considered as the most important source of heavy metal pollutions among various heavy metals. Lead is a significant element metal that contaminated the water both natural and anthropogenic activities. Lead (Pb) found in natural deposits and process include mineral breakdown, sedimentation of from dust storms, volcanic eruptions, forest fires etc. Anthropogenic activities of lead contamination including and smelting operations, commonly used in household plumbing materials and water service lines, metal plating, battery recycling, combustion of leaded gasoline, atomic energy installation, leatherworking, photography, salvages yards, urban and industrial waste, continuous of fertilizer, pesticides and use of Pb bullets (Sing et al., 2006; Heil et al., 1999) automobile, and oil industries produce more heavy metal ions that other industries (Reed and Arunachalam, 1994). It directly or indirectly causes damage or dysfunction to liver, reproductive system, brain and central nervous system, kidney and reduction in hemoglobin formation, mental retardation, infertility and abnormalities in pregnant women etc.

A variety of methods have been proposed for the treatment of wastewaters containing lead metals such as chemical precipitation (Matlock et al., 2001), electrochemical reduction, ion exchange (Inglezakis et al., 2007), membrane separation, flotation, biosorption (Nourbakhsh et al., 2002; Gupta and Ali, 2004) and adsorption (Mohan and Chander, 2006; Gupta and Sharma, 2002). Adsorption is being popular to be an economically viable alternative technique for removing lead from wastewater and water supplies. In recent years, there is an increase interest in using non-chemical and low-cost adsorbent (Salim et. al., 2007) to remove heavy metals from wastewater. The objective of the present study is to determine the functionality and sorption kinetics of silica ceramic as a low-cost adsorbent material to remove Pb(II) from aqueous phase.

## 2. Material and Method

### 2.1 Adsorbent

Study used silica ceramic (powder particle size, <0.05mm) obtained from EKOAIRANDO Co. Ltd. Kochi, Japan having major chemical ingredients SiO<sub>2</sub>, Na<sub>2</sub>O, Al<sub>2</sub>O<sub>3</sub>, CaO and K<sub>2</sub>O.

### 2.2 Adsorbate

The synthetic Stock solution of Pb (II) (1000 mg/L) was prepared using Pb(NO<sub>3</sub>)<sub>2</sub> (Kanto Chemical Inc. Ltd., Japan) by dissolving in acidified ultra distilled water. The stock solution was diluted with distilled water to obtained desired concentration ranging from 5 to 70 mg/L. Solutions of the 0.1 M HCl and 0.1 M NaOH were used for pH adjustment.

### 2.3 Analytical method

The surface area of the silica ceramic was measured by N<sub>2</sub> adsorption using single point Brunauer, Element and Teller (BET) (Micrometric ASAP 2020, USA) procedure. The surface structure was examined by scanning electron microscopy (SEM-EDS, JEOL-JSM-6500F, Japan). Lead analysis was conducted by Atomic Absorption Spectrometer (AAAnalyst200, Perkin-Elmer, Singapore) at a wave length of 283.31 nm. All samples were analyzed after filtering within 24 hours of collection.

### 2.4 Batch kinetics experiments

Batch experiments were conducted for optimum dose, equilibrium time, effect of concentrations, and effects of temperature. Silica ceramic was added as per dose requirements to round bottom glass bottles of 100 ml capacity with 50 ml of Pb solutions of desire concentration (10-50 mg/L) and (5.5 -6.5) pH range. The flasks were capped and placed on a mechanical shaker at a speed of 140 rpm at 30 °C, and samples were taken at predetermined intervals. All samples were filtered by a 0.45 μm membrane filter and analyzed for Pb. The amount of adsorbed Pb was calculated using Eq. (1) by the difference of initial and residuals amounts of Pb in solution divided by the mass of adsorbent. The removal efficiency,  $R_e$ , (determined as the Pb removal percentage relative to initial concentration) using Eq. (2) of the system, was calculated as:

$$q_e = \frac{(C_0 - C_e)}{M} \times V \quad (1)$$

$$R_e = \frac{(C_0 - C_e)}{C_0} \times 100 \quad (2)$$

Where,  $q_e$  (mg/g) is the amount of the Pb adsorbed per unit mass of silica ceramic.  $C_0$  and  $C_e$  are the initial and equilibrium (or at any time) ion concentration (mg/L), respectively,  $V$  is the volume in liter of solution and  $M$  is the mass (g) of the silica ceramic.

### 2.5 Batch isotherms studies

After determining the optimum pH, temp and equilibrium time, isotherm studies were conducted by varying the mass of silica ceramic. Representative masses (0.3, 0.4, 0.5.....0.9 and 1.0 g) of silica ceramic were add into 25 ml of solution containing 10 mg/L of Pb ion for 3h, which is equilibrium time for the silica ceramic ion. The initial pH of the metal solutions was adjusted to an optimum value of 3.5 with 0.1 M NaOH or HCl.

## 3. Results and Discussion

### 3.1 Adsorbent characterization

The details physio-chemical properties are given in Table 1. The major components of chemical compositions of the silica ceramic are silicon, aluminum, sodium, calcium and potassium compounds. Both elemental and mineralogical characterization of silica ceramic verified its compositions. Scanning electron microscopy was performed on silica ceramic at different magnification to determine surface structure. The working tension was 15 KV. Scanning electron micrographs for intra structure of silica ceramic is shown in Figure 1 (A) and (B). The mineralogical analysis is shown in Figure 2. The figures indicate that silica ceramic has an extensive surface area, and it can be used as a potential adsorbent.

### 3.2 Effect of pH

pH of solution is one of the most important parameters for adsorption of heavy metals from contaminated aqueous solution. Adsorption of Pb was studied at various pH and results are given away in Figure 3. The initial pH of solution varied from 2.45 to 11.5. In this experiments adsorbate concentration was 25 mg/L, ceramic mass was 0.3 g to 1.0 g and contact time was 18 h. From this figure it is clear that lead adsorption efficiency is high at bellow pH 4.5. This result showed similar trend to lead removal by zeolite and sepiolite (Turan et al., 2005); and by natural phosphate (Mouflih et. al., 2006).

### 3.3 kinetics study

#### 3.3.1 Effect of concentration

To evaluate the sorption characteristics of silica ceramic for lead ions, the change of sorption capacity with time for different initial solution concentrations has been investigated. A series of experiments were undertaken by varying the initial Pb concentration in the range 10 – 50 mg/L on removal kinetics of Pb from the solution. Figure 4 showed that adsorption of Pb(II) by silica ceramic increases as the initial Pb (III) concentration increased. The contact time required to reach the equilibrium of Pb(II) solution within 180 min. However, the experimental data were measured at 600 min to confirm the complete equilibrium was reached.

#### 3.3.2 Adsorption Kinetics

The adsorption kinetic data of lead are analyzed using three kinetics models were applied mainly, pseudo-first order, pseudo-second order and, intra-particle diffusion model rate equations.

Lagergren suggests the pseudo-first order kinetics rate equation (Lagergren, 1898), which is expressed as follows:

$$\frac{dq_t}{dt} = k_1(q_e - q_t) \quad (3)$$

Where  $k_1$  is the pseudo-first order rate constant,  $q_e$  represents adsorption capacity. The integrating rate law by applying the initial condition of  $t = 0$  to  $t$  and  $q_t = 0$  to  $q_e$ , Eq.(3) becomes:

$$\log(q_e - q_t) = \log q_e - \left( \frac{k_1}{2.303} \right) t \quad (4)$$

Where,  $q_e$  and  $q_t$  both (mg/g) are the amount of Pb(II) adsorbed per unit of mass of silica ceramic at equilibrium and time  $t$ , respectively, and  $K_1$  the rate constant (1/min). The value for the  $K_1$  was calculated from the slope of the linear plot of  $\log(q_e - q_t)$  versus  $t$  [Figure 5. (a)]. The  $K_1$  values and correlation coefficients  $R^2$  are given in Table 2.

The pseudo-second order reaction rate equation used by Ho et al (Ho et al., 1996) to study the kinetics of adsorption of heavy metals on peat. This model was also applied to assess the kinetics of adsorption of Pb(II) on silica ceramic. The equation is as follows:

$$\frac{dq_t}{dt} = k_2(q_e^2 - q_t)^2 \quad (5)$$

where  $k_2$  is the rate constant of pseudo second-order adsorption. The integrating rate law Eq.(5), after applying the initial conditions (McKay and Ho, 1999), and rearranging it gives as linearized form of pseudo second-order rate kinetics expressed as follows:

$$\frac{t}{q_t} = \frac{1}{k_2 q_e^2} + \frac{1}{q_e} t \quad (6)$$

In addition, initial rate of adsorption is  $h$  is:

$$h = k_2 q_e^2 \quad (7)$$

Where,  $q_e$  and  $q_t$  both (mg/g) are the amount of Pb(II) adsorbed per unit of mass of silica ceramic at equilibrium and time  $t$ , respectively, and  $K_2$  is the rate constant of pseudo second order adsorption (g/mg min). The kinetics plots between  $t/q_t$  versus  $t$  were plotted for the different initial concentrations [Figure 5. (b)]. Slope and intercept values were solved to give the value of pseudo-second order rate constant (Table 2).

Figure 5 (b) and Table 2 shows that highly significant regression line ( $R^2 > 0.997$ ) and the data were well fitted only to the pseudo second-order rate equation. The straight line was obtained indicating that the process follow a pseudo second order kinetics for various concentration of Pb(II). While the initial Pb(II) concentration increases from 10 mg/L to 50 mg/L, the adsorption capacity,  $q_{exp}$ , increase from 0.9594 to 2.7048 mg/g. This indicates that the initial Pb(II) concentration plays a key role in determining the adsorption capacity of Pb(II) on silica ceramic. It is also observed in Table 2 that when initial Pb(II) concentration increase from 10 mg/L to 50 mg/L, the rate constant,  $k_2$  decrease from  $277.397 \times 10^{-3}$  to  $19.223 \times 10^{-3}$  g/mg min and values of initial sorption rate  $h$  are also decrease from  $258.853 \times 10^{-3}$  to  $151.849 \times 10^{-3}$  mg/g min.

Lagergren pseudo first order and pseudo second-order rate equations cannot identify the diffusion mechanisms during the sorption process and uptake varies almost proportionately with the half-power of time,  $t^{1/2}$ , rather than  $t$ . A nearly linear variation in the quantity sorbed with  $t^{1/2}$  is predicted for a large initial fraction of reactions controlled by rates of

intra-particle diffusion. Therefore, the experimental kinetic data were tested against intra-particle diffusion model. The initial rate of intra-particle diffusion can be determined by the most-widely applied intra-particle diffusion equation for sorption system is given by Weber and Morris (Weber and Morris, 1963):

$$q_t = k_i t^{1/2} + C \quad (8)$$

Where,  $q$  is the amount of Pb (II) adsorbed (mg/g) at time  $t$ ,  $k_i$  the intra-particle diffusion constant (mg/g min<sup>1/2</sup>), and  $C$  is the intercept.

The values of  $k_i$  indicate an enhancement in the rate of adsorption. It is observed in Table 2 that when initial Pb(II) concentration increase from 10 mg/L to 50 mg/L, the intra-particle diffusion constant,  $C$  and  $k_i$  increase from 0.5316 to 0.9613 and from  $27.1 \times 10^{-3}$  to  $101.6 \times 10^{-3}$  g/mg min respectively.

### 3.3.3 Effect of temperature

Effect of temperature on removal of Pb (II) were performed at three different temperatures, i.e., 20, 30, and 40°C. The results are shown in Figure 6, which indicates that the Pb (II) uptake increases from 2.42 to 2.86 when temperature of the solution increases from 20 to 30°C. After that, sorption uptake increase slowly from 2.86 to 2.90 mg/g when temperature of the solution increases 30 to 40°C. The adsorption of lead on silica ceramic is highest at 40°C. That means the sorption of Pb (II) is in favor of temperature indicates that the mobility of the lead molecule increases with an increase in the temperature. Therefore, it is revealed that the process is endothermic.

### 3.3.4 Effect of adsorbent doses

The effect of adsorbent dose was studied at a fixed initial concentration of 20 mg/L by silica ceramic mass varied from 5 to 40 g/L. The general trend indicates that 5 to 25 g/L of sorbent dose uptake large amount of Pb(II), rapidly and 30 to 40 g/L dose uptake little amount but slowly (Figure 7). At 10 g/L, removal efficiencies of 97.9% were observed and thereafter efficiency was 100% occurred slowly. The reason of removal efficiency increased due to the increase of adsorbent dose that means increase of the total available surface area of the adsorbent particles.

### 3.4 Adsorption Isotherm

The equilibrium adsorption isotherm is of importance in the design of adsorption systems (Wang et al., 2005). Several isotherm equations are available and the Langmuir isotherm is selected in this study. The Langmuir adsorption isotherms assumes that adsorption takes place at specific homogeneous sites within the adsorbent and has found successful application to many sorption process of monolayer adsorption. The Langmuir adsorption isotherm can be written as:

$$q_e = \frac{q_m b C_e}{1 + b C_e} \quad (9)$$

The Langmuir parameters were obtained by fitting the experimental data to the linearized equation derived from Eq. (9):

$$\frac{C_e}{q_e} = \frac{1}{b q_m} + \frac{C_e}{q_m} \quad (10)$$

$$\frac{1}{q_e} = \frac{1}{b q_m C_e} + \frac{1}{q_m} \quad (11)$$

Where,  $q_e$  is the adsorbent amount (mg/g) of the Pb (II),  $C_e$  is the equilibrium concentration of the Pb(II) in solution (mg/L),  $q_m$  is the monolayer adsorption capacity (mg/g) and  $b$  is the constant related to the free energy of adsorption (L/mg).

Based on Eq. (10) and Eq. (11) the isotherms were fitted to the adsorption data obtained. The Langmuir adsorption exponents for Eq. (10) and Eq. (11), the  $q_m$  and  $b$  are determined from the linear plots of  $C_e/q_e$  versus  $C_e$  (Figure not shown) and  $1/q_e$  versus  $1/C_e$  (Figure not shown) and calculated correlation coefficients for these isotherms, are shown in Table 3. The values of the Langmuir constant were calculated from the slopes and intercepts of the plots. The magnitude of Langmuir constant  $b$  is small (1.8561 L/mg) and the adsorption capacity  $q_m$  was determined as 2.7586 mg/g. In order to predict the adsorption efficiency of the adsorption process, the dimensionless equilibrium parameter  $R_L$  was determined by using the following equation (Magdy and Daifullah, 1988):

$$R_L = \frac{1}{(1 + b C_0)} \quad (12)$$

Where,  $C_0$  is the initial concentration and  $b$  is the Langmuir isotherm constant. The parameter  $R_L$  indicates the shape of isotherm. The process is irreversible if  $R_L = 0$ , favorable if  $R_L < 1$ , linear if  $R_L = 1$  and unfavorable if  $R_L > 1$ . The Figure 9 shows that the  $R_L$  values at different initial Pb (II) concentration indicating a highly favorable adsorption. As shown in Table 3 and Figure 8, the Langmuir equation represents adsorption process is very well and the correlation coefficient,  $R^2$  value is indicating a very good mathematical fit.

#### 4. Conclusions

The results of present investigations revealed that silica ceramic is potential adsorbent to removal the Pb(II) from aqueous phase. The pseudo-second order kinetic models fits very well with the adsorption behavior of Pb. The sorption suggested that the adsorption is high at low pH range. The amount of lead uptake at equilibrium increased with increasing solution concentrations, temperatures and decreasing pH, sorbent mass. The findings of the study show that silica ceramic has excellent potential for use in the removal of Pb from waste water, however further work is increase the adsorption capacity of silica ceramic. Currently study is being progress involving the activation of silica ceramic by acid and heat treatment.

#### Acknowledgements

The authors wish to express their thanks to Asst. Prof. Le Thanh Son, Hanoi University of Science, Vietnam National University, Vietnam and Center for Advanced Marine Core Research, Kochi, Japan for chemical and mineralogical analysis of silica ceramic.

#### References

- Gupta, V. K., & Ali, I. (2004). Removal of lead and chromium from wastewater using bagasse fly ash- a sugar industry waste. *J Colloid Interf Sci*, 271, 321–328.
- Gupta, V. K., & Sharma, S. (2002). Removal of cadmium and zinc from aqueous solution using red mud. *Environ Sci Technol*, 36(16), 3612–3617.
- Heil, D. M., Samani, Z., Hanson, A. T., et al. (1999). Remediation of lead contaminated soils by EDTA. I. Batch and column studies. *Water Air Soil Pollut*, 13, 77-95.
- Ho, Y. S., Wase, D. A. J., & Forster, C. F. (1996). Kinetic studies of competitive heavy metal adsorption by sphagnum moss peat. *Environ Technol*, 17(1), 71-77.
- Inglezakis, V. J., Stylianou, M. A., Gkantzou, D., et al. (2007). Removal of Pb(II) from aqueous solutions by using clinoptilolite and bentonite as adsorbents. *Desalination*, 210, 248–256.
- Lagergren, S. (1898). Zur theorie der sogenannten adsorption geloster stoffe. *Kungliga Svenska Vetenskapsakademiens. Handl*, 24(4), 1-39.
- Magdy, Y. H., & Daifullah, A. A. M. (1988). Adsorption of a basic dye from aqueous solutions onto sugar-industry-mud in two modes of operations. *Waste Manage*, 18 (4), 219-226.
- Matlock, M. M., Howerton, B. S., & Atwood, D. A. (2001). Irreversible precipitation of mercury and lead. *J Hazard Mater*, 84, 72–83.
- Mckay, G., & Ho, Y. S. (1999). Pseudo-second-order model for sorption processes. *Process Biochem.*, 34, 451-465.
- Mohan, D., & Chander, S. (2006). Removal and recovery of metal ions from acid mine drainage using lignite-a low cost sorbent. *J Hazard Mater*, B137, 1545–1553.
- Mouflih, M., Akil, A., Jahroud, N., et al. (2006). Removal of lead from aqueous solution by natural phosphate. *Hydrometallurgy*, 81, 219-225.
- Nourbakhsh, M. N., Kiliçarslan, S., İlhan, S., et al. (2002). Biosorption of  $Cr^{+6}$ ,  $Pb^{+2}$  and  $Cu^{+2}$  ions in industrial waste water on *Bacillus* sp. *Chem Eng J*, 85, 351–355.
- Reed, B. E., & Arunachalam, S. (1994). Use of granular activated carbon columns for lead removal. *J Environ Eng, ASCE*, 120, 416- 436.
- Salim, M., Munekage, Y., & Naing, K. M. (2007). Arsenic removal from contaminated water using silica ceramic: A batch adsorption study. *J app. Sci.* 7(16), 2314-2320.
- Sing, S. P., Ma, L. Q., & Hendry, M. J. (2006). Characterization of aqueous lead removal by phosphatic clay: Equilibrium and Kinetic studies. *J Hazard Mater*, B136, 654-662.
- Turan, M., Mart, U., Yuksel, B., et al. (2005). Lead removal in fixed-bed columns by zeolite and sepiolite. *Chemosphere*, 60(10), 1487-1492.

Wang, S., Boyjoo, Y., & Choueib, A. (2005). A Comparative study of dye removal using fly ash treated by different methods. *Chemosphere*, 60(10), 1401-1407.

Weber, W. J., & Morris, J. C. (1963). Kinetics of adsorption on carbon from solution. *J Sanit Eng Div ASCE*, 89 (SA2), 31-59.

Table 1. Physical and chemical properties of absorbent used in the experiments

Chemical properties	wt. %	Physical properties	Value
SiO <sub>2</sub> ,	80.81	Surface area (BET), (m <sup>2</sup> /g)	340.38
CaO	6.93	Median Pore diameter (A)	44.46
Al <sub>2</sub> O <sub>3</sub>	3.80	Pore Volume (cm <sup>3</sup> /g)	0.3274
Na <sub>2</sub> O	2.57	pH (1% Solution)	8.5
K <sub>2</sub> O	1.84	Particle size, mm	< 0.05

Table 2. Lagergren constants, Pseudo second-order rate constants and Intra-particle diffusion constants for lead adsorption on silica ceramic at different initial concentration

Pb (mg/L)	$q_{exp}$	Lagergren constants		Pseudo second-order rate constants				Intra-particle diffusion	
		$K_1 \times 10^{-3}$	R <sup>2</sup>	$q_e$	$K_2 \times 10^{-3}$	$h \times 10^{-3}$	R <sup>2</sup>	C	$K_i \times 10^{-3}$
10	0.9594	34.775	0.7244	0.966	277.397	258.853	1	0.5316	27.1
20	1.8718	33.624	0.9455	1.912	44.380	162.248	0.9999	0.8416	60.4
30	2.5088	22.569	0.9176	2.6596	11.064	78.260	0.999	0.6858	97.5
40	2.6264	31.781	0.9421	2.7563	14.957	113.636	0.9981	0.8395	100.9
50	2.7048	32.703	0.8939	2.8106	19.223	151.849	0.9977	0.9613	101.6

Table 3. Langmuir isotherm constant for adsorption of Pb(II) by silica ceramic

Langmuir isotherm parameters	$C_e/q_e$	$1/q_e$
$q_m$ (mg/g)	2.7586	2.7586
b (L/mg)	1.8561	1.8561
R <sup>2</sup>	0.9999	1

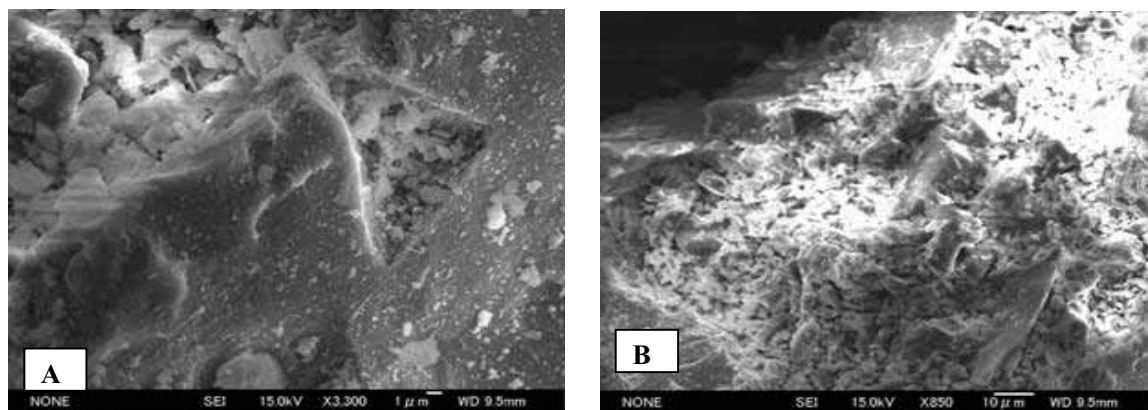


Figure 1. SEM of silica ceramic: (A)  $\times 3300$ , 1 $\mu$ m; (B)  $\times 850$ , 10 $\mu$ m

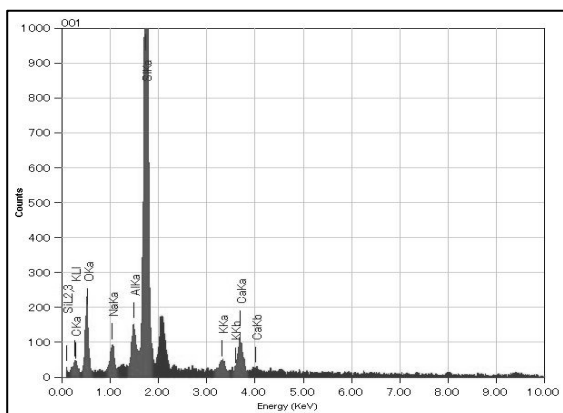


Figure 2. Elements spectrum of a selected silica ceramic obtained by SEM-EDS analysis

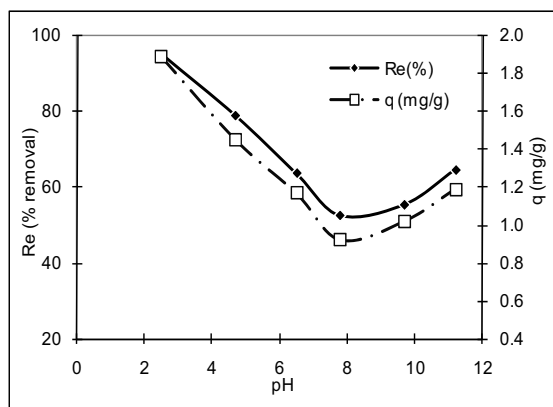


Figure 3. Effect of pH on adsorption of Pb(II) by silica ceramic at temperature 25°C

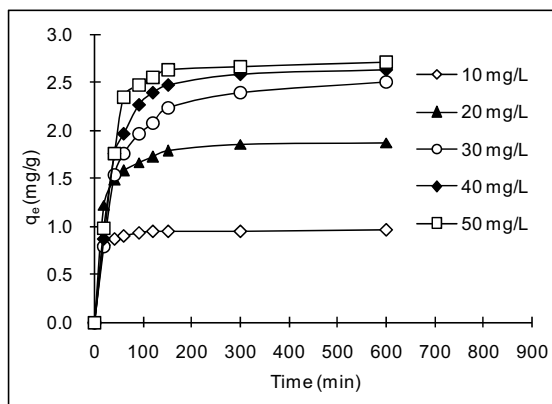


Figure 4. Effect of initial concentration on Pb(II) adsorption by silica ceramic at pH 5.5

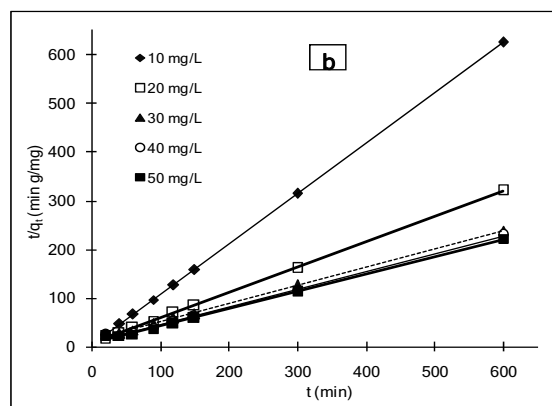
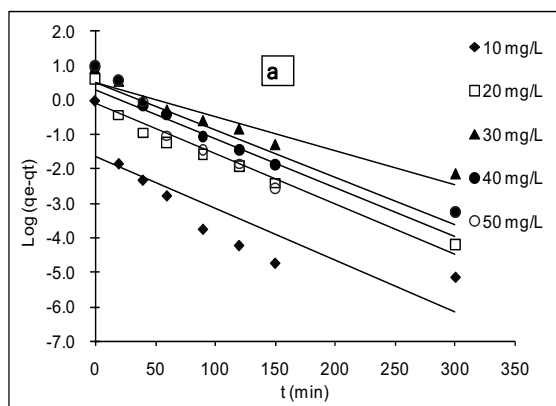


Figure 5. Kinetics analysis of pb(II) adsorption by linear plots of (a) pseudo first-order, (b) pseudo second-order rate equations

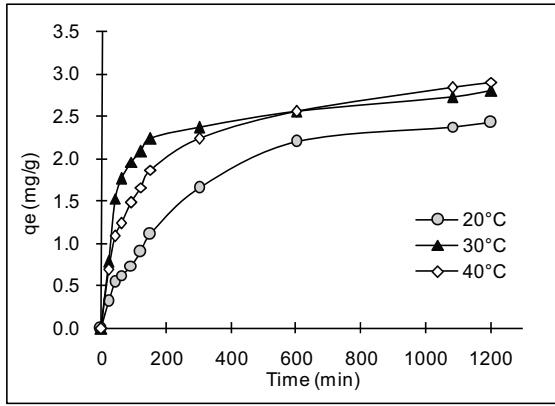


Figure 6. Effect of temperature on Pb(II) adsorption

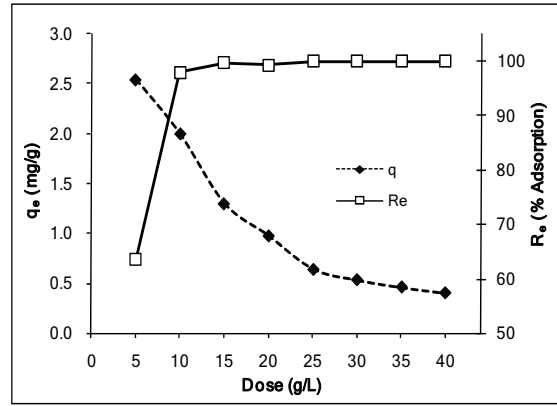


Figure 7. Effect of adsorbent dose on Pb(II) adsorption.

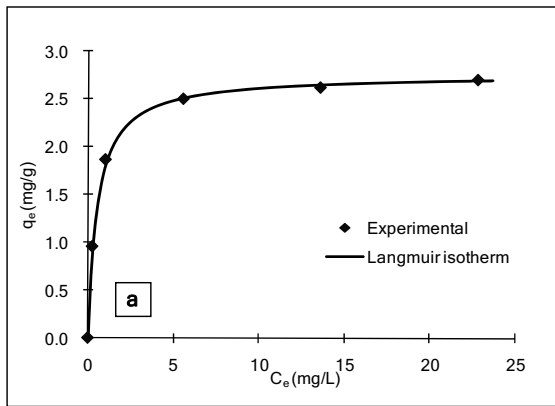


Figure 8. Langmuir adsorption isotherm of Pb(II) on silica ceramic

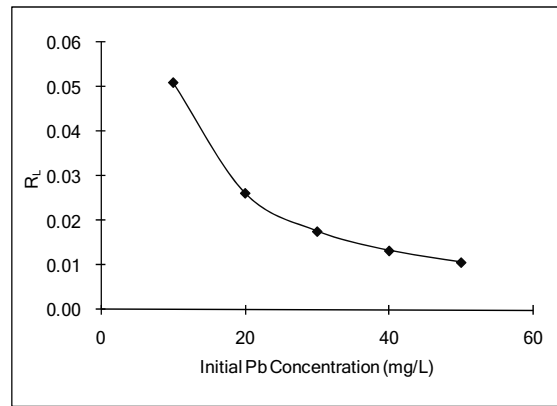


Figure 9. Separation factor for Pb(II) adsorption using silica ceramic



## Synthesis, Characterization and Application of O, O-diethyl Acrylamide Phosphate

Aibing Jiang

Tianjin Municipal Key Laboratory of Fiber Modification and Functional Fiber

Tianjin Polytechnic University, Tianjin 300160, China

School of Textile, Tianjin Polytechnic University, Tianjin 300160, China

E-mail: jiangaibing58@sina.com

Bowen Cheng, Yuanlin Ren & Zhenhuan Li

Tianjin Municipal Key Laboratory of Fiber Modification and Functional Fiber

Tianjin Polytechnic University, Tianjin 300160, China

### Abstract

Taking acrylamide and diethyl chlorophosphate as the reactants, we synthesized a sort of new intumescent flame retardant (IFR) containing phosphorus and nitrogen, O,O-diethyl acrylamide phosphonate. The structure of the title compound could be characterized by FTIR, <sup>1</sup>H NMR and MS. The results show that the structure of the synthesized compound is consistent with the expected structure. The yield of the title compound is 75% under the conditions that the molar ratio between acid-binding agents of triethylamine and acrylamide is 1:1 and the mass fraction of the catalys CuCl is 1% of acrylamide. The optimal reaction temperature range is from 20°C to 30°C. The limiting oxygen index (LOI) value can reach 26.7% when the mass fraction of the title compound in the copolymer is 20%. The scanning electron microscopy (SEM) photos of the fired residue of the flame retarded copolymer show that the surface of the fired residue presents foam-like structure, and the cross section presents cellular structure, which indicate that the title compound is the intumescent flame retardant.

**Keywords:** O, O-diethyl acrylamide phosphate, Intumescent flame retardant, LOI, SEM

### 1. Introduction

In recent years, the intumescent flame retardant is one of R&D hotspots in the domain of flame retardant. It is the composite flame retardant taking nitrogen, phosphorus and carbon as bases and it doesn't contain halogen and adopt antimony pentoxide as synergy agents, but it possesses the synergy function itself (Chigwada, 2003, P.551-557, Duquesne, 2002, P.333-344, Zhang, 2002, P.5463-5472, Horacek, 1996, P.205-215, Wyman, 2006, P.764-771, He, 2008, P.104-108). When this sort of flame retardant is used in the fame retardant materials which are heated, the surface of the materials will form loose carbon layer with closed structure which can retard burning, isolate oxygen and eliminate smoke, so this type flame retardant possesses excellent fame retardant performances (Schartel, 2006, P.8495-8508, Lewin, 2002, P.1091-1102, Yan, 2007, P.6-7, Ju, 2008, P.5-7, Ren, 2007, P.1314-1317, Zhang, 2007, P.831-834). So we synthesize a sort of new intumescent flame retardant containing phosphorus and nitrogen, and copolymerize it with acrylonitrile to form the flame retardant acrylonitrile copolymer. We measure the LOI value of the flame retardant copolymer by the LOI meter and analyze the flame retardant mechanism of the title compound through the SEM test of the carbon residue of burned flame retardant copolymer.

### 2. Experiment

#### 2.1 Reagents and Apparatus

Reagents used in the experiment include acrylamide (analytical reagent, being ready for recrystallizing), acetone (analytical reagent, being ready for distillation), anhydrous (analytical reagent, being ready for distillation), acrylonitrile (analytical reagent, being ready for distillation), phosphorus oxychloride (analytical reagent, it can be used directly), triethylamine (analytical reagent, it can be used directly), and cuprous chloride (analytical reagent, it can be used directly).

Apparatuses used in the experiment include Bruker Vector 22 (Germany) Fourier Infrared Spectrum Meter, KBr pressed disk, Bruker AC-P2000 NMR Equipment (US), solvent  $\text{CDCl}_3$ , internal standard TMS, VG-ZAB-HS mass spectrograph (Germany), Quanta 200 environmental SEM (Zcech), and Stanton Redcroft FTA oxygen analyzer (Britain).

### 2.2 Synthesis of diethyl phosphorus oxychloride

Put 91.54ml phosphorus oxychloride into the flask with four standard necks of 500ml, and put 116.45ml anhydrous ethanol into the press-constant dropping funnel, and slowly drop the anhydrous ethanol into the flask in 2 hours, and control the reaction temperature in  $0^\circ\text{C}\sim 5^\circ\text{C}$  and stop the reaction after 4 hours, and react in the room temperature for 10 hours. Decompress and distill the reaction production ( $73^\circ\text{C}$ , 1.15kPa), and the liquid obtained is O,O-diethyl acrylamide phosphonate (Sundarrajan, 2001, P.41-45 & Devi, 2002, P.2461-2467), and the relative density  $\rho$  is  $1.192\text{ g/cm}^3$ .

### 2.3 Synthesis of O, O-diethyl acrylamide phosphate

Put 120ml acetone, 34.72g acrylamide, 69ml triethylamine and 0.35g CuCl into the flask with four standard necks of 250ml, and mix round by the magnetic force beater evenly, and put 70.71ml diethyl phosphorus oxychloride into the press-constant dropping funnel, and slowly drop the anhydrous ethanol into the flask in 1 hour, and control the reaction temperature in  $20^\circ\text{C}\sim 30^\circ\text{C}$  and stop the reaction after 6 hours, and react in the  $60^\circ\text{C}$  for 18 hours. Filtrate, decompress and distill the reaction production, and the oily liquid obtained is the title compound, and the relative density  $\rho$  is  $1.113\text{ g/cm}^3$ .

### 2.4 Synthesis of flame retardant polyacrylonitrile copolymer

Add nitrogen gas into the flask with four standard necks of 500ml to eliminate the oxygen in the flask, and put 10.35g O,O-diethyl acrylamide phosphonate into the flask, and put 51ml acrylonitrile into the flask with four standard necks, and add 141ml DMSO acting as the solvent, and mix round evenly, and when the temperature increases to  $40^\circ\text{C}$ , add 0.36g azobisisbutyronitrile (AIBN) and control the temperature in  $65^\circ\text{C}$  to react for 8 hours and produce white viscous fluids, and wash the fluids by anhydrous ethanol, and wash the fluids by distilled water three times, and desiccate the fluids, we can obtain the flame retardant polyacrylonitrile copolymer. The synthesis routes include following shemes.

## 3. Result and discussions

### 3.1 Production structure analysis

The infrared spectrum of the title compound is seen in Figure 1. In the figure, the position of 3384 is the flex oscillation absorption peak of N-H bond, and the position of 1711 is the flex oscillation absorption peak of C=O bond, and the position of 1667 is the flex oscillation absorption peak of C=C bond, and the position of 1476 is the symmetric bending oscillation absorption peak of  $-\text{CH}_2-$  bond, and the position of 1397 is the flex oscillation absorption peak of C-O bond, and the position of 1232 is the oscillation absorption peak of P=O bond, and the position of 1036 is the flex oscillation absorption peak of P-O-C bond, and the position of 2988 is the asymmetric flex oscillation peak of  $-\text{CH}_3-$  bond.

The  $^1\text{H}$  NMR spectrum and MS spectrum of the title compound are respectively seen in Figure 2 and Figure 3. There are five groups of peak in the  $^1\text{H}$  NMR spectrum, and the multiple peak between  $\delta=3.9915\sim 4.0868$  is the chemical displacement of H ①, and the multiple peak between  $\delta=5.7238\sim 5.7571$  is the chemical displacement of H ②, and the multiple peak between  $\delta=6.1504\sim 6.3605$  is the chemical displacement of H ③, and the multiple peak between  $\delta=3.1171\sim 3.1399$  is the chemical displacement of H ④, and the multiple peak between  $\delta=1.2884\sim 1.3778$  is the chemical displacement of H ⑤.

From Figure 3, the molecule hydronium peak of the title compound is 207, which accords with the molecular weight of the anticipated title compound.  $m/z=191$  is the corresponding fragment peak of the group of  $\text{C}_7\text{H}_{14}\text{O}_3\text{NP}$ , and  $m/z=177$  is the corresponding fragment peak of the group of  $\text{C}_6\text{H}_{12}\text{O}_3\text{NP}$ , and  $m/z=163$  is the corresponding fragment peak of the group of  $\text{C}_5\text{H}_{10}\text{O}_3\text{NP}$ , and  $m/z=147$  is the corresponding fragment peak of the group of  $\text{C}_5\text{H}_{10}\text{O}_2\text{NP}$ , and  $m/z=133$  is the corresponding fragment peak of the group of  $\text{C}_5\text{H}_{10}\text{O}_2\text{P}$ , and  $m/z=119$  is the corresponding fragment peak of the group of  $\text{C}_4\text{H}_8\text{O}_2\text{P}$ , and  $m/z=73$  is the corresponding fragment peak of the group of  $\text{C}_3\text{H}_5\text{O}_2$ , and  $m/z=59$  is the corresponding fragment peak of the group of  $\text{C}_2\text{H}_3\text{O}_2$ , and  $m/z=45$  is the corresponding fragment peak of the group of  $\text{C}_2\text{H}_5\text{O}$ , and  $m/z=31$  is the corresponding fragment peak of the group of  $\text{CH}_3\text{O}$ .

Through above analysis, the structure of the synthesized title compound is consistent with the anticipated structure.

### 3.2 Influences of acid-binding agent and reactive temperature on the synthesis of title compound

In the synthesis process of O,O-diethyl acrylamide phosphonate, HCl gas will produce, so we adopt the method adding the acid-binding agent to quicken the reaction speed and enhance the yield. The researches indicate that when the triethylamine is singly used as the acid-binding agent, the yield is low, and when a small quantity of CuCl is added as the activator, the yield can achieve 75%, and the reaction time could be reduced. Finally, we add the triethylamine with same molar acrylamide as the acid-binding agent, and add the CuCl which mass fraction is 1% acrylamide as the activator.

Because the synthesis reaction of O,O-diethyl acrylamide phosphonate is the exothermic reaction, so we must strictly control the reaction temperature in the synthesis process, or else, ascending temperature will influence the yield and possibly produce outgrowth. Therefore, we select the optimal reaction temperature in 0°C~5°C.

### 3.3 LOI measurement of flame retardant polyacrylonitrile copolymer

Copolymerize O,O-diethyl acrylamide phosphonate and acrylonitrile with different masses to obtain the flame retardant polyacrylonitrile copolymer containing diethyl acrylamide phosphonate with different mass fractions, and dissolve the copolymers into the solution of DMSO with 20% of mass fraction, and we can obtain even flame retardant polyacrylonitrile copolymer dope. Scrape the membrane and desiccate according the standard of GB2406-8, and measure the LOI. The result indicates that when the mass fraction of O,O-diethyl acrylamide phosphonate in polyacrylonitrile is 20%, the LOI of the flame retardant polyacrylonitrile copolymer can achieve 26.7%, which shows O,O-diethyl acrylamide phosphonate is the reactive flame retardant with better effect.

### 3.4 SEM analysis of burned carbon residue of flame retardant polyacrylonitrile copolymer

From Figure 4, the carbon residue surface of polyacrylonitrile presents foam structure, and the cross-section presents cellular structure, which accords with the flame retardant mechanism of the intumescent flame retardant. That shows the flame retardant synthesized in the article is the intumescent flame retardant, and it is consistent with the anticipated situation.

## 4. Conclusions

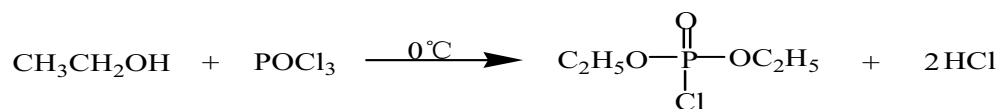
Taking acrylamide and diethyl phosphorus oxychloride as the reactants, we synthesized a sort of new intumescent flame retardant (IFR) containing phosphorus and nitrogen, O,O-diethyl acrylamide phosphonate. The structure of the title compound could be characterized by FTIR, <sup>1</sup>H NMR and MS. And we copolymerize the reactive flame retardant with acrylonitrile to form the flame retardant acrylonitrile copolymer which LOI value can reach 26.7% through LOI testing. The SEM photos of the fired residue of the flame retarded copolymer show that the surface of the fired residue presents foam-like structure, and the cross section presents cellular structure, which indicate that the title compound is the intumescent flame retardant.

## References

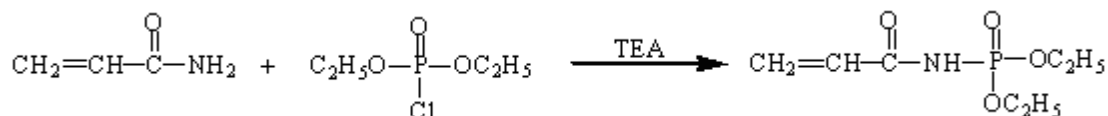
- Chigwada G & Wilkie C A. (2003). Synergy between conventional phosphorus fire retardants and organically-modified clays can lead to fire retardancy of styrenics. *Polym Degrad Stab*, No. 81(3), P. 551-557.
- Devi R R, Saikia C N, Thakur A J, Maji T K. (2002). Modification of rubber wood with styrene in combination with diethyl allyl phosphate as the flame-retardant agent. *J Appl Polym Sci.*, No. 105(5), P. 2461-2467.
- Duquesne S, Delobel R, Le Bras M, et al. (2002). A comparative study of the mechanism of action of ammonium polyphosphate and expandable graphite in polyurethane. *Polym Degrad Stab*, No. 77(2), P. 333-344.
- He, Qingdong, Cao, Youming & Cenlan. (2008). Research Progress on Environment-friendly and High Efficient Intumescent Flame Retardants. *Plastics Science and Technology*, No. 36(2), P. 104-108.
- Horacek H, Grabner R. (1996). Advantages of flame retardants based on nitrogen compounds. *Polym Degrad Stab*, No.54, P. 205-215.
- Ju, Changxun, Majing & Wang, Xinlong. (2008). Recent Advances for Research on Intumescent Flame Retardants. *Plastic Additives*, No. 5, P. 5-7.
- Lewin M, Brozek J. & Martens M M. (2002). The system polyamide/sulfamate/dipentaerythritol: Flame retardancy and chemical reactions. *Polym Adv Tech*, No.13, P. 1091-1102.
- Ren, Yuanlin, Cheng, Bowen & Zhang, Jinshu. (2007). Synthesis and Fire Retardance of N,N'-Bis(2-thio-5,5-dimethyl-1,3,2-dioxaphosphorinane) Ethane. *Chinese Journal of Applied Chemistry*, No. 24(11), P. 1314-1317.
- Schartel B, Braun U, Balabanovich A I, Knoll U, Artner J, Ciesielski M, Doring M, Perez R, Sandler J.K.W, Altstadt V, Hoffmann T, Pospiech D. (2006). Influence of the oxidation state of phosphorus on the decomposition and fire behavior of flame-retarded epoxy resin composites. *Polymer*, No. 47(26), P. 8495-8508.
- Sundarrajan S, Kishore K, Ganesh K. (2001). A new polymeric flame retardant additive for vinyl polymers. *Indian J Chem Technol*, No. 40(1), P. 41-45.
- Wyman P, Crook V, Ebdon J, Hunt B, Joseph P. (2006). Flame-retarding effects of dialkyl-p-vinylbenzyl phosphonates in copolymers with acrylonitrile. *Polymer Int*, No.55(7), P. 764-771.
- Yan, Xiaohong & Zhang, Lifu. (2007). Preparation of New Flame Retardant Containing Nitrogen Phosphorus. *Journal of Flame Retardant Material and Technology*, No. 6, P. 6-7.
- Zhang H, Westmoreland P R, Farris R J, et al. (2002). Thermal decomposition and flammability of fire-resistant

UV/visible-sensitive polyarylates copolymers and blends. *Polymer*, No. 43(20), P. 5463-5472.

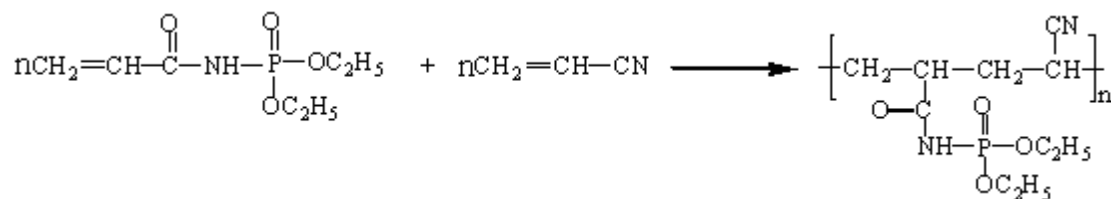
Zhang, Jinshu, Cheng, Bowen & Ren, Yuanlin. (2007). Synthesis and Characterization of 1,4-Di(O,O-diethyl thiophosphorylimine) Benzene. *Chinese Journal of Applied Chemistry*, No. 24(7). P. 831-834.



Scheme 1. Synthesis route of diethyl phosphorus oxychloride



Scheme 2. Synthesis route of the title compound



Scheme 3. Synthesis route of the flame retardant polyacrylonitrile copolymer

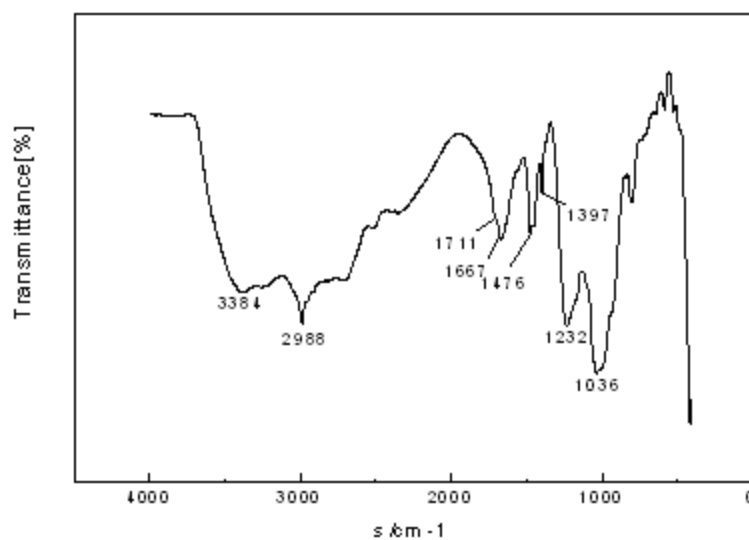


Figure 1. Infrared Spectrum of the Title Compound

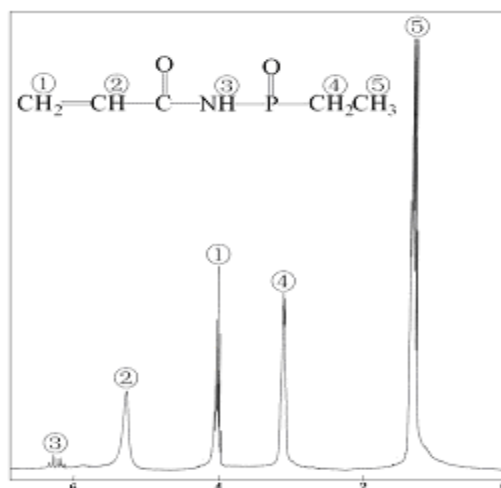


Figure 2. <sup>1</sup>H NMR Spectrum of the Title Compound

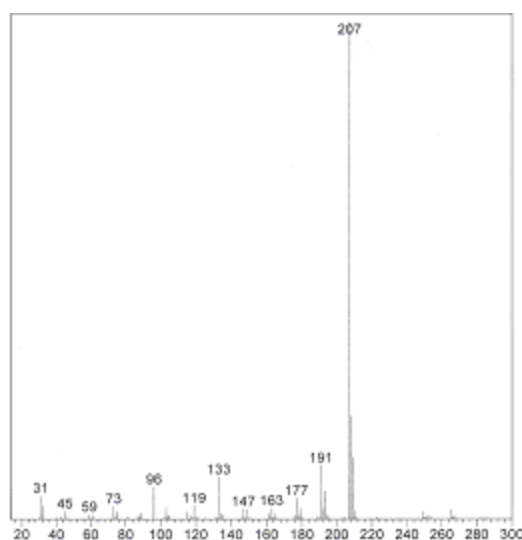
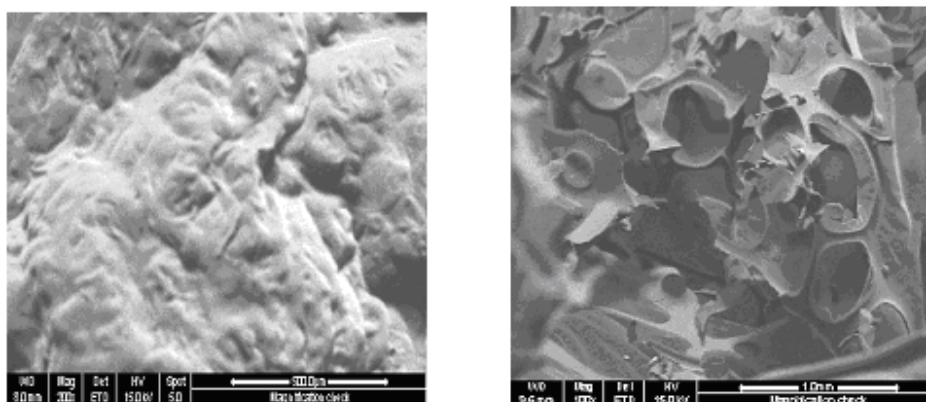


Figure 3. Mass Spectrum of the Title Compound



a. Surface photo of the fired copolymer residue    b. Cross-section photo of the fired copolymer residue

Figure 4. The Surface and Cross-section SEM Photos of the Fired Residue of Flame Retardant polyacrylonitrile copolymer



## Extraction, Separation and Identification of Chemical Ingredients of *Elephantopus Scaber L.* Using Factorial Design of Experiment

Anees Ahmad

Environmental Technology Division

School of Industrial Technology

Univesriti Sains Malaysia

11800 Penang, Malaysia

E-mail: anees@usm.my, aneesahmad@yahoo.com

Abbas F. M. Alkarkhi

Environmental Technology Division

School of Industrial Technology

Univesriti Sains Malaysia

11800 Penang, Malaysia

E-mail: abbas@usm.my

Sufia Hena

Environmental Technology Division

School of Industrial Technology

Univesriti Sains Malaysia

11800 Penang, Malaysia

E-mail: sufiahena@yahoo.co.in

Lim Han Khim

Environmental Technology Division

School of Industrial Technology

Univesriti Sains Malaysia

11800 Penang, Malaysia

E-mail: Hankhimzip@yahoo.com

### Abstract

Soxhlet extraction technique is employed for the extraction and separation of chemical constituents in the medicinal plant, *Elephantopus scaber L.* The effect of parameters, such as different parts of the plant (leaves, roots and stems), extraction time and types of solvent (n-hexane and methanol) on the extracted yield and the percentage of extraction were investigated. The design of experiment was done using factorial design. The data were analyzed using ANOVA as well as factorial design. The experimental results show that the methanol is better than n-hexane but an extraction time of 9 hours was required for stems and roots while 12 hours for leaves. Essential crude of *Elephantopus scaber L.* obtained by Soxhlet extraction was further analyzed by gas chromatography-mass spectrometry detection to identify the chemical ingredients of the plant and used as a standard in the qualitative analysis for certain chemical compounds based on the retention time on the chromatogram. Six compounds such as stigmaterol, lupeol, stearic acid, deoxyelephantopin isomers, analogue 1 and analogue 2 of deoxyelephantopin have been identified. Oven temperature

program of gas chromatography has been developed in this research. The results obtained, enable one to make qualitative and quantitative analysis for the essential oil which was extracted from the herbal plant. Maximum extraction conditions of the stigmasterol and lupeol were determined by comparing the area percentage below the peak in chromatogram with the GCMS standard. Stigmasterol: 6 hours extraction time using n-hexane and stems show the highest area percentage (8.145%). Lupeol: 9 hours extraction time using n-hexane and stems show the highest area percentage (68.580%).

**Key words:** Soxhlet extraction technique, *Elephantopus scaber* L, Separation, GC, GC-MS

## 1. Introduction

The development of organic chemistry took place along with the study of plants, mainly in the 19th century, when the first studies on plants were scientifically recorded. This ended up in the isolation of some active compounds from plants (Wheelwring, E.G, 1974). It is the vegetal kingdom that has contributed, in a more meaningful way, to the supply of useful substances for the treatment of human diseases (Galhiane, M.S., 2006). *Elephantopus scaber* L. is a member of *Asteraceae* family. The whole plant of *Elephantopus scaber* L. is a perennial herb and is well known as a Chinese folk medicine which is widely used in the treatment of nephritis, edema, dampness, pain in the chest, fever and cough of pneumonia, scabies, and arthralgia due to wounding (Peer, L. M., 1980 & Tsai, C. C, 1999). It is also commonly used as a remedy for the treatment of gastropathy, hepatitis, nephritis, edema, chest pain, fever and cough of pneumonia, bronchitis, arthritis, and carbuncle in China.

*Elephantopus scaber* L. is known to contain a large number of bioactive compounds such as lipids, phytochemicals, pharmaceuticals and pigments. For example, ethyl hexadecanoate, ethyl-9, 12-octadecadienoate, ethyl-(Z)-9-octadecenoate, ethyl octadecanoate, lupeol, stigmasterol, stigmasterol glucoside, deoxyelephantopin (1) and two new germacranolide sesquiterpene lactones named 17, 19-dihydrodeoxyelephantopin (2) and iso-17, 19-dihydrodeoxyelephantopin.

In this study, extraction of *Elephantopus scaber* L. with Soxhlet extraction process has been studied experimentally. The advantages of applying conventional Soxhlet extraction include (a) the displacement of transfer equilibrium by repeatedly bringing fresh solvent into contact with the solid matrix (b) maintaining a relatively high extraction temperature and (c) no filtration requirement after leaching. Furthermore, the soxhlet extraction method requires simple and inexpensive equipment which is easy to operate. (Luque de Castro, 1998).

In this study, the soxhlet extraction of *Elephantopus scaber* L. is presented using methanol and n-hexane as extracting solvents because these might extract different compositions (Zarnowski, R., 2004). The most widely-used solvent to extract edible oils from plant sources is hexane which has a fairly narrow boiling point range of approximately 63–69°C and is excellent oil solvent in terms of oil solubility and ease of recovery (Mamidipally, P.K., 2004). Various extraction conditions including the solvent (n-hexane and methanol), time of extraction (3 hours, 6 hours, 9 hours and 12 hours), different parts of plant (leaves, stems, and roots), have been investigated.

On the issue of problem statements, the points which should be highlighted are:

(a) The studies on development of chromatographic method of *Elephantopus scaber* L. rarely found in literature and particularly none in Gas Chromatography (GC) method. As a result, the development of GC method such as oven temperature, carrier gas flow rate and detention time are quite challenging.

(b) Extracted essential oil of *Elephantopus scaber* L. may contain volatile chemical compounds and it is very difficult to trap them while transferring the essential oil into the sample storage bottle after extraction process. Therefore, the essential oil is to be cooled to room temperature before transferring process so that the volatile components will not evaporate easily since it will condense back when temperature is lower than its boiling point. Moreover, some chemical constituents of *Elephantopus scaber* L. were identified using Gas Chromatography – Mass Spectrometry (GCMS) during this research study.

## 2. Material and methods

### 2.1 Sampling

Fresh *Elephantopus scaber* L. with commercial maturity (the plant height approximately 50 cm with corolla 8~10 mm long purple flower) were obtained from a local garden. In order to ensure the sample used was from the same source throughout the experiment, the fresh sample was collected in sufficient quantities (~10 kg) at a time. The standard procedure was followed to collect and store the sample.

The plant of *Elephantopus scaber* L. is separated into leaves, stem and root. First, the plant was washed thoroughly with running tap water, followed by rinsing with distilled water and then each part was cut into small pieces. The leaves,

stems and roots were sun dried (~33 °C) at open area with active ventilation until they attained constant weight (around two weeks).

### 2.2 Particle size

The sun dried parts of the plant were powdered in German Retsch mill, and then sieved into different mesh sizes (>150, 150, 180, 250 and 300 μm) using Vibrator Sieve Shaker (Retsch, German) but only samples of selected particle size were used in this study. Each of the sample size after the sieving process was weighed to calculate the percentage particle size of the material present in the sample. All the samples were stored in air tight container respectively and kept in the refrigerator at temperature below 4 °C to maintain the freshness of sample and preserving the loss of volatile compounds present in the samples.

### 2.3 Moisture content

5 gm of each dried ground leaves, roots and stems respectively was dried in the oven (Model Memert) at 104 °C until constant weight. The initial weight and final weight were taken, the weight difference for each samples represents its moisture content. The moisture content determination process was repeated for three times. The % of moisture content is reported in this study.

### 2.4 Soxhlet extraction

The samples of dried leaves, roots and stems were removed from the refrigerator and kept at room temperature (~28 °C) for 30 minutes to gently release the water vapor from the samples. This was done to retain the quality and amount of oil content in its original condition. The chosen particles sizes selected for the extraction are: leaves <150 μm; roots <150 μm and stems 180 μm.

The weight of a blank thimble filter (22 × 90 mm) (Advantec, Japan) and a blank round bottom extraction flask were weighed before and after placing 3 grams of sample into thimble. The cotton is then placed into the thimble and its weight along with sample was recorded again. The purpose of using cotton was to ensure the presence of samples inside the thimble during the experiment. The Soxhlet extraction processes using n-hexane (99% assay) and methanol (99.8% assay) as extraction solvents were carried out to compare the percentage of extraction and their quality of extraction between the two solvents. 350 mL of solvent is poured into the round bottom extraction flask, weighed and placed on the heating mantle. After this, the thimble containing the sample was placed into the extraction chamber. Lastly, the condenser was placed on top of the extraction flask and all these parts were fixed vertically. The extraction was carried out for four different preset intervals of times, which is 3 hours, 6 hours, 9 hours and 12 hours respectively. The process was repeated three times and an average extraction was taken.

After the extraction process, the weight of thimble containing sample and the weight of round bottom extraction flask containing solvent and extracted crude were weighed. The extracted samples were calculated as percentage of extraction while the extracted oil was stored in a refrigerator at the temperature below 4 °C until analyzed by GC and GCMS after the soxhlet extraction process. The percentage of extraction was calculated by using the equation (1).

$$\% \text{ Extraction} = \frac{m_1 - m_2}{m_1} \times 100 \quad (1)$$

Where:

$m_1$  = mass in grams of thimble and the sample before extraction

$m_2$  = mass in grams of thimble and the sample after extraction

### 2.5 Analytical methods

#### 2.5.1 Gas chromatography (GC)

The extracted crude with solvent was analyzed by Shimadzu GC-17A Gas Chromatography (GC) system equipped with a flame ionization detector (FID). BP-X5 capillary column (30m × 0.25mm id), 0.25 μm film thickness (SGE, Australia) was used. The helium carrier gas flow rate was 25mL/min at 600 kPa. The injector and detector temperature were maintained at 250 °C. Injection was performed in split less mode and the volume was 1 μL. An oven temperature program with total run time of 51.6667 min was used. The column temperature, after an initial isothermal period of 2 min at 60 °C was increased to 200 °C at a rate of 5 °C/min, and maintained at this temperature for 2 min, followed by the temperature was increased to 220 °C at a rate of 3 °C/min, maintained at this temperature for 1 min, and finally increased to 250 °C at a rate of 6 °C/min, and maintained at this temperature for 7 min. A sample of 2 mL of extracted oil with solvent was drawn out by using a 5 mL syringe and placed into a 2 mL vial prior for gas chromatography analysis. The extraction was repeated three times for each extraction by using hexane and methanol respectively.

Crude samples with solvent (1  $\mu$ L) were injected manually and peaks areas were calculated. The compounds in the GC were further identified by comparing its retention time with the results of GC-MS which was used as a standard.

### 2.5.2 Gas chromatography - mass spectrometry (GC-MS)

5 mL of plant extract was evaporated to dryness and reconstituted in 200  $\mu$ L n-hexane or 200  $\mu$ L methanol. The extracts were then subjected to GC-MS analysis. Chromatographic separation was carried out with Hewlett Packard 6890 series Gas Chromatograph with Autosampler and 5973N Mass Selective Detector and Chemstation Data System and a HP-5 crosslinked 5% phenyl methyl siloxane fused silica capillary column, 30m  $\times$  0.25mm (id), 0.25 $\mu$ m film thickness was used. Helium was used as a carrier gas with a flow rate of 0.9mL/min. The GC-MS oven temperature was programmed as follows:

- i. 50  $^{\circ}$ C (hold 2.5 minutes) to 150  $^{\circ}$ C at the rate of 15  $^{\circ}$ C/min
- ii. increased to 200  $^{\circ}$ C at a rate of 3  $^{\circ}$ C/min
- iii. increased to 300  $^{\circ}$ C at a rate of 8  $^{\circ}$ C/min
- iv. kept for another 8 minutes at 300  $^{\circ}$ C

Injection temperature was maintained at 250  $^{\circ}$ C, interface temperature at 280  $^{\circ}$ C, quadruple temperature at 150  $^{\circ}$ C and ion source temperature at 230  $^{\circ}$ C. Injection was performed in split less mode and the volume was 1  $\mu$ L. The mass spectra of compounds in samples were obtained by electron ionization (EI) at 70 eV, and the detector operated in scan mode from 20 to 600 amu. Identifications were based on mass spectral matching with standard compounds in NIST and Wiley libraries ( $\geq$  90%) while identification of Deoxyelephantopin isomers and analogs were based on the molecular structure, molecular mass and calculated fragmentations.

The essential chemical constituents were identified by matching mass spectra with spectra of reference compounds in mass spectral library of National Institute of Standards and Technology (NIST 147). The relative amounts of individual components were expressed as percent peak areas relative to total peak area.

### 2.6 Statistical analysis

Statistical techniques such as analysis of variance (ANOVA) and factorial design were used for analyzing the data obtained from extraction experiment. The effect of three factors on percentage of extraction as a response variable, the factors are extraction time (four levels; 3, 6, 9, 12 hr), type of solvent (two types; n-hexane and Methanol), and part of plant (three parts; leave, Root, Stem). Factorial design of type  $4 \times 2 \times 3$  was used to carry out this experiment in random order (Montgomery, 2005). Three replicates were used for each combination and the total number of runs was 72.

## 3. Result and discussions

### 3.1 Particle size selection

Five particle sizes of samples (leaves, roots and stems) were obtained as shown in Table 2. They are, smaller than 150  $\mu$ m, 150  $\mu$ m, 180  $\mu$ m, 250  $\mu$ m, and 300  $\mu$ m. Leaves and roots with smaller than 150  $\mu$ m particle size were selected for further study due to its abundance compared to other sizes that is about 50.6% (leaves) and 93.9% (roots) of the total samples. Moreover, larger particles may result in prolonged extraction time because the extraction process may be diffusion-controlled where the oil has to diffuse out from the inner part of the particle to the surface through the matrix of the particle before the solubility process occurred. Besides that, the smaller the particle size the higher would be the extraction yield due to higher surface area to volume ratio and the specific surface area that was exposed to the solvent was increased. Therefore, the extraction yield increased with decreasing particle size.

According to Reverchon (Reverchon, E., 1997), if external mass transfer or equilibrium was the controlling step of the extraction process, the particle size could not affect the extraction rate significantly. On the other hand, if the internal mass transfer or diffusion was the controlling step of the extraction process, the particle size could significantly influence the extraction time. As a result, effect of solvents on the extraction time was the main consideration in this experiment and hence the particle size of each sample was fixed. However, stems samples with particles size 180  $\mu$ m was chosen due to the small amount of the smallest particle size (smaller than 150  $\mu$ m) could be obtained in the total samples of stems.

### 3.2 Moisture content on the extraction process

In this study, the sun dried ground samples with particle size of  $\leq$  150 $\mu$ m (leaves and roots) and 180 $\mu$ m (stems) were used rather than the wet basis sample. Moreover, the wet sample will cause mechanical operational failure to the analytical instruments such as GCMS.

The moisture content of *Elephantopus scaber* L. leaves with particle size of  $\leq$  150 $\mu$ m was found to be 8.94%, roots with particle size of  $\leq$  150 $\mu$ m was found to be 8.72% and stems with particle size 180 $\mu$ m was found to be 8.60% as shown in

Table 3. High moisture content could induce 'unwanted phenomenon' which will result in lesser yield and lower quality of extract.

The moisture content of leaves is the highest (8.94%), followed by roots (8.72%) and stems (8.60%). This can be explained that the leaf hairs of the plant minimize the water loss from its stomata. The high storage level of water moisture in the leaf is for the photosynthesis purposes. The moisture content of roots is higher than stem because stem only acts as a passage for water transport in a plant while roots are the sources where water enters and contains a high level of moisture content.

### 3.3 Percentage of extraction

The influences of nature of solvents and total time of extraction on the percentage extraction yield are shown in Table 4, 5 and 6. The different yields of extracts with methanol and n-hexane might be influenced by the polarities of solvents (Luque de Castro, 1994 & Romdhane, M., 2002).

Table 4 shows that the percentage extraction yield for leaves with methanol was better than n-hexane. The average extracted yield by methanol is almost 50% more than average extracted yields by n-hexane. For example, the average yield from leaves in methanol at 12 hours was 14.08% while in n-hexane it was 7.45% and thus, the difference was about 89% higher in methanol. This was also reported by Klejdus et al. (Klejdus, B., 2004 & Klejdus, B., 2005) that methanol is a better solvent during their research on comparing the different extraction conditions including solvents and techniques for extraction of isoflavones soybeans samples.

For root of *Elephantopus scaber L.*, methanol was reported better than n-hexane solvent regarding the yield of extraction in percentage. According to Zlotorzynski, A (Zlotorzynski, A., 1995), methanol has relatively higher dissipation factor, which means that it could absorb much of the microwave energy and transform it into heat better than other solvents. Hence, the most favourable extraction time for methanol in roots' extraction was reported as 9 hours (10.17%) and 6 hours for n-hexane (6.07%) which was related to the extracted yield in percentage of extraction, as reported in Table 5.

Table 6 shows the extraction yield of stem of *Elephantopus scaber L.* which indicate that methanol was better than n-hexane as solvent. The highest percentage of the extraction of stems among four different length of time such as 5.26% of extraction for 9 hours (n-hexane) and 10.18% of extraction for 9 hours (methanol). The best duration of extraction of stem using n-hexane was 9 hours. It was different with other parts of the plant where 6 hours the best extraction period was.

### 3.4 Qualitative and Quantitative Analysis

The quantitative determination of the chemical compounds was based on the comparison of peak areas of samples with those in GCMS library. Some of the identified compounds are stigmasterol, lupeol, stearic acid, deoxyelephantopin, and isomers of deoxyelephantopin as described below:

#### 3.4.1 Stigmasterol

The stigmasterol was identified in all parts of *Elephantopus scaber L.* (leaves, roots and stems) in GCMS analysis. Figure 1 shows that the comparison of abundance of stigmasterol in different parts of the plant extracted by the two solvents. All of the samples show that the peaks were in the range of 35.80 min to 36.10 min for stigmasterol. Stems of *Elephantopus scaber L.* contain high level of stigmasterol compound compared to the other parts of the plants. Furthermore, n-hexane was more favourable than methanol as extracting solvent during Soxhlet extraction. This can be explained from the peaks of stigmasterol in each parts of the plant in the Figure 1 with different extraction solvents. Besides that, result from gas chromatography (Table 7) also show that the highest percentage area is 8.145% of stigmasterol compound at 6 hours extraction time with n-hexane as extraction solvent. On the other hand, the leaves sample contain the least stigmasterol compounds. Although the leaves showing the best extraction time of stigmasterol was at 6 hours with n-hexane is same as the conditions applied to stems but it only managed to fulfill 4.850% area (Table 7). As a result, the best extraction conditions for stigmasterol compound in *Elephantopus scaber L.* were 6 hours extraction period with n-hexane as solvent and the most favourable parts of the plant for Soxhlet extraction process was stems.

#### 3.4.2 Lupeol

Besides stigmasterol, lupeol was also one of the chemical compounds that can be determined from *Elephantopus scaber L.* in the GCMS analysis which was next to the peak of stigmasterol. Peaks of lupeol that were determined from the Figure 2 varied from the time range of 36.80 min ~ 37.10 min. All parts of *Elephantopus scaber L.* plant such as leaves, roots and stems show the presence of lupeol. In addition, n-hexane has been identified as the better extraction solvent than methanol. This was because almost all the parts of plant which were extracted with n-hexane solvent proposed the higher percentage area in the result of gas chromatography as shown in Table 7. Further the exception were found for 6 hours (13.556% area) and 9 hours (68.550% area) extraction of stems with n-hexane which was lower than the percentage area of methanol at the same extraction time such as 38.590% (6 hours) and 69.502 (9 hours). For 6 hours

extraction with n-hexane and methanol in stems, percentages areas for lupeol of both conditions were the lowest. Hence, the result from Table 7 also indicated that the condition of 6 hours extraction time with n-hexane solvent was the most favourable condition for extraction of lupeol compound from leaves (54.423% area) while 9 hours with the same solvent for roots (68.360% area) and stems (68.550% area).

#### 3.4.3 Stearic acid

Stearic acid showed its abundance in roots of *Elephantopus scaber L.* which was extracted using hexane as shown in the Figure 3. Next, the time range for the extraction of stearic acid from *Elephantopus scaber L.* plant was from 21 min to 23 min which also can be identified from the Figure 3.

#### 3.4.4 Deoxyelephantopin

Deoxyelephantopin isomers and analogs were identified based on the molecular structure, molecular mass and calculated fragmentation given by Than, N. N. et al. (Than, N.N., p. 200-204). Deoxyelephantopin isomers and analog 2 were detected in all parts of *Elephantopus scaber L.* plant by GCMS. In addition, they were showing their abundance peaks from 30 min to 35 min resulted from Figure 4. Both leaves samples extracted using n-hexane and methanol showed higher peaks compared to other parts of the plant with same extraction condition. However, deoxyelephantopin analogue 1 was only available in roots sample which was reported in the Figure 5. The time range for the appearance of peaks was 27 min ~ 28 min.

### 3.5 Statistical Analysis

Factorial design was used to study the effect of three factors, namely; extraction time, type of solvent, and parts of plant on the percentage extraction of constituents *Elephantopus scaber L.* The results of factorial design with 72 runs are given in Table 8. The results of analysis of variance (ANOVA) for percentage of extraction obtained from this experiment based on the effect of extraction time, type of solvent and part of plant are given in Table 9. The main effects for all the three parameters were statistically significant ( $P < 0.0001$ ). In addition to the main effect, all interactions between different factors were also statistically significant ( $P < 0.0001$ ). Significant interaction (Table 9) indicates that the factors studied did not work independently, rather depend on each other and affect simultaneously on the extent of extraction.

Plot of the main effect using data means for extraction time, type of solvent and parts of plant, is given in Fig.6, which depicts the behavior of each factor individually regardless of other factors. The interaction plot using data means for percentage of extraction is given in Fig.7 that shows the behavior of each factor in presence of other factors, for instance the behavior of extraction time in the presence of type of solvents and parts of plant, the behavior of type of solvents in presence of extraction time and parts of plant, and the behavior of parts of plant in the presence of extraction time and parts of plant on percentage of extraction. The changes in percentage of extraction values were mainly due to the interaction between factors.

The value of  $R^2$  is high and close to 1. The value of  $R^2$  for percentage of extraction was 0.99 which indicates that 0.99 of the total variation is explained by the model that belongs to the extraction time, type of solvent and part of plant and their significant interactions, and only 0.01 of the total variation is unexplained.

## 4. Conclusions

This study has successfully drawn up several conclusions which contributed to Soxhlet extraction process as an alternative method for extraction and separation of chemical constituents from medicinal herbs, *Elephantopus scaber L.* The conclusions of overall study as follows:

(a) The determination of the percentage of extraction for *Elephantopus scaber L.* were studied at various parts of the plants such as leaves, roots and stems with two types of different solvents, n-hexane and methanol, respectively over various extraction period; 3 hours, 6 hours, 9 hours and 12 hours. The study shows that methanol is better than n-hexane as solvent regarding extracted yield. Moreover, different parts of the plant have different favourable extraction conditions such as leaves: 12 hours with methanol as solvent and 6 hours with n-hexane as solvent, roots: 9 hours with methanol as solvent and 6 hours with n-hexane as solvent, and stems: 9 hours with methanol as solvent and 9 hours with n-hexane as solvent.

(b) The moisture content and particle size are also the important criteria to conduct the extraction process and their importance can be identified from literature review and experimental process in this study. The tolerable limit of moisture content for *Elephantopus scaber L.* was around 12% to 13%.

(c) The study also shows that the extracted crude of *Elephantopus scaber L.* contains of multi-compounds such as stigmaterol, lupeol, stearic acid, deoxyelephantopin and its isomers/analogs. All of these chemical constituents have different quantity in the plant of *Elephantopus scaber L.* Maximum extraction condition of stigmaterol was reported as 6 hours extraction with n-hexane as extraction solvent in the stem and reaching 8.145% area in the gas chromatography

result. Besides that, extraction condition of lupeol was favourable at 9 hours extraction time with n-hexane in the stems as reported 68.580% area in the gas chromatogram.

## References

- Galhiane, M.S., Rissato, S.R., Chierice, G.O., Almeida, M.V., & Silva, L.C. (2006). Influence of different extraction methods on the yield and linalool content of the extracts of *Eugenia uniflora* L. *Talanta*. 70, 286-292.
- Klejdus, B., Mikelova, R., Adam, V., Zehnalek, J., Vacek, J., & Kizek, R. (2004). Liquid chromatographic-mass spectrophotometric determination of genistin and daidzin in soybean food samples after accelerated solvent extraction with modified content of extraction cell. *Analytica Chimica Acta*, 517, 1-11.
- Klejdus, B., Mikelova, R., Petrolova, J., Potesil, D., Adam, V., & Stiborova, M., (2005). Evaluation of isoflavone aglycon and glycoside distribution in soy plants and soybeans by fast column high-performance liquid chromatography coupled with a diode-array detector. *Journal of Agricultural and Food Chemistry*. 53, 5848-5852.
- Luque de Castro, M. D., Valcarcel, M. & Tena, M. T. (1994), Analytical Supercritical Fluid Extraction, Butterworth Publishers, Boston.
- Luque de Castro, M.D. & Garcia-Ayuso, L.E. (1998). Soxhlet extraction of solid materials: An outdated technique with a promising innovative future. *Analytica Chimica Acta*. 369, 1-10.
- Mamidipally, P.K., & Liu, S.X. (2004). First approach on rice bran oil extraction using limonene. *European Journal of Lipid Science and Technology*. 106, 122-125.
- Peer, L. M. & Metzger, J. (1980), Medicinal Plants of East and Southeast Asia: Attributed Properties and Uses. *The MIT Press*. London.
- Reverchon, E. (1997). Supercritical Fluid Extraction and fractionation of Essential Oils and Related Products. *J. of Supercritical Fluids*. 10, 1-37.
- Romdhane, M. & Gourdou, C. (2002). Investigation in solid-liquid extraction influence of ultrasound. *Chem. Eng. J.* 87, 11-19.
- Than, N.N., Fotso, S., Sevvana, M., Sheldrick, G. M., Fiebigd, H. H., Kelter, G., & Laatsch, H. (2005). Sesquiterpene lactones from *Elephantopus scaber*. *Z. Naturforsch.* 60b, 200-204.
- Tsai, C. C & Lin, C. C. (1999). Anti-inflammatory effects of Taiwan folk medicine "Teng-Khia-U" on carrageenan and adjuvant-induced paw edema in rats. *J. Ethnopharm.* 64, 85-89.
- Wheelwring, E.G. (1974), Medicinal Plants and their History. *Dover Publications*, New York.
- Zarnowski, R., & Suzuki, Y. (2004). Expedient Soxhlet extraction of resorcinolic lipids from wheat grains. *Journal of Food Composition and Analysis*, 17, 649-664.
- Zlotorzynski, A. (1995). Methanol has relatively higher dissipation factor, which means that it could absorb much of the microwave energy and transform it into heat better than other solvents. *Crit. Rev. Anal. Chem.* 25, 43-75.

Table 1. Sample Preparation Result

<b>Description</b>	<b>Leave (gm)</b>	<b>Root (gm)</b>	<b>Stem (gm)</b>
Fresh sample	537.94	220.78	219.53
After chop	524.14	212.86	212.45
After grind	492.58	198.47	196.95

Table 2. Particle Size Percentages

Parts	Smaller than 150 $\mu\text{m}$	150 $\mu\text{m}$	180 $\mu\text{m}$	250 $\mu\text{m}$	300 $\mu\text{m}$
Leaves	50.56 %	14.22 %	18.32 %	13.63 %	3.27 %
Steam	0.98 %	2.20 %	95.75 %	0.67 %	0.40 %
Root	93.91%	1.68 %	2.75 %	1.20 %	0.46 %

Table 3. Moisture Content Determinations

Description	Leave			Root			Stem		
	1	2	3	1	2	3	1	2	3
Empty dish ( $m_0$ ) (gm)	39.1941	37.6534	40.6425	36.1688	38.2890	35.8629	37.0875	36.5648	38.7524
Dish + sample (initial) ( $m_1$ ) (gm)	44.1932	42.6545	45.6433	41.1681	43.2893	40.8627	42.0871	41.5653	43.7532
Dish + sample (final) ( $m_2$ ) (gm)	43.7460	42.2076	45.1974	40.7315	42.8535	40.4265	41.6573	41.1360	43.3224
Moisture content percentage	8.95	8.94	8.92	8.73	8.72	8.72	8.60	8.59	8.61
Average percentage	8.94			8.72			8.60		

Table 4. Percentage of Extraction of oil from Leaves using n- hexane and Methanol

Extraction Time (Hours)	Percentage of Extraction (%)							
	n- hexane				Methanol			
	Replications			Average	Replications			Average
	I	II	III		I	II	III	
3	6.61	7.39	6.92	6.97	11.78	12.49	12.53	12.27
6	7.69	7.32	8.36	7.79	11.23	10.75	10.95	10.98
9	6.49	7.35	6.18	6.67	12.91	13.26	12.53	12.90
12	7.25	7.48	7.61	7.45	13.69	14.36	14.18	14.08

Table 5. Percentage of Extraction of oil from Roots using n- hexane and Methanol

Extraction Time (Hours)	Percentage of Extraction (%)							
	n- hexane				Methanol			
	Replications			Average	Replications			Average
	I	II	III		I	II	III	
3	5.25	4.85	4.97	5.02	7.33	6.84	7.14	7.10
6	6.11	6.48	5.63	6.07	8.59	9.38	8.92	8.96
9	5.12	4.76	4.43	4.77	9.73	10.27	10.52	10.17
12	5.20	5.58	5.72	5.50	9.61	10.20	9.92	9.91

Table 6. Percentage of Extraction of oil from stems using n- hexane and Methanol

Extraction Time (Hours)	Percentage of Extraction (%)							
	n- hexane				Methanol			
	Replications			Average	Replications			Average
	I	II	III		I	II	III	
3	3.28	2.87	3.56	3.24	4.47	5.39	4.17	4.68
6	5.00	5.38	4.72	5.03	5.11	5.52	4.76	5.13
9	5.37	5.48	4.92	5.26	10.16	10.63	9.74	10.18
12	4.36	4.76	5.18	4.77	10.10	9.69	10.63	10.14

Table 7. Summary of compounds detected in plant from GC

Parts	Compounds	Percentage Area					
		n-hexane			methanol		
		6 hours	9 hours	12 hours	6 hours	9 hours	12 hours
Roots	Stigmasterol	5.369	-	4.766	-	-	-
	Lupeol	58.890	68.360	53.695	47.445	55.405	41.790
Stems	Stigmasterol	8.145	-	4.447	3.468	-	4.451
	Lupeol	13.556	68.550	58.681	38.590	69.502	54.077
Leaves	Stigmasterol	4.850	3.356	3.939	3.955	4.372	3.666
	Lupeol	54.423	53.017	51.713	53.213	45.272	49.862

Table 8. Factorial design with experimental data values for extraction %

Time	Solvent	plant	Part of plant	Time	solvent	plant	Part of plant
3	n-Hexane	Leaves	6.61	9	n-Hexane	Leaves	6.49
3	n-Hexane	Leaves	7.39	9	n-Hexane	Leaves	7.35
3	n-Hexane	Leaves	6.92	9	n-Hexane	Leaves	6.18
3	n-Hexane	Roots	5.25	9	n-Hexane	Roots	5.12
3	n-Hexane	Roots	4.85	9	n-Hexane	Roots	4.76
3	n-Hexane	Roots	4.97	9	n-Hexane	Roots	4.43
3	n-Hexane	Stems	3.28	9	n-Hexane	Stems	5.37
3	n-Hexane	Stems	2.87	9	n-Hexane	Stems	5.48
3	n-Hexane	Stems	3.56	9	n-Hexane	Stems	4.92
3	Methanol	Leaves	11.78	9	Methanol	Leaves	12.91
3	Methanol	Leaves	12.49	9	Methanol	Leaves	13.26
3	Methanol	Leaves	12.53	9	Methanol	Leaves	12.53
3	Methanol	Roots	7.33	9	Methanol	Roots	9.73
3	Methanol	Roots	6.84	9	Methanol	Roots	10.27
3	Methanol	Roots	7.14	9	Methanol	Roots	10.52
3	Methanol	Stems	4.47	9	Methanol	Stems	10.16
3	Methanol	Stems	5.39	9	Methanol	Stems	10.63
3	Methanol	Stems	4.17	9	Methanol	Stems	9.74
6	n-Hexane	Leaves	7.69	12	n-Hexane	Leaves	7.25
6	n-Hexane	Leaves	7.32	12	n-Hexane	Leaves	7.48
6	n-Hexane	Leaves	8.36	12	n-Hexane	Leaves	7.61
6	n-Hexane	Roots	6.11	12	n-Hexane	Roots	5.2
6	n-Hexane	Roots	6.48	12	n-Hexane	Roots	5.58
6	n-Hexane	Roots	5.63	12	n-Hexane	Roots	5.72
6	n-Hexane	Stems	5	12	n-Hexane	Stems	4.36
6	n-Hexane	Stems	5.38	12	n-Hexane	Stems	4.76
6	n-Hexane	Stems	4.72	12	n-Hexane	Stems	5.18
6	Methanol	Leaves	11.23	12	Methanol	Leaves	13.69
6	Methanol	Leaves	10.75	12	Methanol	Leaves	14.36
6	Methanol	Leaves	10.95	12	Methanol	Leaves	14.18
6	Methanol	Roots	8.59	12	Methanol	Roots	9.61
6	Methanol	Roots	9.38	12	Methanol	Roots	10.2
6	Methanol	Roots	8.92	12	Methanol	Roots	9.92
6	Methanol	Stems	5.11	12	Methanol	Stems	10.1
6	Methanol	Stems	5.52	12	Methanol	Stems	9.69
6	Methanol	Stems	4.76	12	Methanol	Stems	10.63

Table 9. The results of analysis of variance (ANOVA) for percentage of extraction %

Source	D.F	Sum of Squares	Mean Square	F-Value	P-value
Extraction Time	3	49.37	16.46	107.85	< 0.0001
Type of solvent	1	287.40	287.40	1883.63	< 0.0001
Parts of plant	2	186.31	93.15	610.54	< 0.0001
Time*solvent	3	42.14	14.05	92.07	< 0.0001
Time* plant	6	27.97	4.66	30.55	< 0.0001
Solvent *plant	2	17.76	8.88	58.19	< 0.0001
Time*Solvent*Plant	6	8.78	1.46	9.59	< 0.0001
Error	48	7.32	0.15		
Total	71	627.04			

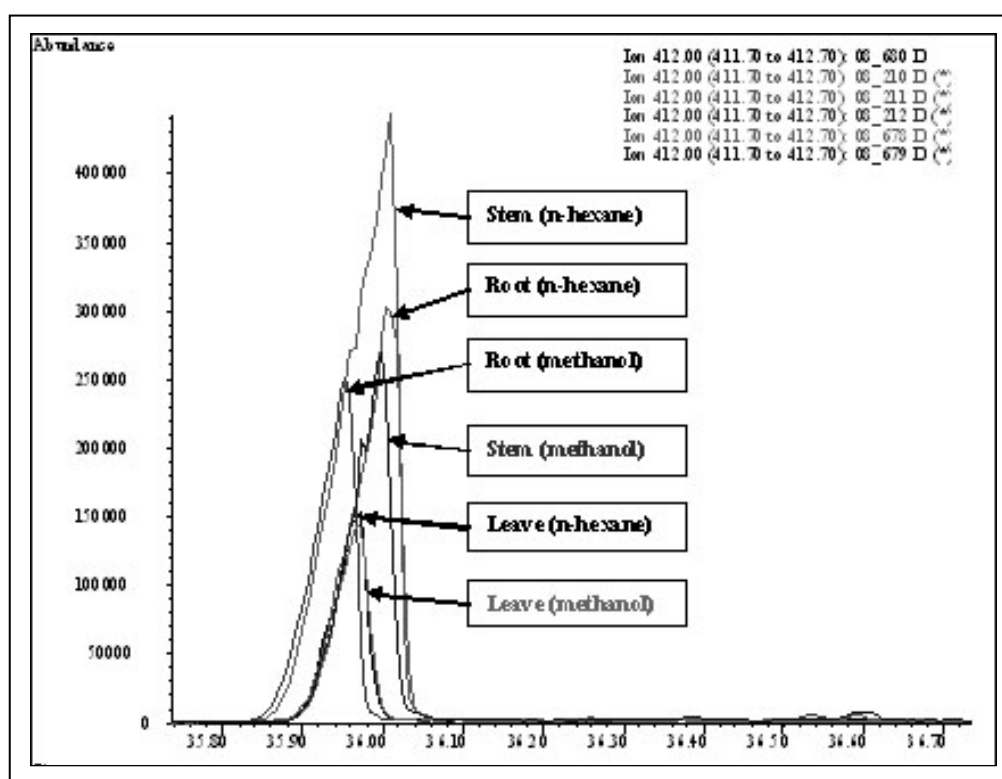


Figure 1. Chromatogram and mass spectrum of Stigmasterol

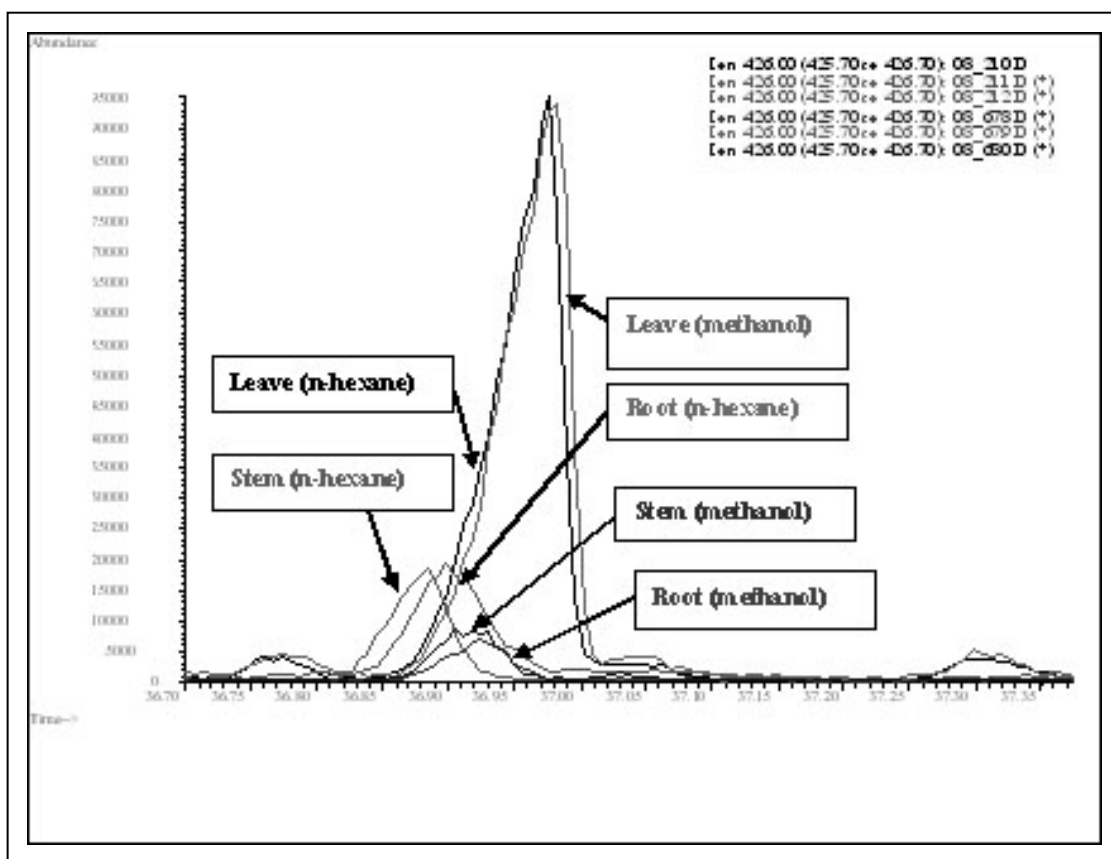


Figure 2. Chromatogram and mass spectrum of lupeol

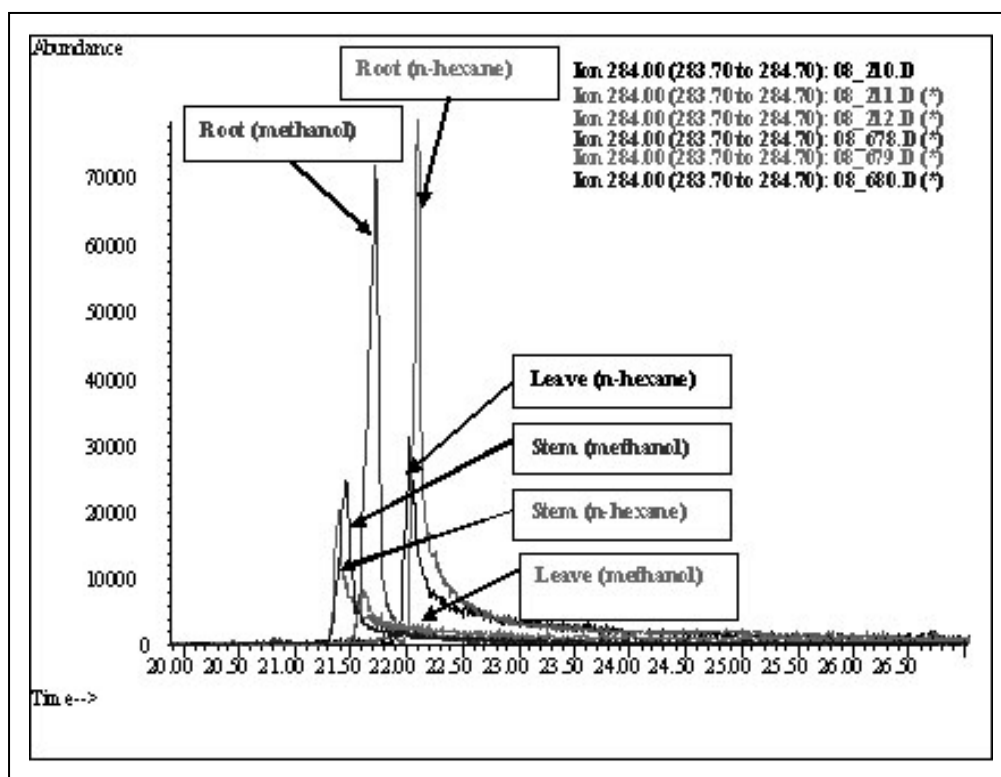


Figure 3. Chromatogram and mass spectrum of stearic acid

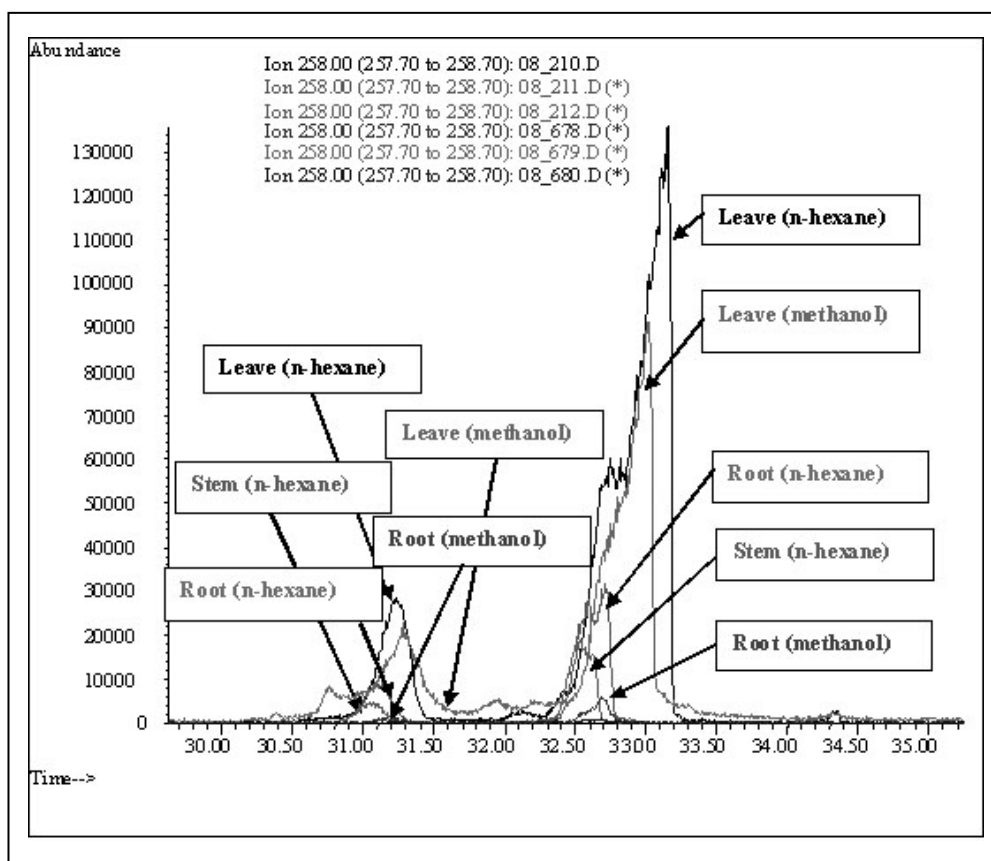


Figure 4. Chromatogram and mass spectrum of deoxyelephantopin isomers and analogue 2

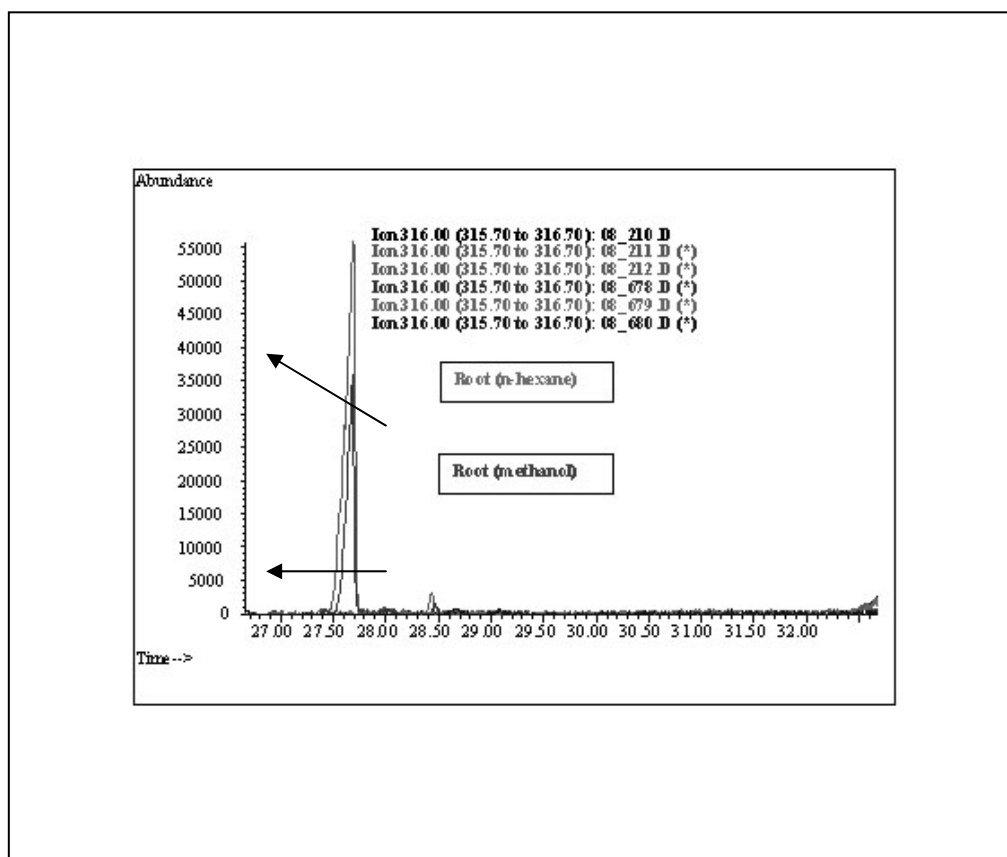


Figure 5. Chromatogram and mass spectrum of deoxyelephantopin analogue 1

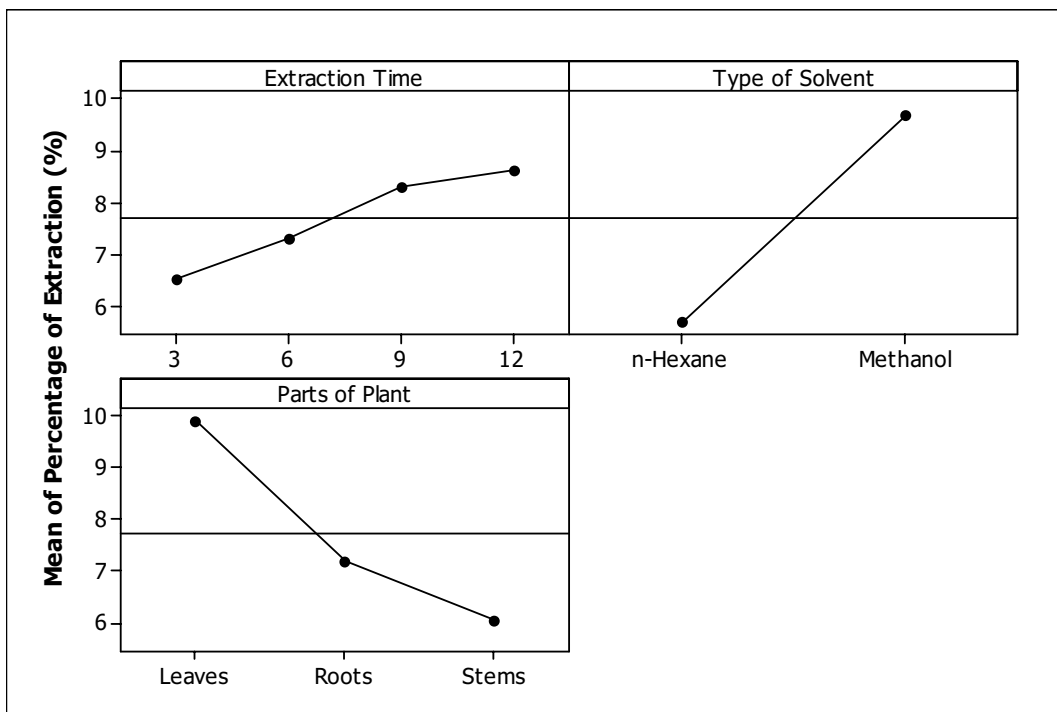


Figure 6. Mean effect plot (data means) of % extraction vs extraction time, type of solvent and part of plant

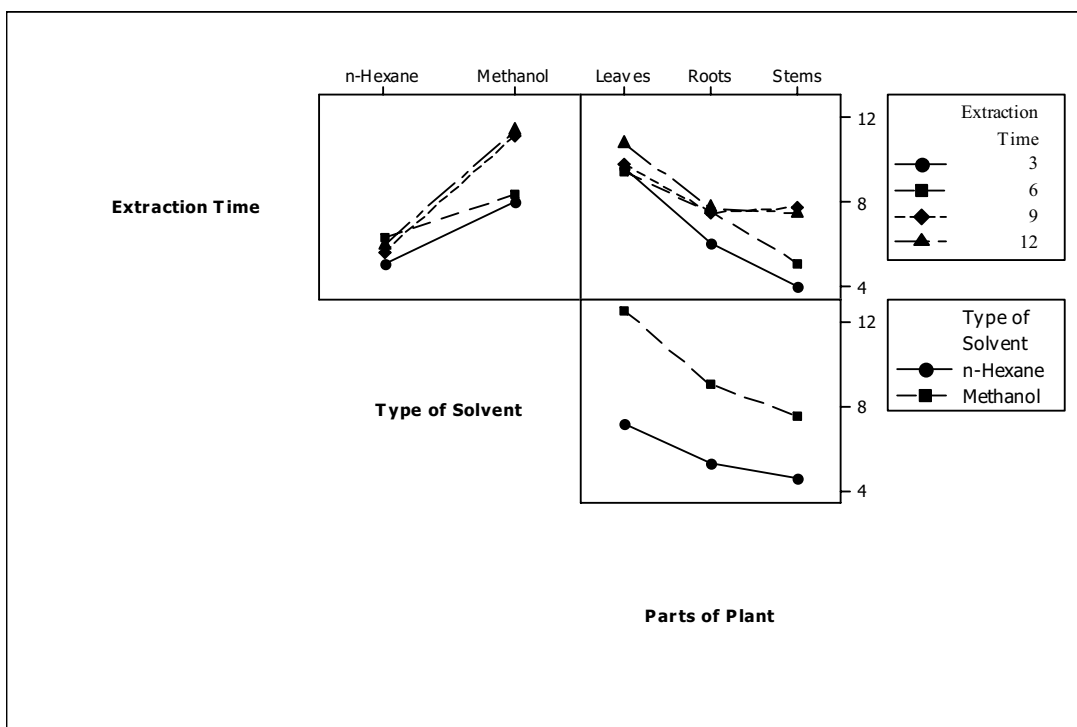


Figure 7. Interaction plot (data means) of Percentage extraction



## Study on the Reaction Kinetics of Ultrasonic Radiation Non-homogeneous Phase Chitin Deacetylation

Cuirong Zhang, Yingde Cui & Zhenyu Jia

Department of Chemistry and Chemical Engineering

Zhongkai College of Agricultural Technology

Guangzhou 510225, China

Tel: 86-20-8816-2869 E-mail: zcr19661115@163.com

### Abstract

Under the condition of ultrasonic radiation, in this article, we studied the reaction kinetics of non-homogeneous phase chitin deacetylation. The results indicated that the deacetylation degree of chitin was obviously enhanced under the condition of ultrasonic radiation, and the reaction process accorded with pseudo-first order kinetics relationship, and the reaction control is diffusion control, and the surface activation energy was  $E=23.45\text{kJ/mol}$ .

**Keywords:** Chitin, Kinetics, Activation energy, Ultrasonic radiation, Non-homogeneous phase

### 1. Introduction

With the increasing deficiency of mineral resources such as oil, the manufacture research of functional materials which take the natural macromolecule as raw materials becomes more and more important in the world. Chitin is a sort of natural macromolecule material of polysaccharide, which is also called as poly-N-acetylglucosamine, and its chemical name is beta-(1,4)-2-acetamido-2-deoxy-d-glucose, and it is the amylase linked with N-acetyl D-glucosamine through  $\beta$ -(1.4) indicant bond. The biological yield of chitin in the world can achieve tens billion ton, and the chitin is sort of natural renewable resource which reserve is only inferior to the cellulose (Jiang, 2001). The chitin could be prepared as various natural macromolecule derivatives with different purposes through chemical modification, and this sort of material possesses many good properties such as harmless, erosion-resistance, good biodegradability and biocompatibility, and it is extensively applied in many industries such as medication, food, textile, paper making, agriculture, printing and dyeing, cosmetic, biomedicine, enzyme preparation and health products (B. Hexing, 2006, p.3069 & Li, 2006, p.374-381). Therefore, in recent years, many domestic colleges and scientific research institutions begin to study it, and many production enterprises with competitive force occur one after the other. The research about functional material development taking natural macromolecule as raw materials has fueled a boom. Someone thought that the chitin will be one pillar industry as synthetic resin and plastic in the 21'st century.

Because strong hydrogen bond function exists in the chitin molecule, so the deacetylation needs longtime function of lye with high concentration, but the products with this method have low deacetylation degree and low viscosity, and so applied performance will be influenced. Many people studied the problem, for example, they adopted precipitation method, pure medium method and microwave method (Cao, 2005, p.120-124 & Cui, 2004) to study the problem and obtained certain effects. Though people have studied the chitin for many years and applied it in many aspects of the industry, but there is still not a complete theory for the preparation of chitosan, especially there are few basic theory researches about the deacetylation of chitin. There are no articles to utilize the ultrasonic radiation technology to study the basic theory of deacetylation, so according to the structure of chitin and the function principle of ultrasonic, we explore the deacetylation to offer the reference for the production of industrialization.

### 2. Experiment and Testing

#### 2.1 Experimental materials and instruments

Experimental materials and instruments include chitin (made by Zhanjiang Botai Biology Chemical and Industrial as Well as Scientific and Technological Co., Ltd), ethanol (95% AR), sodium hydroxide (AR), acetic acid (AR), ultrasonic generator (Branson2200), Ubbelohde viscosity meter, constant temperature water-bathing trough, shear high speed disintegrator and electronic balance.

## 2.2 Chitin deacetylation reaction

Crush the chitin after drying as powders by the disintegrator, respectively take 5g to into three flasks, and add 40% sodium hydroxide solution or add sodium hydroxide-ethanol mixed liquid. Under the condition of circumfluence in the ultrasonic field, control the temperature respectively as 80°C, 100°C, 120°C, and control the time in 1h, 3h, 5h, 7h, and 9h. When the reaction completes, take out flasks, cool, filtrate and wash to neutrality, then drying.

## 2.3 Measure of deacetylation degree (Chen, 1998, p.419-422)

In the experiment, we adopt the acid-based titration method to measure. The chitosan is electrolyte, and to make the measured result exact, we add 0.5% sodium chloride into the acetic acid solution dissolving chitosan.

$$D.D \% = \frac{(C_1 V_1 - C_2 V_2) \times 0.016}{G \times (100 - W) \times 0.0994} \times 100$$

Where, D.D is the degree of deacetylation (%), C1 is the standard solution concentration of hydrochloric acid (mol/L), C2 is the standard solution concentration of sodium hydroxide (mol/L), V1 is 30ml standard solution quantity of 0.1 hydrochloric acid, V2 is the quantity that titration consumes standard solution of sodium hydroxide (ml), G is the quantity of sample (g), W is the water content of sample (%), 0.016 is the amine content equal to 1ml 1mol/L hydrochloric acid solution (g), and 0.0994 is the theoretic amidocyanogen content in chitosan (16/161).

## 2.4 Measure of Characteristic viscosity and molecular weight (Jiang, 2001)

Take 0.5g chitosan into the breaker, add certain acetic acid (0.1mol/L) and sodium acetic acid (0.2mol/L) mixed solution, mix round to make them fully dissolving, and under 25°C in the constant temperature trough, use Ubbelohde viscosity meter to measure the viscosity of chitosan solution.

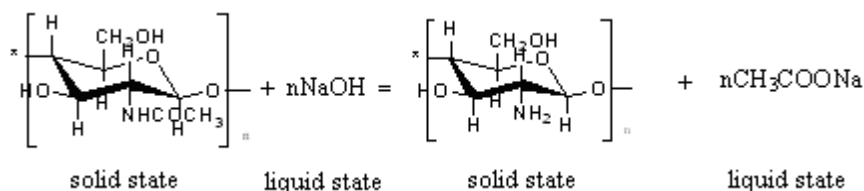
$$[\eta] = K M \alpha$$

Where,  $k=1.81 \times 10^{-3}$ ,  $\alpha=0.93$ .

## 3. Results and Discussion

### 3.1 Diffusion control chitin deacetylation model

The deacetylation of chitin is liquid solid chemical reaction, and with the emersion of acetyl, OH- gradually move to the interior of chitin though the reaction interfaces. In this process, the emersion of acetyl is slow, so the reaction process mainly consider the diffusion control, and we could think the diffusion speed equal to the reaction speed (Cai, 1998, p.352-355, Takanori, 1997, p.649-651, Loth, 1997, Xie, 1996, p.30-33, Chen, 1992, p.1008-1010). The equation of reaction process is



The chitin through crashing could be regard as plate which length, height and thickness respectively are A, B and L, and  $AB \gg L$ , the diffusion area of OH-  $S=AB$ , so the diffusion behavior of OH- in the chitin is seen in Figure 1.

According to the Fick's laws of diffusion (Novikov, 1990, p.64-67 & Zhang, 2000, p.23-26), the diffusion flux of unit area in unit time through vertical diffusion direction is  $\Phi = -D \frac{dC}{dx}$ .

So, the diffusion speed of OH- in chitin is

$$\frac{dG}{dt} = -D S \frac{dC}{dx}$$

Where, D is the diffusion coefficient, S is the transprence area of diffusion direction,  $dc/dx$  is the concentration grads along the diffusion direction. Because the reaction is controlled by the diffusion, so the deacetylation speed (reaction speed) could be thought to equal to the diffusion speed. Implement integral to the above formula, we can get  $-dG/dt = -D S C_0/x$ , where,  $C_0$  is the concentration of sodium hydroxide solution (g/ml) and X is the advance distance of OH-diffusion (cm).

In the deacetylation process of chitin, the interior reaction surface gradually shifts inside, and the shift speed is  $dN = dG = \rho S dx$ .

Combine the diffusion speed with shift speed, and we can obtain  $x dx = DC_0/\rho dt$ .

Solve the above equation, we can get  $x = (2DC_0t/\rho)^{1/2}$ .

Slice-shape chitin is in the sodium hydroxide solution, and the diffusion of OH<sup>-</sup> is seen in Figure 1. So, we can suppose the degree of deacetylation is  $D.D \% = 100 \times 2x/L = 200/L \times (2DC_0t/\rho)^{1/2}$ , where,  $\rho$  is the density of chitin (g/cm<sup>3</sup>),  $L$  is the thickness of chitin (cm),  $C_0$  is the concentration of sodium hydroxide (g/ml),  $t$  is the time of reaction (h), and  $D$  is the diffusion speed.

From the formula of deacetylation degree, we can see that under the condition of constant temperature, the deacetylation degree of chitin is directly proportional to the concentration of sodium hydroxide and reaction time, and the function relationship is  $D.D = f(D, C_0, t, \rho, L)$ . The experiment research showed that the experiment result basically inosculate with the theory. The establishment of the mathematical model possesses certain instructive meaning for actual production.

### 3.2 Reaction kinetics of chitin deacetylation

The molecules of chitin are generally arranged in the crystal lattice of highly crystal micro-fiber, and they are divided into three types such as  $\alpha$ ,  $\beta$  and  $\gamma$  according to their crystal structure, and the  $\alpha$  structure is the most stable structure, and it is the common structure in the nature. Strong -O...H-O- and -O...H-N- hydrogen bond functions exist among chitin molecules, and the function force among big molecules is very strong, which make the chitin molecules present ordered structure and induce the non-melt and highly difficult non-dissolving property of chitin, and the chitin is not dissolved in water and other most solvents (Keeme, 1980, p.293-296, Huang, 1995, Zhou, 1995, p.93-96, Qian, 1998, p.100-104 & Liu, 2002, p.31-34). The structure of chitin is seen in Figure 2. Figure 3 is the structure of chitosan through deacetylation.

The basic hydrolysis of acid amide is a nucleophilic substitution reaction (Zhang, 2004, p.511-515). Under the concentrated alkali, because carbonyl takes positive charge and OH<sup>-</sup> has strong nucleophilicity and small bulk, chitin will first attach carbonyl to make original plane deltoid amides become into tetrahedral transition state, and part of negative charge will be on the oxygen. The tetrahedral transition state will change into the tetrahedral midbody, and the positive charge is on the oxygen. That is the first step of reaction, and it is the addition of OH<sup>-</sup> to the amides, and the balance exists from reaction material to the midbody, so it is reversible. The second step is the leaving of alkalescence group. The reaction course is seen in Figure 4.

The whole reaction process is controlled by the first step, and the reaction could be thought as the first order reaction, so the first order dynamical equation could be denoted as

$$k = \frac{2.303}{t} \log \frac{a}{a-x}$$

Where,  $a$  is the initial concentration of acetylamine, and  $X$  is the amidogen concentration formed after  $t$  time of hydrolyzation.

From the above formula, we can obtain

$$k = \frac{2.303}{t} \log \frac{1}{1-x/a}$$

Suppose  $D.D = x/a$ , where  $X$  is the transformation rate of chitin deacetylation which corresponds with the deacetylation degree of chitin. So we can obtain  $\ln[1/(1-D.D)] = k t$ , where  $K$  is the reaction surface speed constant, and  $D.D$  is the degree of deacetylation.

From Figure 5 and Figure 6, under constant sodium hydroxide concentration and reaction temperature, the deacetylation degree of static reaction chitin is far smaller than the deacetylation degree under dynamic condition, which indicates that the mixing condition enhance the diffusion intension of OH<sup>-</sup>. The condition of ultrasonic radiation could make compact crystal chitin loosen, which makes for the diffusion of OH<sup>-</sup> in the body of chitin, improves the enhancement of deacetylation degree and further proves that the deacetylation reaction of chitin is controlled by diffusion.

In the deacetylation reaction process of chitin, the influence of reaction temperature is very important. From Figure 7, the temperature increases, the deacetylation degree of chitin obviously increase, and with the increase of reaction time, the degree of deacetylation increases. The chitin deacetylation reaction from above hypothesis is the first order reaction dynamics which accords with the experiment research, i.e. the equation of  $\ln[1/(1-D.D)] = k t$  comes into existence.

Under the condition of ultrasonic radiation, the concentration of sodium hydroxide is 40%, and the reaction temperatures respectively are 60°C, 80°C, 100°C and 120°C. Construct  $\ln[1/(1-D.D)]$  to the reaction time  $t$ , we can obtain Figure 8, and parameters all present good linear relationship, and all correlative coefficients exceed 0.995. The

result shows that the deacetylation reaction dynamics of chitin is the first order reaction.

Figure 9 is the relationship between the slope of the first order reaction equation  $\ln[1/(1-D)] = kt$  under different temperatures  $\ln k$  with the time reciprocal  $1/T$ , and both are linear relationship, and the correlative coefficient of beeline is 0.9964. So we can compute the surface activity energy of deacetylation of chitin under ultrasonic radiation,  $E = 23.45 \text{ kJ/mol}$ . The value is obviously smaller than the activity energy  $92.05 \text{ kJ/mol}$  in Sannan's report (Zhang, 2004, p.511-515) which took the homogeneous phase as the hypothesis, which indicates both reaction mechanisms are very different, and the non-homogeneous phase deacetylation of chitin is diffusion control. Chen Bingnian's researches about the deacetylation dynamics to chitin under the mixing condition indicated that the surface activity energy is  $35.63 \text{ kJ/mol}$ . Under the condition of ultrasonic radiation, its surface activity energy is smaller, which shows that the ultrasonic radiation could strengthen the diffusion of  $\text{OH}^-$ , strongly shake the acetyl groups on chitin, and make for the hydrolysis nucleophilic substitution reaction for alkali.

Figure 10 is the fitting curve between deacetylation degrees of chitin with time. The fitting equation is  $D \cdot D\% = -1.15t^2 + 20.17t + 3.04$ ,  $R^2 = 0.992$ . The experiment values basically accord with the computation values from the fitting equation. Under the condition of ultrasonic radiation, the concentration of sodium hydroxide is 40%, and with the process of time, the deacetylation degree continually increases, and when the deacetylation degree achieves 80%, the deacetylation begins to be slow, and when the degree exceeds 90%, the deacetylation goes parallel, and the resistance of diffusion is large. To enhance the degree of deacetylation, we must further crush the chitin.

Figure 11 shows the comparison of average molecular weight of same deacetylation degree prepared under conditions of ultrasonic radiation, static state and mixing, which indicates the ultrasonic radiation could not induce degradability for chitosan.

#### 4. Conclusions

(1) The deacetylation degree of chitin increases obviously under the condition of ultrasonic radiation, and the deacetylation is the pseudo-first-order reaction dynamic relationship, and the surface activation energy of deacetylation is  $E = 23.45 \text{ kJ/mol}$ , which is smaller than the activation energy which takes the homogeneous phase reaction as the hypothesis, and that indicates both reaction mechanisms are very different, and the non-homogeneous phase deacetylation reaction of chitin is diffusion control.

(2) In the deacetylation reaction process of chitin, the influence of reaction temperature is very important, and the temperature increases, the deacetylation of chitin obviously increases. The ultrasonic radiation also has very important influence to the deacetylation of chitin, and under same conditions, the deacetylation degree is enhanced obviously, which indicated that the condition of ultrasonic radiation could make the compact crystal of chitin loosen, and it is propitious to the diffusion of  $\text{OH}^-$  in the chitin and deacetylation.

#### References

- B. Hexing, H. Alata & Y. Inoue. (2006). *Polym. Sci. Part B: Polym. Phys.*, No. 43, p. 3069.
- Cai, Zhongli & Ma, Xiaohong. (1998). Study on Low Alkalinity Chitin Deacetylation Technique and Dynamics. *Chemical World*, No.32(7), p. 352-355.
- Caojian & Dai, Yangyong. (2005). Research on Chitosan Preparation by Microwave Deacetylation of Chitin. *Food Science*, No.26 (11). p. 120-124.
- Chen, Bingnian. (1992). Studies on Kinetics of Deacetylation of Chitin in Heterogeneous Alkaline Solution. *Chemical Journal of Higher Colleges*, No. 13(7), p. 1008-1010.
- Chensheng. (1998). Method and Measure Comparison of Chitin Deacetylation. *Chemical World*, No. 37(8), p. 419-422.
- Cui, Yingde & Liangliang. (2004). Study on Preparation of Chitosan with Microwave New Technology. *Journal of Changshu Institute of Technology*, No. 4.
- Huang, Xiwen. (1995). *Research of Chitin Deacetylation Dynamics and Reaction Mechanism*. Thesis of Tianjin University.
- Jiang, Tingda. (2001). *Chitosan*. Beijing: Chemical Industry Press.
- Keeme L & Lindbery B. (1980). Methods in Carbohydr. *Chem.*, No.8, p. 293-296.
- Li, Lei & You-Lo Hsieh. (2006). Chitosan Bicomponent Nanofibers and Nanoporous FcarbohdrRes. No. 341, p. 374-381.
- Liu, Changxia. (2002). Comment on Deacetylation Kinetics of Chitin. *Journal of Cangzhou Teachers' College*, No. 18(3), p. 31-34.
- Loth Fritz. (1997). Manufacture of Chitosan by Deacetylation of Chitin with Aqueous Lye Solution in Presence of Alcoholols. *Ger.offen. De 19, 530, 689 (clco8b37/08)*. 13 Feb, 1997.

Novikov V. YU, oriovaTA & Voronia IE. (1990). Kinetics of Chitin and Chitosan Deacetylation. *Izvestiya Vysshikh Vchebnykh Zavedeni pishchevaya Tekhnologiya*, No. 5, p. 64-67.

Qian, Hesheng. (1998). Reaction of Chitin Deacetylation. *Journal of China Textile University*, No. 24(2), p. 100-104.

Takanori Sanna. (1997). Study on Chitin.v.Kinetics of Deacetylation Reaction. *Polymer Journal*, No.9(6), p.649-651.

Xie, Liping. (1996). Study on Portunid Chitin Non-homogeneous Phase Dynamics. *Guangzhou Chemical Industry*, No. 24(1), p. 30-33.

Zhang, Zitao & Chen, Donghui. (2000). Deacetylation Kinetics of Chitin. *Journal of Qingdao University*, No. 15(4), p. 23-26.

Zhang, Zitao & Chen, Donghui. (2004). Study on the Kinetics Model of Deacetylation Reaction of Chitin. *Chemical World*, No.10, p. 511-515.

Zhou, Ruzhong. (1995). Study on the Deacetylation of the Chitin. *Journal of China University of Petroleum (Edition of Natural Science)*, No.19(6), p. 93-96.

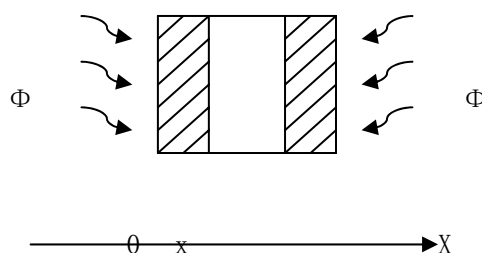


Figure 1. OH-proliferation Direction Schematic Drawing

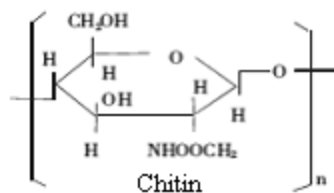


Figure 2. Carapace Element (Chitin) Structural Formula

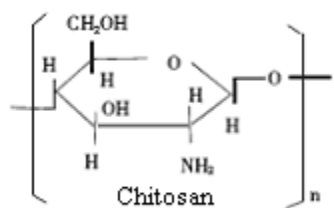


Figure 3. Shell Polyose (Chitosan) Structural Formula

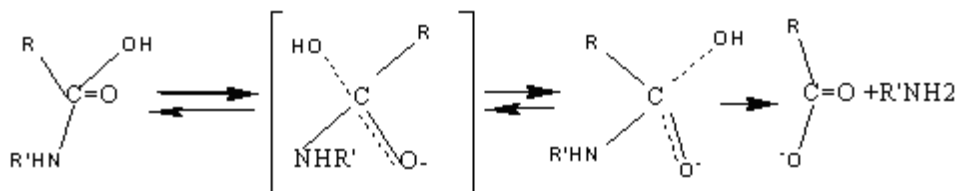


Figure 4. The Drawing of Carapace Element Escape Acetylyze Response under Thick Alkali's Function

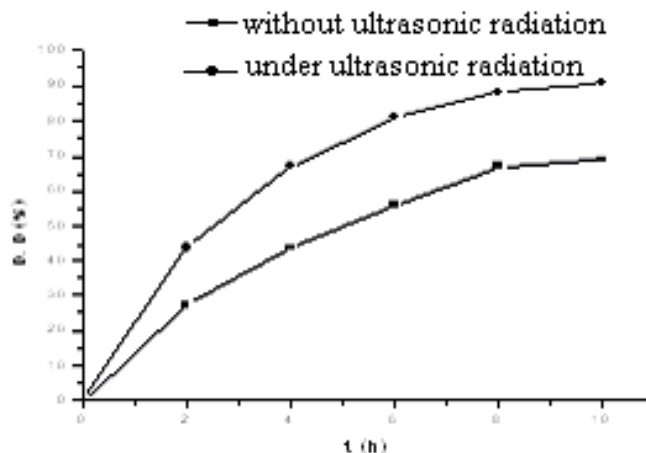


Figure 5. Contrast of Escape Acetyl Influence under Supersonic Radiation Condition

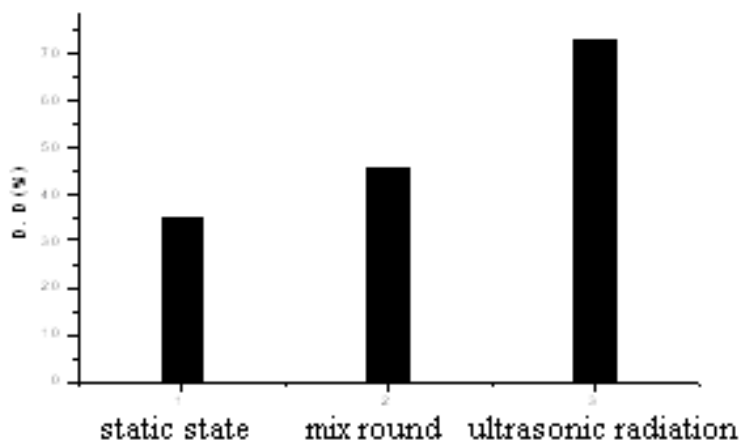


Figure 6. Contrast of Escapes Acetyl under Tendency and Static Condition

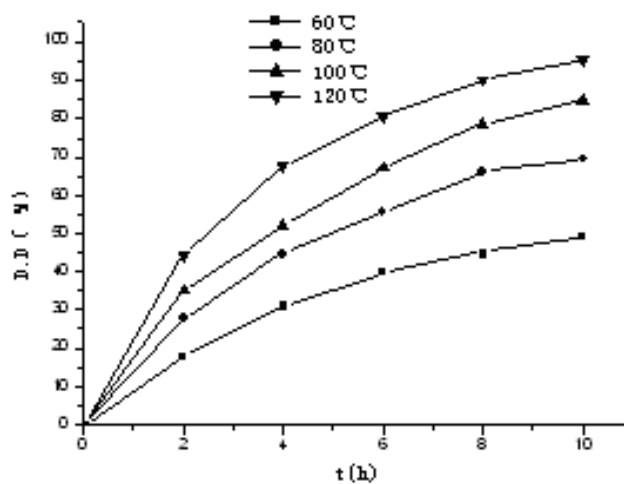


Figure 7. Influence of Temperature to Escapes Acetyl of Carapace Element

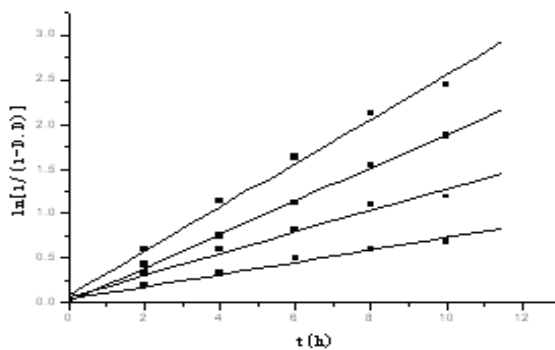


Figure 8. Ln [1/(1-D.D)] with Time t Relational

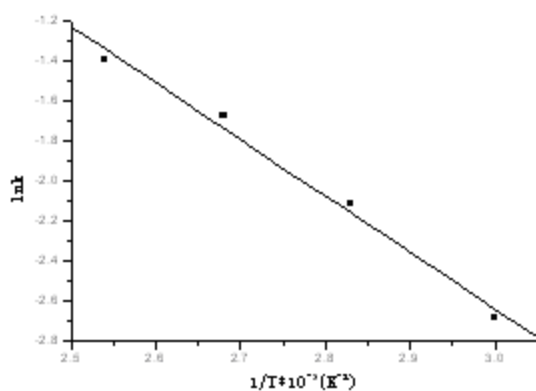


Figure 9. Lnk with 1/T Relational

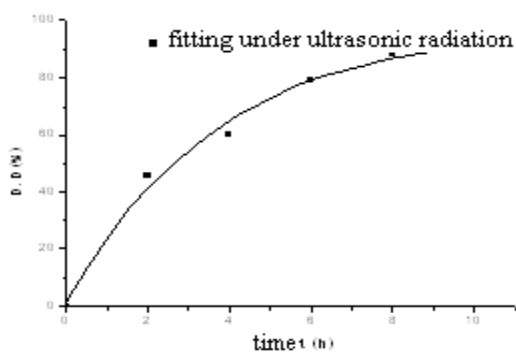


Figure 10. Escape Acetyl with Time Relationship Fitted Curve

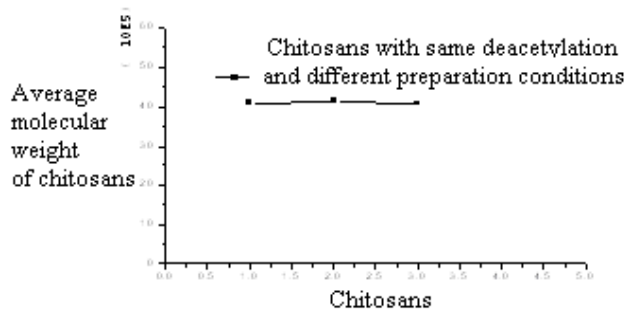


Figure 11. Change of Escapes Acetyl Same Shell Polyose Molecular Weight



## Performance Research of Polyester Fabric Treated by Nano Titanium Dioxide (Nano-TiO<sub>2</sub>) Anti-ultraviolet Finishing

Haixia Li, Hua Deng & Jing Zhao

School of Textiles, Tianjin Polytechnic University

Tianjin 300160, China

E-mail: lhx0829@126.com

### Abstract

Nano-TiO<sub>2</sub> sol and finishing agent was prepared by sol-gel method, during which tetrabutyl titanate was used as precursor and ethanol was used as solvent. The agent was penetrated into polyester fabric through a padding method, the anti-ultraviolet performance of the fabric was analyzed and the external morphology was carefully studied afterward. The results showed that indicated that the Nano-TiO<sub>2</sub> particles distribute evenly with fine dispersity and stability and the finished fabrics demonstrated exceptional anti-ultraviolet performance with a phenomenal UPF ascendance reaching up to 50+ without influencing the breaking strength.

**Keywords:** Sol-gel, Nano-TiO<sub>2</sub>, Polyester, Anti-ultraviolet

### 1. Introduction

With the aggravating greenhouse effect and the getting-severer ozone depletion phenomenon emerge, the total amount of ultraviolet (UV) reached the earth surface increased year by year (Diffey, B., 2004). When intensely interact with human skin, central nervous system and ocular region, various pathological changes would be caused which makes doing research and development on Anti-ultraviolet fabrics a focal point in recent years (Wu, Dacheng, 2003). Nanometer particles are those superfine particles with sizing range around 1-100 nm. Based on the unique characteristics demonstrated by nanometer particles such as quantum size effect, small-geometry effect, surface effect and quantum tunnel effect, wide range of application are applying nanometer technology, e.g. catalyzing, optical filtering and absorbing, pharmaceutical, magnetic medium and novel material. Nano-TiO<sub>2</sub> possesses a multitude of advantages like small particle size, large specific surface area, strong magnetism, photocatalytic, exceptional absorbing property especially on UV, large surface activity, remarkable heat transfer performance and stable suspension liquid. In recent years, the research of function-fabric by application of the Nano-materials and application of Nano-technology were published (such as super-amphiphobic, super-amphiphilic, UV-protection, far-infrared healthy, antistatic, anti-bacterial) (Xin J H, 2004, p.97-100).

There are plenty of inorganic UV-absorbing nanometer material which could be used as UV-absorber, for example, Nano-TiO<sub>2</sub>, Nano-ZnO, Nano-SiO<sub>2</sub>, Nano-Al<sub>2</sub>O<sub>3</sub>, Nano-FeO and etc, among which Nano-TiO<sub>2</sub> is one stable, nontoxic and tasteless UV-absorber. By uniformly distributing Nano-TiO<sub>2</sub> into fiber molecules, the decomposition of the macromolecule chain could be effectively inhibited and free radicals could be reduced (Wang, Shimin, 2004, p.230-234). Nano-TiO<sub>2</sub> shows strong UV-absorbing capability and UVA, UVB could be effectively shielded while visible light could freely penetrate through. Nano-TiO<sub>2</sub> finishing agents could enhance the fabrics' UV-reflection and UV-scattering capability to a good extent and they are secure and pragmatic to use (Zhao, Jiexiang, 2002, p.31- 34). Yalpani M and Johnson F (Yalpani, M, 1995) etc. have done deeply research on the preparation and performance of Nanometer Titanium Dioxide (Nano-TiO<sub>2</sub>); Denghua (Deng, hua, 2007, p.40-42) have done the research about the treatment of cotton fabric using the Nanometer Titanium Dioxide (Nano-TiO<sub>2</sub>), improving the performance of the anti-ultraviolet and anti-bacterial, Haixia Li (Li, Haixia, 2008, p.70-73) have discussed the performance of the Nanometer Titanium Dioxide (Nano-TiO<sub>2</sub>). However most of the research is about the function treatment of cotton fabric using Nanometer Titanium Dioxide, the research about the treatment of polyester fabric was so little. Thought the function of the anti-ultraviolet of polyester fabric is better than that of cotton fabric, the performance of the anti-ultraviolet still can not satisfy the anti-ultraviolet standard (AS/NZS) of fabric when the polyester fabric made into clothing.

### 2. Experimental

#### 2.1 Material

Polyester fabrics with warp density 420p/cm, weft density 300p/cm and thickness 0.099mm.

## 2.2 Reagents

Tetrabutyl titanate, Anhydrous Ethanol, Nitrate, Distilled water.

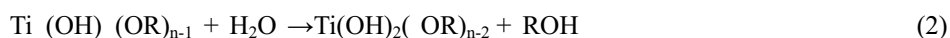
## 2.3 Nano-TiO<sub>2</sub> prepared by sol-gel method

Add certain quantity of Tetrabutyl titanate precursor into the anhydrous ethanol with a 1:10 ratio, sufficient stir to get a fully resolved mixed solution A. Next put the catalyst HNO<sub>3</sub> into distilled water to make mixed solution B and then add A into B drop by drop under quick stirring state. Maintain that state under room temperature for a certain length of time and the uniformly distributed transparent Nano-TiO<sub>2</sub> sol could be prepared.

The chemistry of the sol-gel process can be represented as follows:

It is well-documented that titanium alkoxide react with water through the reactions shown in Eqs. (1) (2) (3) and (4).

Hydrolysis:



Condensation:



## 3. Finishing process

The polyester fabric processed by plasma ion gas with power of 100KW, processing time of 10min, then dipping the fabric into the Nano-TiO<sub>2</sub> sol, at 60°C, processing time of 40 min, then dry out under 80°C.

## 4. Test and Characterization

### 4.1 Performance of the finishing agent

Dilute the Nano-TiO<sub>2</sub> Anti-ultraviolet finishing agent with 100 times of distilled water. The absorbency (A) and transmittance (T) were measured under different wave lengths by using TEC ultraviolet spectrophotometer. Test the particle distribution condition of Nano-TiO<sub>2</sub> sol and the surface potential characteristics of Nano-TiO<sub>2</sub> by using D10-BA38-1436 nanometer particle size analyzer. The crystallization phase situation of the prepared Nano-TiO<sub>2</sub> powder XRD diagram was characterized and analyzed by X-ray diffraction analyzer.

### 4.2 Performance of the finished fabric

The UV transmittance and obstructing rate in the wave section of UVA and UVB(Sliney.D.H., 2000, p.213-228) was got by using Camspec M350 SPF Spectrophotometer in accordance with AATCC Test Method 183-1998), then evaluate the UV-protection effectiveness according to the value of ultraviolet protection factor (UPF) and the rate of UV-protection of fabric Use YG065/PC electronic strength tester by referring to GB/T3923.1-1997 testing method section 1(which is an introduction about the breaking strength and breaking elongation rate by undertaking stripe sampling method) to test the warp-wise breaking strength.

## 5. Results and Conclusions

### 5.1 Finishing agent's performance

The UV-Visible light absorbency spectrum and transmittance spectrum of Nano-TiO<sub>2</sub> anti-ultraviolet finishing agent show as fig.1 and fig.2.

Figure 1. shows that Nano-TiO<sub>2</sub> anti-ultraviolet finishing agent has a very limited UV-absorbing capability around the wavelength of 200nm with absorbency less than1, but when the wavelength surpasses 200nm, the absorbency ascends phenomenally and reaches a maximum value of 4.2 around 250nm. After that section, the absorbency gradually descends until around 320nm a precipitous decline appeared and the absorbency reaches to a minimum level of 0.1 around 360nm with no obvious absorbency change happened thereafter. In the whole visible light section, the finishing agent shows almost none absorption.

Figure 2. shows that a precipitous ultraviolet transmittance decline occurred since 200nm section and the transmittance comes almost to zero between wavelengths 250nm to 370nm. After 370nm section, the transmittance gradually ascends and around 400nm, the transmittance increases the fastest. The transmittance of visible light in all spectrums increases as the wavelengths increase.

So Nano-TiO<sub>2</sub> finishing agent has exceptional anti-ultraviolet effect and UVA, UVB section could be effectively shielded. In the visible light section, the agent has good transmittance and transparence.

### 5.2 The finishing agent's particle size and Zeta potential

Figure 3. shows that the average particle size of the nanometer particles is 23.3nm ranging uniformly between 5nm to 50nm which illustrates that high-purity Nano-TiO<sub>2</sub> sol could be readily prepared undertaking sol-gel method. The particle size distribution of Nano-TiO<sub>2</sub> could also affect the zeta potential: the smaller the Nano-TiO<sub>2</sub> particles are and the more uniformly they distribute, the larger the zeta potential absolute value will be and the more stable of Nano-TiO<sub>2</sub> sol will be. The zeta potential of Nano-TiO<sub>2</sub> tested is 31.97 with positive and large absolute value. The particle size is ideally small and well-distributed, therefore obtains a good distribution stability.

### 5.3 The XRD of Nano-TiO<sub>2</sub> powder

The Nano-TiO<sub>2</sub> powder used for XRD is deserved under a drying condition lower than 50°C Because of a low drying condition, the crystal form could be considered as intact without any breakage. Figure 4 shows that a maximum diffraction peak in the pattern appeared when the diffraction angle(2θ) reaches 25.3°, which just correspondence of the diffraction peak of the crystal plane of anatase type TiO<sub>2</sub>(101) . Different diffraction peaks appeared when the diffraction angle reaches 37.9°, 48°and 55°matching along separately with the crystal plane of anatase type TiO<sub>2</sub>(004), (200) and (211) which illustrates that the prepared Nano-TiO<sub>2</sub> has all been crystallized with phase structure of anatase crystal type. If the maximum diffraction peak of Nano-TiO<sub>2</sub> is narrow-and-acuate-oriented, the half-peak width would be narrow-oriented accordingly and the corresponding crystallinity would be better with comparatively intact crystal form.

### 5.4 Performance of the finished fabrics

#### 5.4.1 Anti-ultraviolet performance of the finished fabrics

In Table1, ①Finished fabrics are fabrics which have prepared Nano-TiO<sub>2</sub> finishing agent without plasma ion; Get the polyester fabric processed by plasma ion and then impregnate the fabric into the Nano-TiO<sub>2</sub> finishing agent, got ②Finished fabrics. In Table.1, compared with the unfinished fibers, the UPF values of ①Finished fabrics did not increase, and the anti-ultraviolet performance of polyester fabrics did not obviously improve; ②Finished fabrics on the whole UV spectrum finished by Nano-TiO<sub>2</sub> is very high, especially for UVB reaching 98.8%. The UPF value of polyester fabrics finished elevates from 15.1 to 65.3 and UPF rate elevates from 15 to 50+ belonging to exceptional protecting class which illustrates that the anti-ultraviolet performance of polyester fabrics enhanced to a good extent after being firstly pretreated by plasma and retreated by the finishing agent.

#### 5.4.2 SEM analysis

Figure 5 and Figure 6 are the fiber surface topography after 1000 times of magnification. By comparing the two images, we can see that the unfinished fiber surface is smooth and sleek while the finished has deposited Nano-TiO<sub>2</sub> on the fiber surface ranging in an inconsecutive way with some aggregation formed due to the minimal-particle-size-led self-aggregating phenomenon of Nano-TiO<sub>2</sub>. Consecutive Nano-TiO<sub>2</sub> particles ranged in a dispersed way leading to an irregular surface.

Nano-TiO<sub>2</sub> anti-ultraviolet mechanism analysis: (1) the valence band of Nano-TiO<sub>2</sub> is formed by the electron-filled-O<sub>2p</sub> track and the conduction band is formed by the unoccupied Ti<sub>3d</sub> orbital, which jointly configures a typical n-type semiconductor band gap. Based on its broadband-absorption performance, the energy of photonic (UV wavelength less than 410nm) would exceed the band gap if being radiated by UV when the energy of UV would be transformed into excitation energy to overcome the band gap. e<sup>-</sup> is going to be stimulated and transit into a high-power conduction band from the valence band to form a e<sup>-</sup> - h<sup>+</sup> hole and impart the TiO<sub>2</sub> the power of UV absorption. (2) Nano-TiO<sub>2</sub> also has a remarkable capability of UV-scattering. The particle size of Nano-TiO<sub>2</sub> is smaller than the wavelength of UV and when the UV energy propagates into the Nano-TiO<sub>2</sub> particles in the form of electromagnetic wave to collide with the electrons within the Nano-TiO<sub>2</sub> particles, vibration would be triggered in the frequency of the incident UV thus becoming a source of propagation of the electromagnetic wave and scatter UV light in all directions (Cao, Jianjun, 2005). Due to the powerful UV absorption and scattering capability, fabrics finished by Nano-TiO<sub>2</sub> would be imparted with excellent UV-shielding performance.

#### 5.4.3 Breaking strength

Mark: F(N)-Breaking strength; ΔL(mm)-breaking elongation; L(%) -elongation at break; W(J)-fracture work; T(s)-Breaking Time.

Table 2 shows that the breaking strength of the finished polyester fabric has decreased because the surface etching when being pretreated by plasma has caused damage to the fabric. The breaking force descending magnitude is fairly slight because of a low-level etching.

## 6. Conclusions

(1) The particle size of Nano-TiO<sub>2</sub> prepared by sol-gel method distributed fairly evenly showing fine dispersion and stability and has a remarkable shielding performance on the ultraviolet of UVA and UVB section.

- (2) Finished Fabrics demonstrate excellent anti-ultraviolet performance with a UPF value over 60 and UPF rate over 50+.
- (3) Discontinuous and unevenly distributed Nano-TiO<sub>2</sub> particles were deposited on the fabric surface after being finished by Nano-TiO<sub>2</sub>.
- (4) The breaking strength of the fabrics finished has decrease with a fairly slight or even unperceivable magnitude.

### Acknowledgement

This study was supported by Municipal Natural Science Foundation of Tianjin, China. (Approved by No. 06YFJMJC02700).

### References

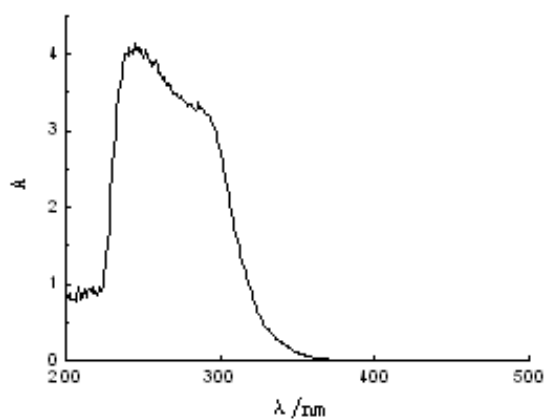
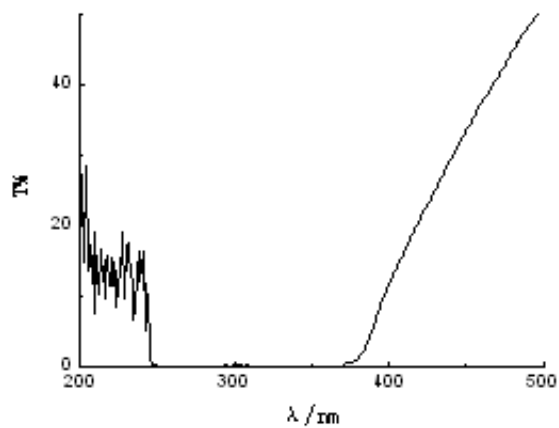
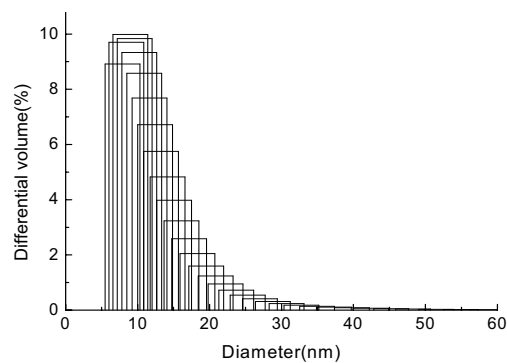
- AS/NZS 43991996 Sun protective Clothing-Evaluation and classification. Published jointly by Standards Australian and Standards New Zealand.
- Cao, Jianjun, Guo, Gang & Wang, Binhua. (2005). Use rutile Nano-TiO<sub>2</sub> to improve the photo-ageing performance of powder coating material. *Iron steel vanadium titanium*, Vol. 26, No.1, 2005, p. 34239.
- Deng, Hua, Deng Baoxiang and Xiao, Changfa. (2007). Nano-materials in UV protection textiles. *Textile Asia*. June 2007, p. 40-42.
- Diffey, B. Climate change. (2004). Ozone depletion and the impact on ultraviolet exposure of human skin. *Physics in Medicine and Biology*, Vol. 49, No.1, 2004, p. R1-R11.
- Li, Haixia & Deng, Hua. (2008). Preparation of Nano-titanium dioxide and its application in cotton fabric. *The eighth symposium of functional textiles and nanotechnology*, April 2008, p. 70-73.
- Sliney, D.H. (2000). Ultraviolet radiation exposure criteria. *Radiation Protection Dosimetry*, No. 91, p. 213-228.
- Wang, Shimin, Xu, Zuxun & Fu, Jing. *Nanometer material preparing technology*, Beijing: Chemistry Industry Press. P. 230-234.
- Wu, Dacheng & Du, Zhongliang and Gao Xushan. (2003). *Nanometer fiber*. Beijing: Chemistry Industry Press.
- Xin J H & Daoud W A. (2004). A new approach to UV-Blocking treatment for cotton fabrics, Vol. 72, No. 2, TRJ, 2004, p. 97-100.
- Yalpani, M, Johnson, F & Roblnson, L E. (1995). Advances in chitin and chitosan. *Elsevier Applied Science*, 1995, p. 543-561.
- Zhao, Jiayang. (2002) The status quo of skin protecting fabrics research in Japan. *Textile Science Research*, Vol. 13, No. 2, 2002, p. 31- 34.

Table 1. Anti-ultraviolet performance of the finished and unfinished fabrics

Sample	UVA blockage%	UVB blockage%	UPF value	UPF rate
Unfinished fabrics	81.4	95.6	15.1	15
① Finished fabrics	84.5	96.2	17.4	15
② Finished fabrics	94.3	98.8	65.3	50+

Table 2. Strength comparison of fabrics

Sample	F(N)	ΔL(mm)	L(%)	W(J)	T(s)
Original polyester fabric	227.7	20.8	20.80	2.3	12.48
Polyester fabric finished	225.9	21.2	21.20	2.3	12.75

Figure 1. UV-absorbance spectra of Nano-TiO<sub>2</sub> solFigure 2. UV-transmission spectra of Nano-TiO<sub>2</sub> solFigure 3. The Nano-TiO<sub>2</sub> particle size distribution

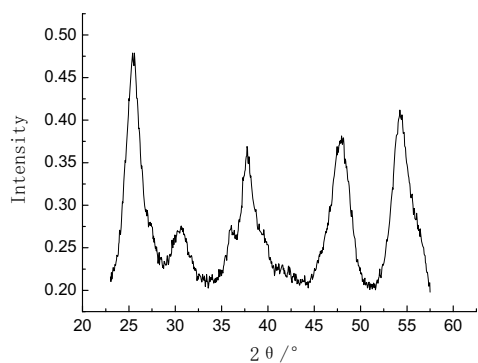


Figure 4. X-ray diffraction patterns of Nano-TiO<sub>2</sub> crystals

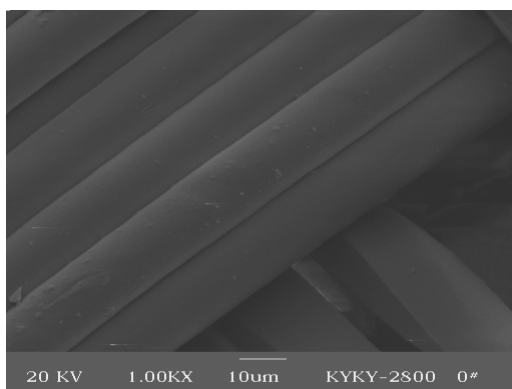


Figure 5. SEM image of the surface distribution of unfinished polyester fabrics

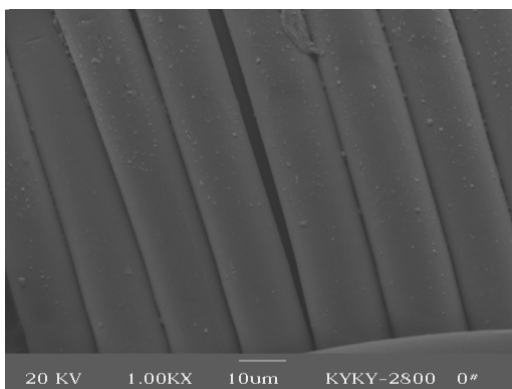


Figure 6. SEM image of the surface distribution of finished polyester fabrics



## Synthesis of $\beta$ -Lactam Fused Eneidyne by Intramolecular Kinugasa Reaction: Comparison of Reactivity with Monocyclic Analogues

Amit Basak (Corresponding author)

Department of Chemistry, Indian Institute of Technology

Kharagpur 721 302, India

Tel: 91-3222-283-301 E-mail: absk@chem.iitkgp.ernet.in

Runa Pal

Department of Chemistry, Indian Institute of Technology

Kharagpur 721 302, India

Sanket Das

Department of Chemistry, Indian Institute of Technology

Kharagpur 721 302, India

*The research is financed by DST, Government of India. (Sponsoring information)*

### Abstract

$\beta$ -lactam fused eneidyne have been successfully synthesized by intramolecular Kinugasa reaction in moderate yields. DSC studies indicated significant influence of the  $\beta$ -lactam ring upon the reactivity of eneidyne. None of the  $\beta$ -lactam fused eneidyne (under ring opening conditions) as well as the 11-membered monocyclic eneidyne as the tosylate salt showed any cleavage of plasmid DNA. Interestingly, the 10-membered eneidyne as the tosylate salt cleaved both single and double strands of plasmid DNA at micromolar concentration.

**Keywords:** Eneidyne,  $\beta$ -lactam, Kinugasa reaction, Hybrid, Plasmid DNA

### 1. Introduction

N-containing cyclic eneidyne including the  $\beta$ -lactam fused ones, are potential candidates for evaluation as antitumor and antibiotic agents.<sup>10</sup> The N-atom in monocyclic eneidyne serves as a handle for incorporation of various appendages. The advantage of using  $\beta$ -lactam as a molecular lock<sup>10,6</sup> lies in the fact that it imparts the strain to the fused eneidyne system, thereby preventing it from undergoing Bergman cyclisation<sup>4</sup> and the 4-membered lactam can be easily opened up by nucleophiles (thiol) or enzymes like transpeptidase or  $\beta$ -lactamase or under basic conditions for activation. Because of the instability of both the  $\beta$ -lactam ring as well as the cyclic eneidyne, the previously reported synthesis of these "lacteneidyne" by Guanti *et al.*<sup>1</sup> (via route a and b) and our group<sup>3</sup> (via route a and c) and may not be the ideal choice (Scheme 1). The concerted formation of both eneidyne and  $\beta$ -lactam rings via route d, has the advantage of not handling the sensitive  $\beta$ -lactam or cyclic eneidyne until the last step. In a preliminary communication<sup>11</sup>, we have reported the one step synthesis of  $\beta$ -lactam fused eneidyne via Kinugasa reaction.<sup>5,8</sup> In this paper, we describe the full experimental details for the synthesis of both the aromatic and non-aryl  $\beta$ -lactam fused eneidyne (1-8) along with their reactivity (thermal and biological) which were compared with the corresponding monocyclic eneidyne 10-11. Incidentally, the eneidyne 9, a counterpart of the aromatic eneidyne 7 could not be prepared.

<Space for Scheme 1>

Kinugasa reaction is a simple [3+2] cycloaddition between a nitron and *in situ* generated Cu (I) - acetylide producing both *cis* and *trans* isomers. The reaction has the advantage for its mild condition and also the availability of large repertoire of nitrones and alkynes makes it quite attractive. In 2003 Fu *et al.*<sup>12</sup> first reported the intramolecular Kinugasa reaction. Ours is only the second report of intramolecular Kinugasa reaction applied to the synthesis of  $\beta$ -lactam fused eneidyne.

<Space Figure 1>

Since intramolecular Kinugasa reaction is the final step, the construction of an acyclic enediyne with one arm carrying the nitron while the other terminal acetylene was required. The synthesis of the oxacyclic enediynes were first attempted because of easy accessibility of the precursor. For 1 the following steps are involved: i) Sonogashira coupling<sup>13</sup> to construct the acyclic enediyne framework ii) O-propargylation, iii) generation of the nitron by functional group modification. The final Kinugasa reaction was carried out by dissolving the nitron 17 in deoxygenated acetonitrile at 0 °C (c 0.003M) followed by addition of cuprous iodide (0.5 eq) and triethyl amine (1 eq) and stirring for 24 h at 15 °C. The desired  $\beta$ -lactams 1 and 2 were isolated by careful chromatography over Si-gel and finally purified by hplc (ODS column, H<sub>2</sub>O/MeOH, 5%). A third slower running compound characterized as the elimination product 5 was isolated (Scheme 2). It is interesting to note that the higher homologous nitron 23 when subjected to similar conditions produced only the *cis* and the *trans*  $\beta$ -lactams 3 and 4 respectively; no such elimination product was isolated (Scheme 3).

<Space for Scheme 2-7>

We then turned our attention to the synthesis of the 11-membered enediyne systems 6 and 33. For this the precursor nitron 32 was prepared as shown in Scheme 4. When this nitron was subjected to Kinugasa reaction conditions, two  $\beta$ -lactam containing products were isolated. One is the *trans* fused system 6 and the other was the elimination product 7. Gratifyingly the reaction was much cleaner and the yields were better than what were obtained in case of the synthesis of the oxacycles. Similar strategy has been adopted to synthesize the non-aromatic  $\beta$ -lactam fused enediynes. The nitron 44 under Kinugasa reaction condition gave only one product namely the *trans* fused hydroxyl-containing isomer 8 (Scheme 5). No elimination product 9 could be isolated. Perhaps the incorporation of double bond in the 11-membered enediyne framework makes the system too unstable for isolation. It was unfortunate to note that all our attempts to induce the intramolecular Kinugasa reaction for the synthesis of the 10-membered  $\beta$ -lactam fused enediyne 46 were not successful; the nitron 45 decomposing under the reaction conditions.

For the synthesis of monocyclic enediynes 10-11, our reported method\* based on intramolecular N-alkylation was used. Both the 10 and 11-membered cyclic enediynes were deprotected and the free amines were isolated as the tosylate salts 10c and 11c.

### 1.1 Characterization

The structures of both the compounds were determined by NMR, IR and mass spectroscopic data. The stereochemistry was confirmed by extensive decoupling experiments. Thus for compound 2, upon irradiation of the H-5 methylene, the signal for the H-4 appearing as a broad signal in the range  $\delta$  4.17-4.14, collapsed to a narrow singlet with half-width of 2.3 Hz, which indicated *trans* stereochemistry.<sup>9</sup> For the compound 1, similar irradiation collapsed the signal for the H-4 into a doublet of coupling constant 5 Hz confirming the *cis* stereochemistry. For this compound the H-3 and H-4 protons appeared in the range of  $\delta$  3.86-3.70 as complex multiplet. For the elimination product 5 characteristic<sup>2</sup> broad singlets at  $\delta$  5.75 and 5.21 for the exomethylene hydrogens appeared.

The structures of the *trans* fused  $\beta$ -lactam 6 and the elimination product 7 were confirmed by decoupling experiment, <sup>13</sup>C and HRMS analysis. For compound 6 the carbinol proton came at  $\delta$  4.89 as doublet with  $J = 10.0$  Hz, the NCH<sub>2</sub>Ph appeared as separate double doublets at  $\delta$  4.71 and 4.08 ( $J = 15.0$  Hz). H-4 appeared as a multiplet at  $\delta$  3.51 and H-3 as a dd at  $\delta$  3.36 with  $J$  values of 15.0 and 2.5 Hz. The coupling constant of 2.5 Hz indicated *trans* configuration. In the decoupling experiment, upon irradiation of H-13 the H-3 proton signal appeared as multiplet and irradiation of H-3 proton H-13 appeared as singlet and H-4 became a triplet. The assignments of chemical shifts and the coupling between the different protons is the elimination compound 7 has also been unambiguously settled by extensive decoupling experiments. The characteristic double bonded proton H-13 appeared at  $\delta$  6.28 as doublet with  $J$  value 1.5 Hz and H-4 at  $\delta$  3.98 as multiplet. Upon irradiation of H-4, H-13 changed to singlet and on irradiation of H-13, the pattern of H-4 changed to a dd confirming the elimination compound. Apparently the diastereomer 33 having *trans* relationship between the H-3 and carbinol OH, undergoes elimination under the reaction conditions which cannot happen for the major isomer 6.

The assignments of aliphatic  $\beta$ -lactam fused enediyne 8 were similarly done by decoupling experiment, <sup>13</sup>C and HRMS. In <sup>1</sup>H spectra characteristics H-3, H-4 proton appeared at  $\delta$  3.22 as dd ( $J = 2.5$  Hz) and 3.38 as multiplet, NCH<sub>2</sub>Ph appeared at  $\delta$  4.63, 3.98 as a separate double doublets with coupling constant 14.8 Hz. The CHOH proton resonates at  $\delta$  4.75 as doublet ( $J = 10.4$  Hz). The corresponding aromatic analogue was similarly characterized.

#### 1.1.1 Thermal reactivity

The thermal reactivity of both the aliphatic and aromatic  $\beta$ -lactam fused enediynes (6-8) was then studied. The onset temperatures for BC were determined using Differential Scanning Calorimetric measurements (DSC). The enediynes 6 and 7 showed the onset temperature of BC at 207 °C and 192 °C respectively.

The slight lowering of onset temperature of elimination compound can be attributed to be due to the incorporation of endocyclic double bond into the enediyne framework; however, the effect is not very significant. For the corresponding

aliphatic analogue 8 the exothermic rise started at  $\sim 79$  °C. This experimental result is in agreement with the fact that on going from aromatic to corresponding aliphatic analogue there is a substantial drop in onset temperature and thus lowering the activation barrier of BC. The reactivity of the  $\beta$ -lactam fused enediyne was then compared with the 11-membered N-substituted enediyne which revealed little difference in reactivity as recorded by DSC. The various onset temperatures for BC are shown in Table 1.

### 1.1.2 DNA Cleavage Activity

The higher reactivity of the  $\beta$ -lactam fused aliphatic enediyne prompted us to check whether it possesses any DNA-cleaving activity. Gel electrophoresis experiment carried out at 37 °C, however, revealed no such activity even at millimolar concentration. Since the free amine as salts are activated towards BC, the tosylate salt of the 11-membered enediynyl amine was also prepared and the onset temperature for BC was recorded which came out to be 100 °C. Although there is considerable lowering of activation barrier, the extent of lowering is not sufficient to bring down the reactivity to the level of room temperature. Consequently, it also failed to show any DNA-cleavage activity. Interestingly, the tosylate salt of the corresponding 10-membered enediynyl amine having a half life of 12 h at 30 °C turned out to be a potent DNA cleaving agent at micromolar concentration; the cleavage also produced significant proportion of Form III corresponding to double strand cleavage (Figure 2).

### 1.1.3 Experimental

#### Synthesis of 2-{5-[2-(3-Prop-2-ynyloxy-prop-1-ynyl)-phenyl]-pent-4-ynyloxy}-tetrahydro-pyran (14)

To a suspension of sodium hydride (60% suspension in mineral oil, before using it was washed with petroleum ether to remove the oil, 250 mg, 10.4 mmol) in THF, solution of 3-{2-[5-(Tetrahydro-pyran-2-yloxy)-pent-1-ynyl]-phenyl}-prop-2-yn-1-ol (13) (1.55 gm, 5.20 mmol) in THF (15 ml) was added dropwise at 0 °C and the solution was stirred for 30 minutes at 0 °C. Propargyl bromide (537  $\mu$ l, 6.24 mmol) dissolved in THF was added dropwise. The mixture was stirred for 4 hours at room temperature. Evaporation in vacuum gave solid mass which was quenched with  $\text{NH}_4\text{Cl}$  and extracted with EtOAc (50 ml). The organic layer was washed with brine (50 ml) and dried over  $\text{Na}_2\text{SO}_4$ . Evaporation in vacuum gave an oil from which the title compound (14) was isolated by column chromatography (Si-gel, PE: EA = 25:1) as a yellowish oil; Yield: 1.49 gm, 85%; State: yellow oil;  $\nu_{\text{max}}$  (neat) 3293, 3014, 2947, 2117, 1719, 1508, 1480, 1443, 1347, 1269 and 1028  $\text{cm}^{-1}$ ;  $\delta_{\text{H}}$  1.96-1.52 [8H, m,  $\text{CCCH}_2\text{CH}_2\text{CH}_2$ ,  $\text{CH}_2\text{CH}_2\text{CH}_2$  (pyran)], 2.48 (1H, t,  $J = 2.4$  Hz,  $\text{OCH}_2\text{CCH}$ ), 2.59 (2H, t,  $J = 7.0$  Hz,  $\text{CCCH}_2\text{CH}_2$ ), 3.62-3.45 [2H, m,  $-\text{OCH}_2\text{CH}_2$  (pyran)], 3.96-3.82 (2H, m,  $\text{CH}_2\text{CH}_2\text{OTHP}$ ), 4.38 (2H, d,  $J = 2.4$  Hz,  $\text{OCH}_2\text{CCH}$ ), 4.55 (2H, s,  $\text{CCCH}_2\text{O}$ ), 4.62 [1H, t,  $J = 2.8$  Hz, OCH (pyran)], 7.28-7.16 (2H, m, Ar-H), 7.44-7.37 (2H, m, Ar-H);  $\delta_{\text{C}}$  16.5, 19.4, 25.4, 28.8, 30.6, 56.1, 57.2, 62.1, 65.9, 74.9, 79.0, 79.4, 85.8, 87.3, 93.9, 98.7, 124.6, 126.5, 127.2, 127.3, 131.7, 131.8; Mass (ESI)  $m/z$  336 ( $\text{M}^+$ ).

#### Synthesis of 5-[2-(3-Prop-2-ynyloxy-prop-1-ynyl)-phenyl]-pent-4-yn-1-ol (15)

To a solution of compound 14 (1.50 gm, 4.46 mmol) in dry ethanol (20 ml) pyridinium *p*-toluene sulfonate (PPTS) (112 mg, 0.45 mmol) was added and stirred for 8 h at room temperature. Solvent was removed under vacuum and the title compound (15) was isolated by column chromatography (Si-gel, PE: EA= 3:1) as a very pale yellow viscous liquid; Yield: 876 mg, 78%; State: pale yellow;  $\nu_{\text{max}}$  (neat) 3447, 2960, 2224, 1709, 1262, 1185, 1097, 760 and 667  $\text{cm}^{-1}$ ;  $\delta_{\text{H}}$  1.94-1.87 (2H, m,  $\text{CCCH}_2\text{CH}_2\text{CH}_2\text{OH}$ ), 2.52 (1H, t,  $J = 2.4$  Hz,  $\text{OCH}_2\text{CCH}$ ), 2.63 (2H, t,  $J = 6.7$  Hz,  $\text{CCCH}_2\text{CH}_2\text{CH}_2\text{OH}$ ), 3.90 (2H, t,  $J = 6.2$  Hz,  $\text{CH}_2\text{CH}_2\text{OH}$ ), 4.41 (2H, d,  $J = 2.4$  Hz,  $\text{OCH}_2\text{CCH}$ ), 4.59 (2H, s,  $\text{CCCH}_2\text{O}$ ), 7.29-7.24 (2H, m, Ar-H), 7.45-7.41 (2H, m, Ar-H);  $\delta_{\text{C}}$  15.9, 31.0, 56.3, 57.3, 61.3, 75.1, 78.9, 79.7, 85.9, 87.3, 93.8, 124.6, 126.4, 127.3, 128.2, 131.7, 131.9; Mass (ESI)  $m/z$  252 ( $\text{M}^+$ ).

#### Synthesis of 5-[2-(3-Prop-2-ynyloxy-prop-1-ynyl)-phenyl]-pent-4-ynal (16)

To a solution of 5-[2-(3-Prop-2-ynyloxy-prop-1-ynyl)-phenyl]-pent-4-yn-1-ol 15 (791 mg, 3.14 mmol) in dry DCM (15 ml), PCC (1.01 gm, 4.71 mmol) was added and stirred for 3 h at room temperature under argon. The mixture was filtered through silica gel bed, which was thoroughly washed with DCM and the combined filtrate and washings were evaporated. The titled compound 16 was isolated by column chromatography (Si gel, PE: EA = 7:1) as a pale brown oil; Yield: 510 mg, 65%; State: pale brown oil;  $\nu_{\text{max}}$  (neat) 3448, 2919, 2226, 1718, 1218, 1078 and 761  $\text{cm}^{-1}$ ;  $\delta_{\text{H}}$  2.47 (1H, t,  $J = 2.4$  Hz,  $\text{OCH}_2\text{CCH}$ ), 2.79 (4H, s,  $\text{CH}_2\text{CH}_2\text{CHO}$ ), 4.38 (2H, d,  $J = 2.4$  Hz,  $\text{OCH}_2\text{CCH}$ ), 4.54 (2H, s,  $\text{CCCH}_2\text{O}$ ), 7.26-7.21 (2H, m, Ar-H), 7.42-7.36 (2H, m, Ar-H), 9.87 (1H, s,  $\text{CH}_2\text{CHO}$ );  $\delta_{\text{C}}$  12.8, 42.4, 56.2, 57.2, 74.9, 78.9, 79.9, 85.6, 87.5, 92.0, 124.8, 125.9, 127.5, 128.2, 131.8, 131.9, 200.4; Mass (ESI)  $m/z$  250 ( $\text{M}^+$ ).

#### Synthesis of 5-[2-(3-Prop-2-ynyloxy-prop-1-ynyl)-phenyl]-pent-4-ynyl-N-benzyl nitron (17)

To a solution of 5-[2-(3-Prop-2-ynyloxy-prop-1-ynyl)-phenyl]-pent-4-ynal (16) (550 mg, 2.20 mmol) in dry MeOH (20 ml) N-benzyl hydroxylamine (406 mg, 3.30 mmol) was added and stirred for 2 h at room temperature under argon atmosphere. Evaporation in vacuum gave an oily residue from which title compound 17 was isolated by column chromatography (Si-gel, PE: EA = 1:4) as brown oil; Yield: 625 mg, 80%; State: brown oil;  $\delta_{\text{H}}$  2.49 (1H, t,  $J = 2.0$  Hz,

OCH<sub>2</sub>CCH), 2.87-2.74 (4H, m, CCCH<sub>2</sub>CH<sub>2</sub>CH<sub>2</sub>), 4.31 (2H, d, *J* = 2.2 Hz, OCH<sub>2</sub>CCH), 4.48 (2H, s, CCCH<sub>2</sub>O), 5.04 (2H, s, NCH<sub>2</sub>Ph), 7.45-7.17 [10H, m, Ar-H, CHN (O) CH<sub>2</sub>Ph];  $\delta_c$  15.8, 26.1, 43.0, 56.3, 57.3, 68.9, 75.2, 78.9, 80.4, 85.7, 87.5, 92.2, 124.7, 125.8, 127.6, 128.2, 128.8, 128.8, 129.2, 129.3, 131.8, 132.4; Mass (ESI) *m/z* 355 (*M*<sup>+</sup>).

Synthesis of Sulfuric acid methyl ester 3-{2-[5-(tetrahydro-pyran-2-yloxy)-pent-1-ynyl]-phenyl}-prop-2-ynyl ester (18)

To a solution of 3-{2-[5-(Tetrahydro-pyran-2-yloxy)-pent-1-ynyl]-phenyl}-prop-2-yn-1-ol (13) (1.26 gm, 4.23 mmol) in CH<sub>2</sub>Cl<sub>2</sub> (20 ml) at 0 °C, methane sulfonyl chloride (490  $\mu$ l, 6.34 mmol) and triethyl amine (882  $\mu$ l, 6.34 mmol), were added. The reaction mixture was stirred for 15 mins at room temperature after which it was poured into water (50 ml) and extracted with CH<sub>2</sub>Cl<sub>2</sub> (2 x 50 ml). The organic layer was washed with water (2 x 50 ml), dried and then evaporated. The residue on chromatography (Si-gel, hexane: EtOAc = 2:1) furnished the title compounds (18) as pale yellow oil; Yield: 1.41 gm, 85%; State: pale yellow oil;  $\delta_H$  1.97-1.58 [8H, m, CCCH<sub>2</sub>CH<sub>2</sub>CH<sub>2</sub>, CH<sub>2</sub>CH<sub>2</sub>CH<sub>2</sub> (pyran)], 2.60 (2H, t, *J* = 7.0 Hz, CCCH<sub>2</sub>CH<sub>2</sub>CH<sub>2</sub>), 3.14 (3H, s, OSO<sub>2</sub>CH<sub>3</sub>), 3.61-3.45 (2H, m, OCH<sub>2</sub>CH<sub>2</sub>OHP), 3.91-3.85 (2H, m, CCCH<sub>2</sub>CH<sub>2</sub>CH<sub>2</sub>OHP), 4.62 (1H, t, *J* = 2.8 Hz, OCH-Pyran), 5.03 (2H, s, CH<sub>2</sub>OMs), 7.26-7.19 (2H, m, Ar-H), 7.40-7.36 (2H, m, Ar-H); Mass (ESI) *m/z* 392 (*M*<sup>+</sup>).

Synthesis of 2-{5-[2-(3-Bromo-prop-1-ynyl)-phenyl]-pent-4-ynyloxy}-tetrahydro-pyran (19)

To a solution of mesylate 18 (1.4 gm, 3.57 mmol) in dry THF (20 ml) at 0 °C, LiBr (463 mg, 5.36 mmol) was added to it and stirred at 0 °C for 3 h. After completion of the reaction it was poured onto a saturated solution of NaHCO<sub>3</sub> (25 ml). The layers were separated and the aqueous layer was extracted with EtOAc. The combined organic extracts were washed with brine, dried over Na<sub>2</sub>SO<sub>4</sub>, and concentrated *in vacuo*. The crude oil was purified *via* chromatography (Si-gel, hexane: EtOAc = 25:1) to yield the bromide compound 19; Yield: 1.03 gm, 80%; State: yellow oil;  $\delta_H$  1.98-1.58 [8H, m, CCCH<sub>2</sub>CH<sub>2</sub>CH<sub>2</sub>, CH<sub>2</sub>CH<sub>2</sub>CH<sub>2</sub> (pyran)], 2.60 (2H, t, *J* = 7.0 Hz, CCCH<sub>2</sub>CH<sub>2</sub>CH<sub>2</sub>), 3.61-3.45 (2H, m, OCH<sub>2</sub>CH<sub>2</sub>OHP), 3.91-3.85 (2H, m, CCCH<sub>2</sub>CH<sub>2</sub>CH<sub>2</sub>OHP), 4.23 (2H, s, CCCH<sub>2</sub>Br), 4.62 [1H, t, *J* = 2.8 Hz, OCH (Pyran)], 7.26-7.19 (2H, m, Ar-H), 7.40-7.36 (2H, m, Ar-H);  $\delta_c$  15.3, 16.6, 19.5, 25.5, 28.9, 30.7, 62.2, 65.9, 79.3, 85.7, 87.5, 94.4, 98.8, 124.5, 126.8, 127.2, 128.4, 131.8, 132.0; Mass (ESI) *m/z* 363, 361 (*M*<sup>+</sup>).

Synthesis of 2-{5-[2-(3-But-3-ynyloxy-prop-1-ynyl)-phenyl]-pent-4-ynyloxy}-tetrahydro-pyran (20)

To a suspension of sodium hydride (80 mg, 3.33 mmol) in THF, solution of 3-butyn-1-ol (251  $\mu$ l, 3.33 mmol) in THF (5 ml) was added dropwise at 0 °C and it was stirred for 30 minutes at 0 °C. Then 2-{5-[2-(3-Bromo-prop-1-ynyl)-phenyl]-pent-4-ynyloxy}-tetrahydro-pyran (19) (1 gm, 2.77 mmol) dissolved in THF (15 ml) was added dropwise. It was stirred for 4 hours at room temperature. Evaporation in vacuum gave a solid mass which was quenched with NH<sub>4</sub>Cl and extracted with EtOAc (50 ml). The organic layer was washed with brine (50 ml) and dried over Na<sub>2</sub>SO<sub>4</sub>. Evaporation in vacuum gave an oil from which the title compound 20 was isolated by column chromatography (Si-gel, PE: EA = 25:1) as a yellowish oil; Yield: 679 mg, 70%; State: yellow liquid;  $\nu_{max}$  (neat) 3293, 3014, 2947, 2117, 1719, 1508, 1480, 1443, 1347, 1269 and 1028 cm<sup>-1</sup>;  $\delta_H$  1.95-1.54 [8H, m, CCCH<sub>2</sub>CH<sub>2</sub>CH<sub>2</sub>, CH<sub>2</sub>CH<sub>2</sub>CH<sub>2</sub> (pyran)], 2.00 (1H, t, *J* = 2.8 Hz, OCH<sub>2</sub>CCH), 2.62-2.49 (4H, m, CCCH<sub>2</sub>CH<sub>2</sub>CH<sub>2</sub>, OCH<sub>2</sub>CH<sub>2</sub>CCH), 3.59-3.54 [2H, m, OCH<sub>2</sub>CH<sub>2</sub> (pyran)], 3.93-3.74 (4H, m, CH<sub>2</sub>CH<sub>2</sub>OHP, OCH<sub>2</sub>CH<sub>2</sub>CCH), 4.47 (2H, s, OCH<sub>2</sub>CCH), 4.62 [1H, t, *J* = 2.8 Hz, OCH (pyran)], 7.25-7.20 (2H, m, Ar-H), 7.41-7.37 (2H, m, Ar-H);  $\delta_c$  16.6, 19.5, 19.7, 25.5, 29.0, 30.7, 58.9, 62.1, 65.9, 67.6, 69.4, 79.5, 81.1, 85.5, 88.2, 93.9, 98.8, 124.9, 126.5, 127.2, 128.1, 131.8, 131.9; Mass (ESI) *m/z* 350 (*M*<sup>+</sup>).

Synthesis of 5-[2-(3-But-3-ynyloxy-prop-1-ynyl)-phenyl]-pent-4-yn-1-ol (21)

Procedure same as 15; Yield: 297 mg, 78%; State: pale yellow;  $\nu_{max}$  (neat) 3447, 2960, 2224, 1709, 1262, 1185, 1097, 761, 667 cm<sup>-1</sup>;  $\delta_H$  1.91-1.77 (2H, m, CCCH<sub>2</sub>CH<sub>2</sub>CH<sub>2</sub>OH), 1.99 (1H, t, *J* = 2.6 Hz, OCH<sub>2</sub>CCH), 2.61-2.49 (4H, m, CCCH<sub>2</sub>CH<sub>2</sub>CH<sub>2</sub>OH, OCH<sub>2</sub>CH<sub>2</sub>CCH), 3.89-3.72 (4H, m, CH<sub>2</sub>CH<sub>2</sub>OH, OCH<sub>2</sub>CH<sub>2</sub>CCH), 4.47 (2H, s, CCCH<sub>2</sub>O), 7.24-7.19 (2H, m, Ar-H), 7.43-7.35 (2H, m, Ar-H);  $\delta_c$  16.1, 19.7, 31.2, 58.9, 60.4, 67.9, 69.6, 79.8, 81.0, 85.5, 88.1, 93.8, 124.9, 126.4, 127.3, 128.2, 131.8, 132.0; Mass (ESI) *m/z* 266 (*M*<sup>+</sup>).

Synthesis of 5-[2-(3-But-3-ynyloxy-prop-1-ynyl)-phenyl]-pent-4-ynal (22)

Procedure same as 16; Yield: 323 mg, 65%; State: pale brown oil;  $\nu_{max}$  (neat) 3448, 2919, 2226, 1718, 1218, 1078, 761 cm<sup>-1</sup>;  $\delta_H$  2.00 (1H, t, *J* = 2.4 Hz, OCH<sub>2</sub>CH<sub>2</sub>CCH), 2.59-2.50 (2H, m, OCH<sub>2</sub>CH<sub>2</sub>CCH), 2.79 (4H, s, CH<sub>2</sub>CH<sub>2</sub>CHO), 3.77 (2H, t, *J* = 7.0 Hz, OCH<sub>2</sub>CH<sub>2</sub>CCH), 4.47 (2H, s, CCCH<sub>2</sub>O), 7.25-7.21 (2H, m, Ar-H), 7.41-7.36 (2H, m, Ar-H), 9.87 (1H, s, -CH<sub>2</sub>CHO);  $\delta_c$  12.6, 19.4, 42.1, 58.6, 67.4, 69.1, 80.1, 80.7, 84.9, 87.9, 91.6, 124.6, 125.6, 127.2, 127.8, 131.5, 131.6, 200.1; Mass (ESI) *m/z* 264 (*M*<sup>+</sup>).

Synthesis of 5-[2-(3-But-3-ynyloxy-prop-1-ynyl)-phenyl]-pent-4-ynyl-N-benzyl nitrene (23)

Procedure same as 17; Yield: 447 mg, 80%; State: brown oil;  $\delta_H$  1.99 (1H, t, *J* = 2.6 Hz, OCH<sub>2</sub>CH<sub>2</sub>CCH), 2.55-2.47 (2H, m, CCCH<sub>2</sub>CH<sub>2</sub>CH<sub>2</sub>), 2.81-2.71 (4H, m, CCCH<sub>2</sub>CH<sub>2</sub>, OCH<sub>2</sub>CH<sub>2</sub>CCH), 3.73 (2H, t, *J* = 7.0 Hz, OCH<sub>2</sub>CH<sub>2</sub>CCH), 4.41 (2H, s, CCCH<sub>2</sub>O), 4.93 (2H, s, NCH<sub>2</sub>Ph), 6.96 [1H, t, *J* = 8.4 Hz, CHN (O) CH<sub>2</sub>Ph], 7.45-7.22 (9H, m, Ar-H);  $\delta_c$  11.6, 15.4, 21.8, 25.3, 54.6, 63.5, 65.2, 76.1, 76.7, 80.9, 83.9, 88.0, 95.2, 120.6, 121.6, 123.3, 123.8, 123.9, 124.6, 124.9,

127.6, 127.7, 128.4; Mass (ESI)  $m/z$  369 ( $M^+$ ).

#### Synthesis of {2-[5-(Tetrahydro-pyran-2-yloxy)-pent-1-ynyl]-phenyl}-propynal (24)

To a solution of alcohol (13) (900 mg, 3.01 mmol) in dry DCM was added Dess- Martin reagent (1.54 gm, 3.62 mmol) under argon atmosphere and the mixture stirred at room temperature in the dark for 4 h. The reaction mixture was diluted with ethyl acetate and the oxidant quenched with a saturated solution of  $Na_2S_2O_3$ . The organic layer was washed (sat.  $NaHCO_3$ ), dried over  $Na_2SO_4$ , filtered and concentrated. Evaporation in vacuum gave oil from which the title compound (24) was isolated by column chromatography (Si-gel, PE: EA = 15:1) as a brown oil. Yield: 858 mg, 96%; State: yellow oil;  $\nu_{max}$  (neat) 3016, 2945, 2187, 1719, 1656, 1354, 1216, 1032, 759  $cm^{-1}$ ;  $\delta_H$  1.96-1.52 [8H, m,  $CCCH_2CH_2$ ,  $CH_2CH_2CH_2$  (Pyran)], 2.61 (2H, t,  $J = 7.0$  Hz,  $CCCH_2CH_2CH_2$ ), 3.61-3.45 [2H, m,  $OCH_2CH_2$  (pyran)], 3.96-3.80 (2H, m,  $CH_2OTHP$ ), 4.62 [1H, t,  $J = 2.8$  Hz, O-CH (pyran)], 7.80-7.35 (4H, m, Ar-H), 9.46 (1H, s,  $CCCHO$ ); Mass (ESI)  $m/z$  296 ( $M^+$ ).

#### Synthesis of 1-{2-[5-(Tetrahydro-pyran-2-yloxy)-pent-1-ynyl]-phenyl}-5-trimethylsilanyl-penta-1, 4-diyne-3-ol (25)

Dry degassed THF (70 ml) was placed in a two neck round bottom flask under argon atmosphere and temperature was reduced to 0 °C. Trimethylsilyl acetylene (1.023 ml, 7.39 mmol) was added and then n-butyllithium soln. in hexane (1.6 M in hexane) 4.62 ml (3 equivalent) was added dropwise. The mixture was stirred at 0 °C under argon atmosphere for 20 minutes. The aldehyde 24 (730 mg, 2.46 mmol) dissolved in dry degassed THF (5 ml) was added dropwise at that condition. Reaction was continued for 30 minutes at 0 °C and then quenched with aq.  $NH_4Cl$  soln. (30 ml). The mixture was poured into EtOAc (200 ml) and the organic layer was washed with saturated  $NaHCO_3$  soln. followed by brine (100 ml each) and dried over  $Na_2SO_4$  and then evaporated. Evaporation in vacuum gave oil from which the title compound (25) was isolated by column chromatography (Si-gel, PE: EA = 10:1) as a brown oil; Yield: 826 mg, 85%; State: brown oil;  $\nu_{max}$  (neat) 3432, 2946, 2206, 1623, 1443, 1293, 1137, 994  $cm^{-1}$ ;  $\delta_H$  0.06 (9H, s, TMS), 1.98-1.67 [8H, m,  $CCCH_2CH_2$ ,  $CH_2CH_2CH_2$  (Pyran)], 2.69-2.57 (2H, m,  $CCCH_2CH_2CH_2$ ), 3.75-3.54 [2H, m,  $OCH_2CH_2$  (OTHP)], 4.28-3.78 (2H, m,  $CCCH_2CH_2CH_2OTHP$ ), 4.78 [1H, bs, OCH (pyran)], 5.36 (1H, bs, CHOH), 7.29-7.16 (2H, m, Ar-H), 7.48-7.34 (2H, m, Ar-H);  $\delta_C$  19.1, 35.3, 37.7, 44.7, 48.4, 49.7, 72.1, 75.0, 80.9, 85.1, 99.4, 102.1, 109.6, 113.0, 117.6, 121.8, 144.1, 146.6, 146.9, 147.8, 151.5, 152.0; Mass (ESI)  $m/z$  394 ( $M^+$ ).

#### Synthesis of 1-{2-[5-(Tetrahydro-pyran-2-yloxy)-pent-1-ynyl]-phenyl}-penta-1,4-diyne-3-ol (26)

To a solution of the silylated compound 25 (700 mg, 1.78 mmol) in dry methanol (50 ml), potassium fluoride (205 mg, 3.54 mmol) was added and the mixture was stirred for 4 h at room temperature under argon atmosphere. Evaporation in vacuum gave oil from which the title compound (26) was isolated by column chromatography (Si-gel, PE: EA = 10:1) as a brown oil; Yield: 458 mg, 80%; State: brown oil;  $\delta_H$  1.97-1.54 [(8H, m,  $CCCH_2CH_2$ ,  $CH_2CH_2CH_2$  (Pyran)], 2.65-2.55 (3H, m,  $CCCH_2CH_2$   $CHOHCCH$ ), 3.76-3.75 [2H, m,  $OCH_2CH_2$  (OTHP)], 4.15-3.85 (2H, m,  $OCH_2CH_2$  (OTHP)], 4.75 (1H, bs, OCH (pyran)], 5.37 (1H, bs, CHOH), 7.29-7.19 (2H, m, Ar-H), 7.46-7.35 (2H, m, Ar-H);  $\delta_C$  16.2, 18.8, 25.2, 28.1, 30.3, 51.9, 61.5, 65.6, 72.1, 79.7, 81.5, 82.7, 89.5, 93.7, 97.9, 124.3, 125.1, 126.4, 128.0, 131.6, 132.3; Mass (ESI)  $m/z$  322 ( $M^+$ ).

#### Synthesis of tert-Butyl-(1-ethynyl-3-{2-[5-(tetrahydro-pyran-2-yloxy)-pent-1-ynyl]-phenyl}-prop-2-ynyloxy)-diphenyl-silane (27)

To a solution of 26 (650 mg, 2.02 mmol) in dry  $CH_2Cl_2$  (50 ml), imidazole (342 mg, 5.04 mmol) and then TBDPS-Cl (613  $\mu$ l, 2.42 mmol) were added at room temperature. After addition of DMAP (25 mg, 0.20 mmol), the mixture was stirred for 3 h. It was then poured into  $CH_2Cl_2$  (100 ml) and the organic layer was washed with 0.1 (N) HCl and brine (100 ml each), dried over  $Na_2SO_4$  and then evaporated. Evaporation in vacuum gave oil from which the title compound (27) was isolated by column chromatography (Si-gel, PE: EA = 25:1) as a brown oil; Yield: 904 mg, 80%; State: brown oil;  $\delta_H$  1.10 (9H, s, t-Bu of TBDPS), 1.96-1.56 [8H, m,  $CCCH_2CH_2$ ,  $CH_2CH_2CH_2$  (Pyran)], 2.35 (2H, t,  $J = 6.9$  Hz,  $CCCH_2CH_2CH_2$ ), 2.50 (1H, d,  $J = 2.4$  Hz, CCH), 3.75-3.70 [2H, m,  $OCH_2CH_2$  (pyran)], 4.15-3.80 (2H, m,  $CH_2OTHP$ ), 4.68 [1H, bs, OCH (pyran)], 5.37 (1H, d,  $J = 2.1$  Hz, CHOTBDPS), 7.38-7.30 (10H, m, Ar-H), 7.70-7.64 (4H, m, Ar-H);  $\delta_C$  19.0, 19.2, 24.8, 25.5, 26.0, 27.9, 31.5, 52.3, 62.3, 64.8, 71.9, 77.8, 80.1, 81.4, 90.6, 97.9, 120.8, 121.5, 122.8, 127.5, 127.6, 127.8, 127.8, 128.1, 128.3, 128.7, 129.6, 129.6, 130.5, 131.8, 134.6; Mass (ESI)  $m/z$  560 ( $M^+$ ).

#### Synthesis of 5-{2-[3-(tert-Butyl-diphenyl-silanyloxy)-penta-1, 4-diyne]-phenyl}-pent-4-yn-1-ol (28)

Procedure same as 15; Yield: 680 mg, 80%; State: yellow oil;  $\nu_{max}$  (neat) 3435, 2377, 2067, 1638  $cm^{-1}$ ;  $\delta_H$  1.11 (9H, s, t-Bu of TBDPS), 1.79 (2H, m,  $CCCH_2CH_2CH_2$ ), 2.51 (2H, t,  $J = 7.2$  Hz,  $CCCH_2CH_2$ ), 2.56 (1H, d,  $J = 2.4$  Hz, CCH), 3.80 (2H, t,  $J = 6.2$  Hz,  $CH_2CH_2CH_2OH$ ), 5.36 (1H, d,  $J = 2.1$  Hz, CHOTBDPS), 7.47-7.21 (10H, m, TBDPS), 7.84-7.77 (4H, m, Ar-H);  $\delta_C$  16.1, 19.3, 26.7, 31.0, 54.4, 61.5, 72.3, 79.6, 81.4, 83.2, 89.5, 93.9, 124.7, 126.6, 127.2, 127.7, 127.7, 128.3, 129.9, 130.0, 131.6, 132.1, 132.5, 132.8, 135.9, 135.9; Mass (ESI)  $m/z$  476 ( $M^+$ ).

#### 5-{2-[3-(tert-Butyl-diphenyl-silanyloxy)-penta-1,4-diyne]-phenyl}-pent-4-ynal (29)

Procedure same as described for 24; Yield: 1.14 gm, 95%; State: yellow oil;  $\nu_{max}$  (neat) 3433, 2377, 1638, 772  $cm^{-1}$ ;  $\delta_H$

1.11 (9H, s, t-Bu of TBDPS), 2.53 (1H, d,  $J = 2.2$  Hz, CCH), 2.68 (4H, s, CH<sub>2</sub>CH<sub>2</sub>CHO), 5.35 (1H, bs, CHOTBDPS), 7.43-7.22 (10H, m, Ar-H of TBDPS), 7.84-7.77 (4H, m, Ar-H), 9.75 (1H, s, CCCH<sub>2</sub>CH<sub>2</sub>CHO);  $\delta_C$  32.3, 38.8, 46.1, 62.0, 73.8, 91.7, 99.3, 100.8, 102.5, 109.1, 111.8, 144.2, 145.6, 146.9, 147.1, 147.2, 147.4, 147.8, 149.3, 149.5, 151.1, 151.5, 152.7, 152.9, 155.3, 220.0; Mass (ESI)  $m/z$  474 ( $M^+$ ).

#### Synthesis of 1-[2-(5, 5-Dimethoxy-pent-1-ynyl)-phenyl]-penta-1, 4-diyn-3-ol (30)

A solution of silylated compound (750 mg, 1.58 mmol) in 3% methanolic HCl (12N) (10 ml) was treated and the mixture was stirred for 2 h at room temperature. It was then partitioned between EtOAc and water (50 ml each). The organic layer was washed with saturated solution of NaHCO<sub>3</sub>, brine solution and dried (Na<sub>2</sub>SO<sub>4</sub>) and concentrated under vacuum at room temperature. After purification by column chromatography (Si-gel, PE: EA = 2:1), compound 30 was isolated as a pale yellow oil; Yield: 335 mg, 75%; State: pale yellow oil;  $\nu_{max}$  (neat) 3433, 2377, 1637, 1219, 771 cm<sup>-1</sup>;  $\delta_H$  2.00-1.90 (2H, m, CCCH<sub>2</sub>CH<sub>2</sub>CH<sub>2</sub>), 2.54 (2H, t,  $J = 6.6$  Hz, CCCH<sub>2</sub>CH<sub>2</sub>CH<sub>2</sub>), 2.57 (1H, d,  $J = 2.2$  Hz, CHOHCCH), 3.37 (6H, d,  $J = 3.0$  Hz, OCH<sub>3</sub>), 5.02 [1H, t,  $J = 5.8$  Hz, CH (OMe)<sub>2</sub>], 5.35 (1H, bs, CHOH), 7.37-7.19 (2H, m, Ar-H), 7.47-7.38 (2H, m, Ar-H);  $\delta_C$  15.3, 30.8, 52.3, 52.5, 72.7, 78.9, 81.5, 81.9, 92.8, 97.6, 102.8, 124.2, 125.0, 126.5, 128.6, 130.6, 133.2; Mass (ESI)  $m/z$ : 282 ( $M^+$ ).

#### Synthesis of 5-[2-(3-Hydroxy-penta-1,4-diynyl)-phenyl]-pent-4-ynal (31)

A solution of the compound 30 (600 mg, 2.13 mmol) in THF (30 ml) containing aqueous HCl (2M, 3 ml) was stirred for 6 hours at room temperature. The mixture was quenched with saturated NaHCO<sub>3</sub> (30 ml), and extracted with EtOAc. Drying over Na<sub>2</sub>SO<sub>4</sub> and evaporation gave the yellow oily material which was purified by column chromatography (Si-gel, PE: EA = 1:1). Yield: 427 mg, 85%; State: yellow oil;  $\nu_{max}$  (neat) 3433, 2079, 1637, 771 cm<sup>-1</sup>;  $\delta_H$  2.60 (1H, d,  $J = 2.0$  Hz, CHOHCCH), 2.80 (4H, s, CH<sub>2</sub>CH<sub>2</sub>CHO), 5.40 (1H, d,  $J = 2.4$  Hz, CHOH), 7.28-7.17 (2H, m, Ar-H), 7.44-7.34 (2H, m, Ar-H), 9.86 (1H, s, CH<sub>2</sub>CH<sub>2</sub>CHO);  $\delta_C$  12.6, 41.9, 51.9, 73.9, 80.9, 82.6, 87.3, 89.2, 92.4, 124.1, 126.0, 126.6, 128.7, 130.7, 133.2, 202.1; Mass (ESI)  $m/z$ : 236 ( $M^+$ ).

#### 5-[2-(3-Hydroxy-penta-1,4-diynyl)-phenyl]-pent-4-ynyl-N-benzyl nitron (32)

Yield: 686 mg, 95%; State: brown oil;  $\delta_H$  2.55 (1H, d,  $J = 2.4$  Hz, CCH), 2.88-2.68 (4H, m, CCCH<sub>2</sub>CH<sub>2</sub>), 4.95 (2H, s, NCH<sub>2</sub>Ph), 5.29 (1H, d,  $J = 2.2$  Hz, CHOH), 6.89 [1H, m, CH=N(O)CH<sub>2</sub>Ph], 7.44-7.18 (9H, m, Ar-H);  $\delta_C$  16.2, 26.2, 58.7, 68.8, 72.2, 80.8, 81.5, 81.6, 90.7, 92.6, 125.1, 125.8, 127.6, 128.2, 128.7, 128.8, 129.5, 131.4, 131.6, 132.1, 141.6; Mass (ESI)  $m/z$ : 341 ( $M^+$ ).

#### Synthesis of 2-(7-Chloro-hept-6-en-4-ynyloxy)-tetrahydro-pyran (34)

To a solution of *cis*-dichloroethylene (1 ml, 13.24 mmol) in dry degassed benzene (20 ml) at room temperature, Pd (PPh<sub>3</sub>)<sub>4</sub> (453 mg, 0.40 mmol) and *n*-BuNH<sub>2</sub> (3.93 ml, 52.95 mmol) were added and stirred for 5 mins under argon. CuI (503 mg, 2.65 mmol) was then added and the solution was stirred for 20 min followed by addition of THP protected 4-Pentyn 1-ol (2.43 gm, 14.55 mmol). The reaction was carried out for 2 hours. The mixture was then partitioned between EtOAc and aqueous NH<sub>4</sub>Cl (2 x 100 ml each). The combined organic layers were washed with aqueous NH<sub>4</sub>Cl (2 x 70 ml), dried (Na<sub>2</sub>SO<sub>4</sub>), and evaporated under reduced pressure. The product 34 was isolated as brown oil by column chromatography (Si-gel, PE: EA = 15: 1); Yield: 2.72 gm, 90%; State: brown oil;  $\delta_H$  1.89-1.51 [8H, m, CCCH<sub>2</sub>CH<sub>2</sub>CH<sub>2</sub>, CH<sub>2</sub>CH<sub>2</sub>CH<sub>2</sub> (Pyran)], 2.49 (2H, t,  $J = 7.0$  Hz, CCCH<sub>2</sub>CH<sub>2</sub>CH<sub>2</sub>), 3.54-3.43 [2H, m, OCH<sub>2</sub>CH<sub>2</sub> (pyran)], 3.89-3.76 (2H, m, CH<sub>2</sub>OHP), 4.59 [1H, t,  $J = 2.8$  Hz, OCH (pyran)], 5.81 (1H, td,  $J = 1.9, 7.3$  Hz, CHCHCl), 6.27 (1H, d,  $J = 7.4$  Hz, CHCl);  $\delta_C$  16.5, 19.4, 25.4, 28.7, 30.6, 62.1, 65.8, 74.8, 98.5, 98.8, 112.4, 126.9; Mass (ESI)  $m/z$ : 228 ( $M^+$ ).

#### Synthesis of 10-(Tetrahydro-pyran-2-yloxy)-dec-4-ene-2,6-diyn-1-ol (35)

Procedure same as described for 34; Yield: 2.32 gm, 88%; State: brown oil;  $\delta_H$  1.89-1.49 [8H, m, CCCH<sub>2</sub>CH<sub>2</sub>CH<sub>2</sub>, CH<sub>2</sub>CH<sub>2</sub>CH<sub>2</sub> (Pyran)], 2.53 (2H, t,  $J = 6.0$  Hz, CCCH<sub>2</sub>), 3.64-3.52 [2H, m, OCH<sub>2</sub>CH<sub>2</sub> (pyran)], 4.09-3.83 (2H, m, CH<sub>2</sub>OHP), 4.40 (2H, s, CCCH<sub>2</sub>OH), 4.73 [1H, t,  $J = 3.0$  Hz, OCH (pyran)], 5.77 (2H, s, CHCH);  $\delta_C$  16.4, 18.9, 25.4, 28.2, 30.4, 51.3, 61.6, 65.2, 78.9, 82.4, 94.9, 97.7, 98.3, 118.2, 120.5; Mass (ESI)  $m/z$ : 248 ( $M^+$ ).

#### Synthesis of 10-(Tetrahydro-pyran-2-yloxy)-dec-4-ene-2, 6-diynal (36)

Procedure same as described for 24; Yield: 1.13 gm, 95%; State: yellow oil;  $\delta_H$  1.94-1.24 [8H, m, CCCH<sub>2</sub>CH<sub>2</sub>, CH<sub>2</sub>CH<sub>2</sub>CH<sub>2</sub> (Pyran)], 2.58 (2H, t,  $J = 6.9$  Hz, CCCH<sub>2</sub>CH<sub>2</sub>CH<sub>2</sub>), 3.57-3.46 [2H, m, OCH<sub>2</sub>CH<sub>2</sub> (pyran)], 3.93-3.80 (2H, m, CH<sub>2</sub>OHP), 4.60 [1H, t,  $J = 3.2$  Hz, O-CH (pyran)], 5.87 (1H, d,  $J = 10.8$  Hz, CHCHCCCH<sub>2</sub>CH<sub>2</sub>), 6.13 (1H, dt,  $J = 2.4, 8.4$  Hz, CHCHCCCHO), 9.34 (1H, s, CCCHO);  $\delta_C$  16.8, 19.4, 25.4, 28.5, 30.6, 62.1, 65.7, 84.4, 91.7, 94.3, 98.8, 103.0, 114.9, 132.1, 176.5; Mass (ESI)  $m/z$  246 ( $M^+$ ).

#### Synthesis of 12-(Tetrahydro-pyran-2-yloxy)-1-trimethylsilyl-dodec-6-ene-1, 4, 8-triyn-3-ol (37)

Procedure same as described for 25; Yield: 1.19 gm, 85%; State: brown oil;  $\delta_H$  0.18 (9H, s, TMS-H), 1.86-1.56 [8H, m, CCCH<sub>2</sub>CH<sub>2</sub>CH<sub>2</sub>, CH<sub>2</sub>CH<sub>2</sub>CH<sub>2</sub> (Pyran)], 2.54 (2H, t,  $J = 6.1$  Hz, CCCH<sub>2</sub>CH<sub>2</sub>CH<sub>2</sub>), 3.64-3.58 [2H, m, OCH<sub>2</sub>CH<sub>2</sub> (pyran)],

4.21-3.90 (2H, m, CH<sub>2</sub>OTHP), 4.77 [1H, t, *J* = 3.2 Hz, OCH (pyran)], 5.26 (1H, bs, CHOH), 5.81 (2H, s, CH=CH); Mass (ESI) *m/z* 344 (M<sup>+</sup>).

Synthesis of 12-(Tetrahydro-pyran-2-yloxy)-dodec-6-ene-1, 4, 8-triyn-3-ol (38)

Procedure same as that of 26; Yield: 506 mg, 80%; State: yellow oil;  $\delta_{\text{H}}$  1.89-1.52 [8H, m, CCCH<sub>2</sub>CH<sub>2</sub>CH<sub>2</sub>, CH<sub>2</sub>CH<sub>2</sub>CH<sub>2</sub> (Pyran)], 2.63-2.49 (3H, m, CCCH<sub>2</sub>CH<sub>2</sub>CH<sub>2</sub>, CHOHCCH), 3.65-3.58 [2H, m, OCH<sub>2</sub>CH<sub>2</sub>(OTHP)], 4.19-3.93 (2H, m, CH<sub>2</sub>CH<sub>2</sub>CH<sub>2</sub>OTHP), 4.98-4.78 (1H, m, OCH (pyran)), 4.97 (1H, d, *J* = 8.8 Hz, CHOH), 5.25 (1H, d, *J* = 4.8 Hz, CH=CHCCCH<sub>2</sub>CH<sub>2</sub>), 5.86-5.77 (1H, m, CH=CHCCCHOH);  $\delta_{\text{C}}$  16.3, 18.5, 25.3, 27.9, 30.3, 52.0, 61.2, 65.1, 72.1, 79.0, 81.2, 81.4, 92.7, 97.6, 97.8, 117.6, 121.6; Mass (ESI) *m/z* 272 (M<sup>+</sup>).

Synthesis of tert-Butyl-[1-ethynyl-10-(tetrahydro-pyran-2-yloxy)-dec-4-ene-2,6-diynyl]-diphenyl-silane (39)

Procedure same as 27; Yield: 1.05 gm, 80%; State: yellow oil;  $\delta_{\text{H}}$  1.15 (9H, s, t-Bu of TBDPS), 1.76-1.41 [8H, m, CCCH<sub>2</sub>CH<sub>2</sub>CH<sub>2</sub>, CH<sub>2</sub>CH<sub>2</sub>CH<sub>2</sub> (Pyran)], 2.37 (2H, t, *J* = 6.9 Hz, CCCH<sub>2</sub>CH<sub>2</sub>CH<sub>2</sub>), 2.43 (1H, d, *J* = 2.4 Hz, CCH), 3.40-3.36 [2H, m, OCH<sub>2</sub>CH<sub>2</sub> (pyran)], 3.75-3.70 (2H, m, CH<sub>2</sub>OTHP), 4.49 [1H, t, *J* = 3.2 Hz, OCH (pyran)], 5.19 (1H, bs, CHOH), 5.66 (1H, dd, *J* = 1.2, 10.8 Hz, CH=CHCCCH<sub>2</sub>CH<sub>2</sub>), 5.76 (1H, d, *J* = 10.8 Hz, CH=CHCCCHOTBDPS), 7.38-7.30 (5H, m, Ar-H), 7.71-7.64 (5H, m, Ar-H);  $\delta_{\text{C}}$  19.3, 19.4, 25.4, 26.5, 26.6, 28.8, 30.6, 54.3, 62.1, 65.9, 72.3, 78.1, 81.1, 81.6, 92.7, 98.7, 117.3, 121.3, 121.4, 127.4, 127.6, 127.6, 127.7, 129.9, 130.0, 132.6, 134.8; Mass (ESI) *m/z* 510 (M<sup>+</sup>).

Synthesis of 10-(tert-Butyl-diphenyl-silanyloxy)-dodec-6-ene-4, 8, 11-triyn-1-ol (40)

Procedure same as 15; Yield: 802 mg, 80%; State: yellow viscous oil;  $\delta_{\text{H}}$  1.15 (9H, s, t-Bu of TBDPS), 1.74 (2H, t, *J* = 6.4 Hz, CCCH<sub>2</sub>CH<sub>2</sub>CH<sub>2</sub>), 2.45 (2H, t, *J* = 4.8 Hz, CCCH<sub>2</sub>CH<sub>2</sub>CH<sub>2</sub>), 2.52 (1H, d, *J* = 2.4 Hz, CHOHCCH), 3.75 (2H, d, *J* = 6.4 Hz, CH<sub>2</sub>CH<sub>2</sub>CH<sub>2</sub>OH), 5.25 (1H, d, *J* = 1.6 Hz, CHCCCH), 5.73 (1H, d, *J* = 10.8 Hz, CH=CHCCCH<sub>2</sub>CH<sub>2</sub>), 5.82 (1H, td, *J* = 1.6, 11.2 Hz, CH=CHCCCH), 7.45-7.38 (5H, m, Ar-H), 7.77-7.75 (5H, m, Ar-H);  $\delta_{\text{C}}$  16.3, 19.3, 26.7, 30.9, 54.3, 61.5, 72.3, 78.5, 81.2, 81.7, 92.7, 98.3, 117.6, 121.4, 127.6, 127.7, 129.6, 129.9, 130.0, 132.5, 132.7, 135.9; Mass (ESI) *m/z*: 426 (M<sup>+</sup>).

Synthesis of 10-(tert-Butyl-diphenyl-silanyloxy)-dodec-6-ene-4, 8, 11-triynal (41)

Procedure same as described for 24; Yield: 946 mg, 95%; State: brown oil;  $\delta_{\text{H}}$  1.09 (9H, s, t-Bu of TBDPS), 2.50 (1H, d, *J* = 2.1 Hz, CHOHCCH), 2.62 (4H, s, CH<sub>2</sub>CH<sub>2</sub>CHO), 5.27 (1H, d, *J* = 1.6 Hz, CHCCCH), 5.77 (2H, dd, *J* = 1.6, 5.3 Hz, CH=CH), 7.49-7.33 (5H, m, Ar-H), 7.79-7.75 (5H, m, Ar-H), 9.71 (1H, s, CH<sub>2</sub>CH<sub>2</sub>CHO);  $\delta_{\text{C}}$  13.0, 19.3, 26.7, 42.5, 54.3, 74.3, 78.8, 81.2, 81.5, 93.0, 96.4, 118.1, 120.9, 127.6, 127.7, 129.8, 129.9, 132.6, 132.7, 135.8, 135.9, 200.2; Mass (ESI) *m/z*: 424 (M<sup>+</sup>).

Synthesis of 12, 12-Dimethoxy-dodec-6-ene-1, 4, 8-triyn-3-ol (42)

Procedure same as that of 30; Yield: 369 mg, 75%; State: yellow oil;  $\delta_{\text{H}}$  1.91-1.86 (2H, m, CCCH<sub>2</sub>CH<sub>2</sub>CH<sub>2</sub>), 2.48 (2H, t, *J* = 6.4 Hz, CCCH<sub>2</sub>CH<sub>2</sub>CH<sub>2</sub>), 2.55 (1H, d, *J* = 2.4 Hz, CHOHCCH), 3.35 (6H, d, *J* = 7.2 Hz, OCH<sub>3</sub>), 4.33 (1H, d, *J* = 8.4 Hz, CHOH), 4.93 [1H, t, *J* = 5.6 Hz, CH(OMe)<sub>2</sub>], 5.27 (1H, d, *J* = 8.4 Hz, CHOH), 5.83 (2H, d, *J* = 2.4 Hz, CH=CH);  $\delta_{\text{C}}$  15.4, 30.9, 52.1, 52.3, 72.4, 78.8, 81.0, 81.6, 92.7, 97.9, 102.4, 117.9, 121.5; Mass (ESI) *m/z*: 232 (M<sup>+</sup>).

Synthesis of 10-Hydroxy-dodec-6-ene-4, 8, 11-triynal (43)

Procedure same as 31; Yield: 682 mg, 85%; State: yellow oil;  $\delta_{\text{H}}$  2.63 (1H, d, *J* = 2.0 Hz, CHOHCCH), 2.75 (4H, s, CH<sub>2</sub>CH<sub>2</sub>CHO), 3.75 (1H, d, *J* = 7.6 Hz, CHOH), 5.30 (1H, d, *J* = 6.4 Hz, CHOH), 5.84 (2H, s, CH=CH), 9.86 (1H, s, CH<sub>2</sub>CH<sub>2</sub>CHO);  $\delta_{\text{C}}$  13.1, 42.0, 52.1, 72.6, 78.9, 80.8, 81.4, 92.5, 96.5, 118.2, 121.2, 201.9; Mass (ESI) *m/z*: 186 (M<sup>+</sup>).

Synthesis of 10-Hydroxy-dodec-6-ene-4, 8, 11-triynyl-N-benzyl nitron (44)

Procedure same as 17; Yield: 892 mg, 95%; State: brown oil;  $\delta_{\text{H}}$  2.54 (1H, d, *J* = 2.4 Hz, CCH), 2.92-2.76 (4H, m, CCCH<sub>2</sub>CH<sub>2</sub>), 4.95 (2H, s, -NCH<sub>2</sub>Ph), 5.20 (1H, d, *J* = 7.2 Hz, CHOH), 5.91-5.78 (2H, m, CH=CH), 6.77 (1H, t, *J* = 5.6 Hz, CH=N(O)CH<sub>2</sub>Ph), 7.43-7.37 (5H, m, Ar-H);  $\delta_{\text{C}}$  16.4, 26.3, 51.8, 68.9, 72.2, 80.8, 81.4, 94.0, 96.8, 118.9, 120.6, 128.7, 128.9, 129.1, 129.7, 132.1, 141.0; Mass (ESI) *m/z*: 291 (M<sup>+</sup>).

Synthesis of 5-(2-Buta-1, 3-diynyl-phenyl)-pent-4-ynyl-N-benzyl nitron (45)

Procedure same as 17; Yield: 883 mg, 90%; State: brown oil;  $\delta_{\text{H}}$  2.53 (1H, s, CCCCH), 2.81-2.71 (4H, s, CCCH<sub>2</sub>CH<sub>2</sub>), 4.96 (2H, s, NCH<sub>2</sub>Ph), 7.07 [1H, t, *J* = 5.2 Hz, CH=N(O)CH<sub>2</sub>Ph], 7.52-7.22 (9H, m, Ar-H);  $\delta_{\text{C}}$  15.9, 25.8, 68.2, 69.4, 72.4, 74.3, 79.7, 79.8, 93.4, 123.5, 127.3, 127.5, 127.6, 128.8, 128.9, 129.1, 131.67, 131.8, 133.0, 137.6; Mass (ESI) *m/z* 311 (M<sup>+</sup>).

General procedure for intramolecular Kinugasa reaction:

To a solution of different nitrones (1.10 mmol) in deoxygenated acetonitrile (30 ml) at 0 °C at a high dilution (0.003 M) under argon at 0 °C, Et<sub>3</sub>N (1.10 mmol) was added and the mixture was stirred for 30 minutes. Cuprous iodide (0.55 mmol) was added and the solution was stirred for another 5 min at 0 °C. The mixture was then stirred for 24 h at room

temperature (15-20 °C). It was diluted with water (50 ml) and filtered through celite. The celite bed was washed with ethyl acetate (50 ml). The combined filtrate and washings were extracted with ethyl acetate (3 x 50 ml). The organic layer was washed with NH<sub>4</sub>Cl, water and brine and dried over Na<sub>2</sub>SO<sub>4</sub> and evaporated. The residue, obtained after evaporation, upon chromatography afforded an oil from which the products separated by conventional column chromatography over silica gel using hexane/ ethyl acetate (1:1) as eluent.

7-Benzyl-11-oxa-7-aza-tricyclo[13.4.0.06,9]nonadeca-1(15),16,18-triene-2,13-diyn-8-one (*cis* and *trans* fused) (1 and 2)

Cis: Yield: 10%, overall yield: 55%; State: white solid;  $\nu_{\max}$  (neat) 3423, 2917, 2849, 2362, 2335, 1742, 1652 cm<sup>-1</sup>;  $\delta_{\text{H}}$  (200 MHz, d<sub>6</sub>-Acetone) 2.63-2.12 (4H, m, CCCH<sub>2</sub>CH<sub>2</sub>), 3.86-3.70 (2H, m, H-3, H-4), 4.27 (2H, d,  $J = 4.45$  Hz, OCH<sub>2</sub>CH), 4.52, 4.71 (2H, ABq,  $J = 17.1$  Hz, OCH<sub>2</sub>CC), 4.41, 4.63 (2H, ABq,  $J = 15.6$  Hz, NCH<sub>2</sub>Ph), 7.38-7.22 (9H, m, Ar-H),  $\delta_{\text{C}}$  16.2, 26.3, 44.3, 52.6, 55.4, 58.9, 64.2, 80.8, 86.7, 89.3, 94.2, 125.9, 126.3, 127.5, 127.7, 127.9, 128.0, 128.8, 130.1, 130.5, 135.8, 167.6; HRMS calcd for C<sub>24</sub>H<sub>21</sub>NO<sub>2</sub> + H<sup>+</sup> 356.1651 found 356.1653.

Trans: Yield: 30%, overall yield: 55%; State: white solid;  $\nu_{\max}$  (neat) 3423, 2917, 2849, 2362, 2335, 1742, 1652 cm<sup>-1</sup>;  $\delta_{\text{H}}$  1.91-1.83 (2H, m, CCCH<sub>2</sub>CH<sub>2</sub>), 2.58-2.43 (2H, m, CH<sub>2</sub>CC), 3.06-3.04 (1H, m, H-3), 4.07-4.03 (2H, m, OCH<sub>2</sub>CH), 4.17-4.14 (1H, m, H-4), 4.46, 4.36 (2H, ABq,  $J = 15.6$  Hz, OCH<sub>2</sub>CC), 4.60, 4.25 (2H, ABq,  $J = 16.9$  Hz, NCH<sub>2</sub>Ph), 7.38-7.12 (9H, m, Ar-H),  $\delta_{\text{C}}$  16.0, 29.4, 44.6, 53.7, 54.9, 58.7, 64.2, 81.1, 85.0, 88.9, 91.1, 125.2, 125.4, 127.3, 127.5, 127.7, 127.8, 128.4, 130.7, 131.4, 136.0, 167.2; HRMS calcd for C<sub>24</sub>H<sub>21</sub>NO<sub>2</sub> + H<sup>+</sup> 356.1651 found 356.1642.

7-Benzyl-12-oxa-7-aza-tricyclo[14.4.0.06,9]jicosa-1(16),17,19-triene-2,14-diyn-8-one (*cis* and *trans* fused) (3 and 4)

Cis: Yield: 15%, overall yield: 60%; State: white solid;  $\nu_{\max}$  (neat) 1747 cm<sup>-1</sup>,  $\delta_{\text{H}}$  2.36-1.63 (5H, m, 1H of CCCH<sub>2</sub>CH<sub>2</sub>, CCCH<sub>2</sub>CH<sub>2</sub>, OCH<sub>2</sub>CH<sub>2</sub>), 2.67-2.50 (1H, m, CCCH<sub>2</sub>CH<sub>2</sub>), 3.68-3.53 (2H, m, H-3, OCH<sub>2</sub>CH<sub>2</sub>), 3.96-3.81 (2H, m, H-4, OCH<sub>2</sub>CH<sub>2</sub>), 4.45, 4.30 (2H, d,  $J = 18.3$  Hz, OCH<sub>2</sub>CC), 4.53, 4.22 (2H, ABq,  $J = 15.5$  Hz, NCH<sub>2</sub>Ph), 7.38-7.19 (9H, m, Ar-H);  $\delta_{\text{C}}$  16.9, 24.5, 26.9, 44.1, 50.1, 55.1, 58.8, 67.8, 81.1, 85.0, 89.1, 92.2, 125.4, 127.2, 127.3, 127.6, 127.6, 127.6, 128.4, 128.5, 130.9, 131.2, 169.1; HRMS calcd. for C<sub>25</sub>H<sub>23</sub>NO<sub>2</sub> + H<sup>+</sup> 370.1808 found 370.1793.

Trans: Yield: 45%, overall yield: 60%; State: white solid;  $\nu_{\max}$  (neat) 2362, 2335, 1742 cm<sup>-1</sup>;  $\delta_{\text{H}}$  2.53-1.90 (6H, m, CCCH<sub>2</sub>CH<sub>2</sub>, CCCH<sub>2</sub>CH<sub>2</sub>, OCH<sub>2</sub>CH<sub>2</sub>), 2.90-2.82 (1H, m, H-3), 3.55-3.50 (1H, m, 1H of OCH<sub>2</sub>CH<sub>2</sub>), 3.85-3.79 (1H, m, H-4), 4.17-4.05 (1H, m, 1H of OCH<sub>2</sub>CH<sub>2</sub>), 4.44, 4.28 (2H, d,  $J = 16.3$  Hz, OCH<sub>2</sub>CC), 4.46, 4.30 (2H, ABq,  $J = 15.3$  Hz, NCH<sub>2</sub>Ph), 7.39-7.20 (9H, m, Ar-H);  $\delta_{\text{C}}$  16.3, 27.6, 31.0, 44.9, 52.7, 57.5, 58.4, 66.8, 88.7, 92.2, 93.0, 125.4, 126.4, 127.0, 127.6, 128.1, 128.7, 128.8, 131.2, 131.7, 136.5, 169.7; HRMS calcd for C<sub>25</sub>H<sub>23</sub>NO<sub>2</sub> + H<sup>+</sup> 370.1808 found 370.1821.

7-Benzyl-7-aza-tricyclo[11.4.0.05,8]heptadeca-1(17),4,13,15-tetraene-2,11-diyn-6-one (7)

Yield: 13%, overall yield: 65%; State: white solid;  $\nu_{\max}$  (neat) 2925, 1745 cm<sup>-1</sup>;  $\delta_{\text{H}}$  2.19- 1.97 (2H, m, CCCH<sub>2</sub>CH<sub>2</sub>), 2.63-2.56 (2H, m, CCCH<sub>2</sub>CH<sub>2</sub>), 3.98 (1H, m, CHCH<sub>2</sub>CH<sub>2</sub>CC), 4.82, 4.20 (2H, ABq,  $J = 15.0$  Hz, NCH<sub>2</sub>Ph), 6.28 (1H, d,  $J = 1.5$  Hz, CCCH), 7.44-7.20 (9H, m, Ar-H);  $\delta_{\text{C}}$  19.9, 28.8, 44.3, 60.9, 80.9, 89.7, 96.3, 96.6, 104.0, 126.4, 127.6, 128.1, 128.4, 128.8, 129.4, 130.0, 130.0, 134.7, 154.6, 167.3; HRMS calcd for C<sub>23</sub>H<sub>17</sub>NO + H<sup>+</sup> 324.1389 found 324.1429.

7-Benzyl-4-hydroxy-7-aza-tricyclo[11.4.0.05,8]heptadeca-1(17),13,15-triene-2,11-diyn-6-one (6)

Yield: 52%, overall yield: 65%; State: white solid;  $\nu_{\max}$  (neat) 2925, 1735 cm<sup>-1</sup>;  $\delta_{\text{H}}$  2.65-2.25 (4H, m, CCCH<sub>2</sub>CH<sub>2</sub>), 3.36 (1H, dd,  $J = 2.5$  Hz, H-3), 3.51 (1H, m, H-4), 4.71, 4.08 (2H, ABq,  $J = 15.0$  Hz, NCH<sub>2</sub>Ph), 4.89 (1H, d,  $J = 10.0$  Hz, CHOH), 7.38-7.23 (9H, m, Ar-H);  $\delta_{\text{C}}$  18.1, 30.0, 44.0, 55.5, 63.0, 63.6, 85.5, 81.0, 92.0, 93.5, 125.7, 127.3, 127.6, 128.1, 128.2, 129.1, 129.5, 129.7, 134.9, 168.2; HRMS calcd for C<sub>23</sub>H<sub>19</sub>NO<sub>2</sub> + H<sup>+</sup> 342.1495 found 342.1526.

12-Benzyl-2-hydroxy-12-aza-bicyclo[9.2.0]tridec-5-ene-3,7-diyn-13-one (8)

Yield: 60%; State: white solid;  $\nu_{\max}$  (neat) 2925, 1735 cm<sup>-1</sup>;  $\delta_{\text{H}}$  2.60-1.95 (4H, m, CCCH<sub>2</sub>CH<sub>2</sub>), 3.22 (1H, dd,  $J = 2.5$  Hz, H-3), 3.38 (1H, m, H-4), 4.63, 3.98 (2H, ABq,  $J = 14.8$  Hz, -NCH<sub>2</sub>Ph), 4.75 (1H, d,  $J = 10.4$  Hz, CHOH), 5.76 (2H, s, CH=CH), 7.30-7.16 (5H, m, Ar-H);  $\delta_{\text{C}}$  18.6, 30.4, 43.9, 55.4, 63.0, 63.9, 80.5, 84.8, 95.4, 98.1, 120.4, 122.8, 127.8, 128.1, 128.6, 128.9, 129.0, 134.4, 167.6; HRMS calcd for C<sub>19</sub>H<sub>17</sub>NO<sub>2</sub> + H<sup>+</sup> 292.1338 found 292.1356.

Synthesis of compound 10a

The mesylate (47) (170 mg, 0.4 mmol), dissolved in dry DMF (30 ml) was treated with K<sub>2</sub>CO<sub>3</sub> (83 mg, 0.6 mmol) and the mixture was stirred for 3 h at room temperature. It was then partitioned between EtOAc and water (60 ml each). The organic layer was further washed with water (3 x 50 ml), dried and evaporated. From this residue, the title compound (10a) was isolated by column chromatography (Si-gel, PE: EA = 5:1) as yellowish solid; Yield: 119 mg, 90%; State: yellowish solid;  $\delta_{\text{H}}$  2.04-1.98 (2H, m, CH<sub>2</sub>CH<sub>2</sub>CH<sub>2</sub>N), 2.40 (2H, t,  $J = 6.0$  Hz, CH<sub>2</sub>CH<sub>2</sub>CH<sub>2</sub>N), 3.68 (2H, t,  $J = 7.4$  Hz, CH<sub>2</sub>CH<sub>2</sub>N), 4.34 (2H, s, NCH<sub>2</sub>CC), 5.76 (2H, dd,  $J = 10.0, 18.0$  Hz, CHCH), 7.99 (2H, d,  $J = 8.8$  Hz, SO<sub>2</sub>CCHCHCNO<sub>2</sub>), 8.38 (2H, d,  $J = 8.8$  Hz, SO<sub>2</sub>CCHCHCNO<sub>2</sub>);  $\delta_{\text{C}}$  17.8, 27.8, 39.4, 44.7, 81.9, 87.5, 88.3, 100.4,

120.7, 123.7, 124.5, 128.6, 143.7, 150.2; Mass (ESI) m/z 330 ( $M^+$ ).

#### Synthesis of 10b & 10c

To a solution of compound 10a (20 mg, 0.06 mmol) in DMF (6 ml), thiophenol (8  $\mu$ l, 0.07 mmol) and  $K_2CO_3$  (25 mg, 0.18 mmol) were added and the mixture was stirred for 40 minutes at room temperature. After partitioning between water and EtOAc, the organic layer was evaporated using liquid  $N_2$  in the vacuum pump and the free amine 10b was isolated by column chromatography (Si-gel, 10%  $CH_3OH$  in  $CH_2Cl_2$ ) as a brown oil. Yield: 8 mg, 90%; Immediately the diethyl ether solution of the amine compound 10b was added drop wise to the solution of *p*-toluene sulfonic acid in diethyl ether with few drops of methanol mixture. The reaction mixture was stirred for few minutes until the brownish precipitate appeared. The solid material 10c was isolated as a white solid by washing with diethyl ether by several times.

#### Spectral data of compound 10b:

$\delta_H$  1.82-1.76 (2H, m,  $CH_2CH_2CH_2N$ ), 2.54 (2H, t,  $J = 6.4$  Hz,  $CH_2CH_2CH_2N$ ), 3.29 (2H, t,  $J = 6.0$  Hz,  $CH_2CH_2N$ ), 3.64 (2H, s,  $NCH_2CC$ ), 5.82 (2H, s, CHCH);  $\delta_C$  16.8, 24.8, 39.1, 43.9, 82.4, 85.2, 97.2, 97.5, 121.4, 122.7; Mass (ESI) m/z 145 ( $M^+$ ).

#### Spectral data of compound 10c:

$\delta_H$  1.98 (2H, t,  $J = 6.4$  Hz,  $CH_2CH_2CH_2N$ ), 2.37 (3H, s, Ar- $CH_3$ ), 2.57 (2H, t,  $J = 6.4$  Hz,  $CH_2CH_2CH_2N$ ), 3.72 (2H, bs,  $CH_2CH_2N$ ), 4.10 (2H, s,  $NCH_2CC$ ), 5.85 (2H, dd,  $J = 10.0, 13.8$  Hz, CHCH), 7.16 (2H, d,  $J = 7.6$  Hz,  $SO_3CCHCHCCH_3$ ), 7.73 (2H, d,  $J = 8.0$  Hz,  $SO_3CCHCHCCH_3$ );  $\delta_C$  16.9, 31.3, 23.0, 37.3, 42.6, 82.9, 86.7, 89.4, 98.3, 120.2, 124.3, 125.8, 128.9, 140.4, 141.4; Mass (ESI) m/z 146 ( $MH^+$ ).

#### Synthesis of compound 11b & 11c

The title compound 11b and 11c were prepared from the corresponding cyclic sulphonamide<sup>7, 3c</sup> compound 11a following the same procedure as described for 10b & 10c. The free amine 11b was isolated by column chromatography (Si-gel, 10%  $CH_3OH$  in  $CH_2Cl_2$ ) as a brown oil, Yield: 60%; and 11c was obtained as a brownish solid.

#### Spectral data of compound 11b

$\delta_H$  2.52 (2H, t,  $J = 5.2$  Hz,  $CH_2CH_2CH_2N$ ), 3.26 (2H, t,  $J = 5.2$  Hz,  $CH_2CH_2N$ ), 3.62 (2H, s,  $NCH_2CC$ ), 5.85 (2H, s, CHCH); Mass (ESI) m/z 131 ( $M^+$ ).

#### Spectral data of compound 11c

$\delta_H$  2.33 (3H, s, Ar- $CH_3$ ), 2.86 (2H, t,  $J = 4.4$  Hz,  $CH_2CH_2N$ ), 3.59 (2H, bs,  $CH_2CH_2N$ ), 4.08 (2H, s,  $NCH_2CC$ ), 5.89 (2H, d,  $J = 7.6$  Hz, CHCH), 7.13 (2H, d,  $J = 7.6$  Hz,  $SO_3CCHCHCCH_3$ ), 7.69 (2H, d,  $J = 8.0$  Hz,  $SO_3CCHCHCCH_3$ ), 9.50 (2H, bs,  $NH_2^+$ );  $\delta_C$  19.4, 21.3, 40.4, 49.7, 84.8, 89.8, 91.3, 100.5, 121.8, 124.6, 125.9, 128.9, 140.5, 141.1; Mass (ESI) m/z 132 ( $MH^+$ ).

## 2 Conclusion

We have successfully developed a general synthetic route to aromatic and non-aromatic  $\beta$ -lactam-fused enediynes by intramolecular Kinugasa reaction. The method has widened the scope of Kinugasa reaction in the synthesis of sensitive systems like heterocyclic and 11-membered carbocyclic  $\beta$ -lactam fused enediynes. The thermal reactivity of these enediynes indicated very little effect of endocyclic double bonds. The aliphatic enediyne expectedly showed higher reactivity as compared to the aromatic counterparts. There was significant effect of the  $\beta$ -lactam ring on the reactivity of the fused enediynyl system because of larger ring size. The 10-membered monocyclic amine, as the tosylate salt, was found to be a potent DNA-cleaving agent.

## Acknowledgements

Author AB thanks DST, Government of India for a research grant. RP and SD are grateful to CSIR, Government of India for a Research Fellowship

## References

- Banfi, L., Guanti, G. (1998). Synthesis of N-fused "lactenediynes". *Eur. J. Org. Chem.* 1543-1548.
- Basak, A., Bdour, H. M., Bhattacharya, G. (1997). An enantiospecific nitronc cycloaddition route to 3-hydroxy-2-azetidiones. *Tetrahedron Lett.* 38, 2535-2538; b) Basak, A., Ghosh, S. C. (2004). L-proline-mediated one-pot synthesis of 3-exomethylene  $\beta$ -lactams via Kinugasa reaction. *Synlett* 1637-1639.
- Basak, A., Khamrai, U. K., Mallick, U. K. (1996). The synthesis and reactivity of novel azetidynyl enediynes. *J. Chem. Soc. Chem. Commun.* 749-750; b) Basak, A., Mandal, S. (2002). A carbene insertion route to  $\beta$ -lactam fused cyclic enediynes. *Tetrahedron Lett.* 43, 4241-4243; c) Shain, J. C., Khamrai, U. K., Basak, A. (1997). The synthesis and reactivity of a novel 10-membered azaenediyne. *Tetrahedron Lett.* 38, 6067-6070; d) Banfi, L., Guanti, G. (1995). Lactenediynes: a new class of triggered cyclic enediynes. *Angew. Chem. Int. Ed. Engl.* 34, 2393-95;

Bergman, R. G. (1973). Reactive 1,4-dehydroaromatics. *Acc. Chem. Res.* 6, 25-31; b) Lockhart, T. P., Bergman, R. G. (1981). Evidence for the reactivity spin state of 1,4-dehydrobenzenes. *J. Am. Chem. Soc.* 103, 4091-4096.

Ding, L. K., Irwin, W. J. (1976). Cis- and trans-Azetidin-2-ones from nitrones and copper acetylide. *J. Chem. Soc. Perkin Trans I* 2382-2386.

Example of an artificial molecular lock (a cyclic carbonate) was first reported by Nicolaou *et al.*: Nicolaou, K. C., Sorensen, E. J., Discordia, R., Hwang, C-K., Minto, R. E., Bharucha, K. N., Bergman, R. G. (1992). Ten-membered cyclic enediynes with remarkable chemical and biological properties. *Angew. Chem. Int. Ed. Engl.* 104, 1094 -1096.

Kar, M., Basak, A. (2007). Design, synthesis and biological activity of unnatural enediynes and related analogues equipped with pH – dependent or phototriggering devices. *Chem. Rev.* 107, 2861-2890.

Kinugasa, M., Hashimoto, S. (1972). Reactions of copper(I) phenylacetylide with nitrones. *J. Chem. Soc. Chem. Commun.* 466-467.

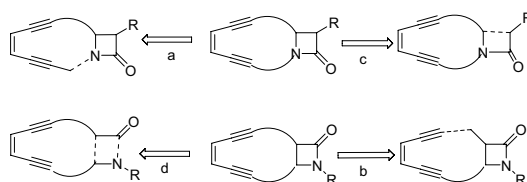
Luche, J. L., Kagan, H. B., Parthasarathi, R., Tsoucaris, G., de Rongo, C., Zewlar, C. (1968). Stereochemistry in the  $\beta$ -lactam series – III. *Tetrahedron* 24, 1275-1281.

Nature uses small epoxide ring as a molecular lock, *e. g.* in dynemicin and kedercidin. For reference: a) Langley, D. R., Doyle, T. W., Beveridge, D. L. (1991). The dynemicin-DNA intercalation complex: a model based on DNA affinity cleavage and molecular dynamics simulation. *J. Am. Chem. Soc.*, 113, 4395-403; b) Kawata, S., Ashizawa, S., Hiramama, S. (1997). Synthetic study of Kedarcidine chromophore: revised structure. *J. Am. Chem. Soc.* 119, 12012-12013 and references are therein.

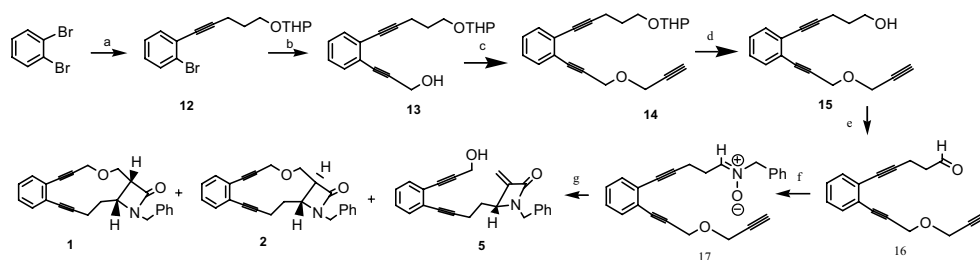
Pal, R., Basak, A. (2006). Anovel synthesis of  $\beta$ -lactam fused cyclic enediynes by intramolecular Kinugasa reaction. *Chem. Commun.* 2992-2994.

Shintani, R., Fu, G. C. (2003). Catalytic enantioselective synthesis of  $\beta$ -lactams: intramolecular Kinugasa reactions and interception of an intermediate in the reaction cascade. *Angew. Chemie. Int. Ed.* 42, 4082-4085.

Sonogashira, K., Tohoda, Y., Hagihara, N. (1975). A convenient synthesis of acetylenes: catalytic substitutions of acetylenic hydrogen with bromoalkenes, iodoarenes and bromopyridines. *Tetrahedron Lett.* 16, 4467-4470; b) Takahashi, S., Kuroyama, Sonogashira, Y., K., Hagihara, N. (1980). A convenient synthesis of ethynylarenes and diethynylarenes. *Synthesis* 627-630.

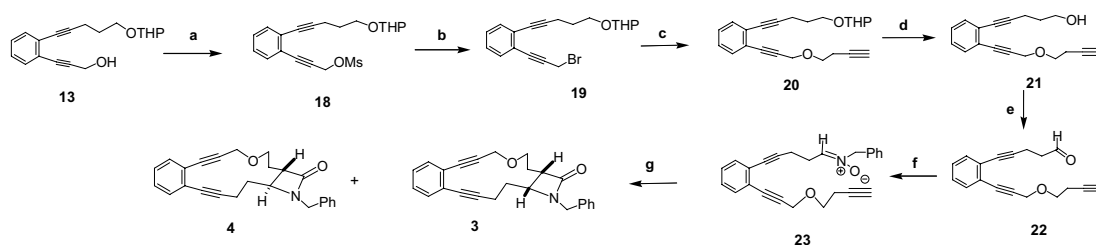


Scheme 1. Possible approaches to  $\beta$ -lactam fused enediynes



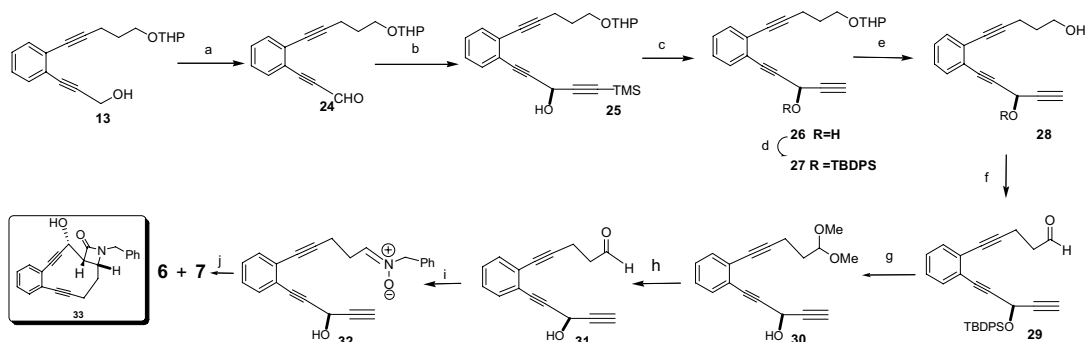
a) THP-protected 4-Pentyn-1-ol, Pd(PPh<sub>3</sub>)<sub>4</sub>, n-BuNH<sub>2</sub>, reflux; b) Propargyl alcohol, Pd(PPh<sub>3</sub>)<sub>4</sub>, n-BuNH<sub>2</sub>, reflux (overall 70%); c) NaH, Propargyl bromide, THF, rt. (85%); d) PPTS, EtOH (78%); e) PCC, DCM, rt (65%); f) PhCH<sub>2</sub>NHOH, MeOH (80%); g) CuI, Et<sub>3</sub>N, CH<sub>3</sub>CN (overall yield 55%, trans = 30%, cis = 10%, elimination = 15%)

Scheme 2. Synthesis of enediynes 1, 2 and 5



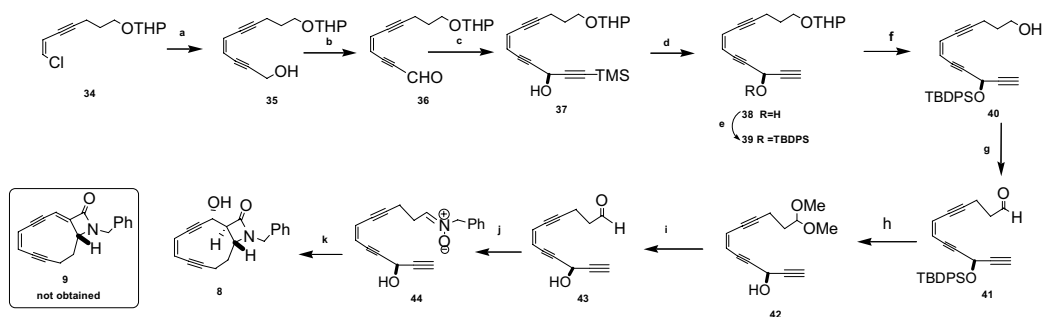
a) MsCl, Et<sub>3</sub>N, CH<sub>2</sub>Cl<sub>2</sub>, 0 °C (85%); b) LiBr, THF (80%); c) NaH, homopropargyl alcohol, THF (70%) d) PPTS, EtOH (78%); e) PCC, DCM, rt. (65%); f) PhCH<sub>2</sub>NHOH, MeOH (80%); g) CuI, Et<sub>3</sub>N, CH<sub>3</sub>CN (overall yield 60%, trans = 45%, cis = 15%).

Scheme 3. Synthesis of enediyne 3 and 4



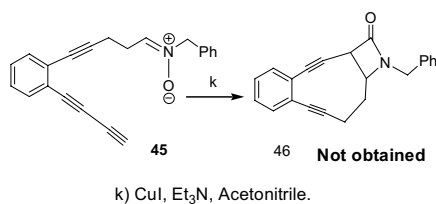
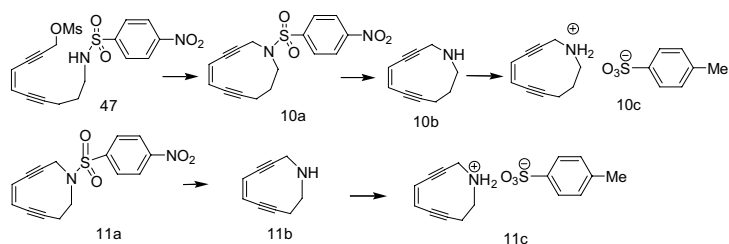
a) Dess-Martin Oxidation (> 90%); b) TMS-acetylene, BuLi, THF, 0 °C (85%); c) KF, MeOH (80%); d) TBDPSCI, DMAP, DCM (80%); e) PPTS, EtOH (80%); f) Dess-Martin Oxidation (>90%); g) 3% HCl-MeOH (75%); h) THF-H<sub>2</sub>O, HCl (85%); i) PhCH<sub>2</sub>NHOH, MeOH (>90%); j) CuI, Et<sub>3</sub>N, Acetonitrile (overall yield : 65%, trans : elimination product = 4:1)

Scheme 4. Synthesis of 11-membered aryl fused enediyne 8



a) propargyl alcohol, Pd[(PPh)<sub>3</sub>]<sub>4</sub>, n-BuNH<sub>2</sub>, 88%; b) Dess-Martin Oxidation (> 90%); c) TMS-acetylene, BuLi, THF, 0 °C (85%); d) KF, MeOH (80%); e) TBDPSCI, DMAP, DCM (80%); f) PPTS, EtOH (80%); g) Dess-Martin Oxidation (>90%); h) 3% HCl-MeOH (75%); i) THF-H<sub>2</sub>O, HCl (85%); j) PhCH<sub>2</sub>NHOH, MeOH (>90%); k) CuI, Et<sub>3</sub>N, Acetonitrile (overall yield : 65%, trans : elimination product = 4:1)

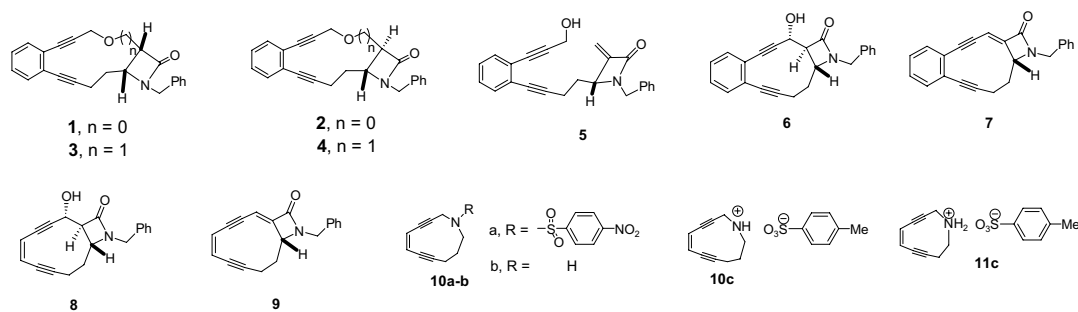
Scheme 5. Synthesis of enediyne 8

Scheme 6. Attempted synthesis of 10-membered  $\beta$ -lactam fused enediyne

Scheme 7. Synthesis of monocyclic enediyne

Table 1. DSC results

Compound number	Onset temperature in °C	Compound number	Onset temperature in °C
6	207	10a	140
7	192	10c	100
8	79	11c	38

Figure 1. Our target  $\beta$ -Lactam-fused enediyne

Form I  
Form III  
Form II

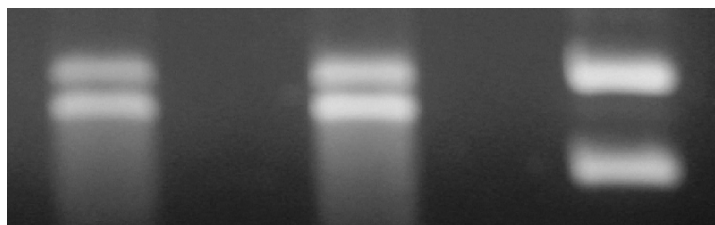


Figure 2. Gel electrophoresis of the tosylate salt 11c



## Synthesis and Modification of Polypropylene by Radiation-induced Grafting

Feng Yuan, Junfu Wei (Corresponding author), En-qi Tang, Kong-yin Zhao & Yang Xue

Tianjin Municipal Key Lab of Fiber Modification and Functional Fibers

Tianjin 300160, China

E-mail: jfwei@tjpu.edu.cn

School of Material Science and Chemical Engineering

Tianjin Polytechnic University

Tianjin 300160, China

E-mail: yuanfeng840106@hotmail.com

### Abstract

Polypropylene fiber (PP) was radiation-induced graft polymerization of lauryl acrylate (LA) and butyl acrylate (BA) using a  $^{60}\text{Co}$  gamma radiation source. Then the grafted polypropylene fiber was characterized by a Fourier transform infrared (FT-IR) spectrometer, Scanning Electron Microscopy (SEM), differential scanning calorimetry (DSC) and thermogravimetry (TG), which indicated that LA and BA have been grafted onto PP. The article focused on some factors that influenced on the graft degree, such as the cross-linking agent concentration, monomer concentration. The results showed that: the degree of grafting BA reached the maximum of 20.53%, while the maximum graft degree of LA was 29.90%.

**Keywords:** Polypropylene, Butyl acrylate, Lauryl acrylate, Radiation grafting, Fiber

### 1. Introduction

Polymers have generated considerable interest as biomaterials in medical science and biotechnology. With increasing demands for a biomaterial with better acceptability and functionality to the biosystem, stress has been focussed on the development of newer materials. One of the ways to develop such materials is to modify existing polymers and design them keeping in view their specific application areas. Sutures are used in surgical operations and require optimum physico-chemical characteristics. Polypropylene (PP) is one of the widely used biostable sutures due to its optimum tensile strength and low level of tissue reaction. PP fibers possess good hydrophobic and lipophilic properties with lower density than water, which can suspend in the surface of water and have a high adsorption capacity of organic solvents such as hydrocarbons, esters, ketones, halohydrocarbons and so on. Therefore, Modification or introduction of new characteristics to those based on synthetic polymers such as polypropylene, can be achieved by several methods. Grafting, whether initiated chemically or by ionizing radiations, constitutes one of the methods that is being applied successfully. The radiation-induced graft polymerization of monomers such as acrylates, methacrylic acid, acrylamide and acrylonitrile onto PP has been reported to introduce hydrogel characteristics in the polymer for biomedical applications (Bhuvanesh, 2006, PP. 161-167, Park, 2006, PP.46-54, Vahdata, 2007, PP.787-793). Chen Xiaoting (2005, PP.536-54 ) reported that using acrylates, methacrylates as monomers, butylene glycol diacrylate as crosslinking agent, BPO as initiator, the high oil absorption resins polyacrylate were synthesized by suspension polymerization. The oil absorption ability of the resin is more than 15(g/g) for toluene, 10(g/g) for gasoline and 9(g/g) for machine oil. Zhang Yudong (1999, PP. 79-82) reported that grafting of ethyl acrylate(EA) onto PP powder had been carried out by preirradiation method using gamma rays from  $3.7 \times 10^{14} \text{Bq } ^{60}\text{Co}$  source as initiator. Chen Jie (1999, PP.193-198) reported that the surface of polypropylene (PP) film was modified by preirradiation grafting of polyethylene glycol methacrylate (PEGMA) with three kind of different molecular weight. Dong Yuan (2006, PP. 569-572) et al have indicated that the matrix of non-woven polypropylene fabrics could be grafted with the monomer of acrylic acid by means of pre-irradiation induced solid phase graft copolymerization. Jung-Dae Cho et al (2006, PP. 1446-1461) reported that 1,6-Hexanediol diacrylate (HDDA) was grafted onto polypropylene (PP) substrates in the presence of benzophenone (BP) using UV radiation and the UV-radiation grafting polymerizations were characterized in detail using contact-angle measurements, Fourier transform infrared spectroscopy with attenuated total internal reflection, and scanning electron microscopy. In the present study, the graft polymerization of LA and BA onto PP monofilament is

carried out by a radiation-induced grafting method to develop sutures with different graft levels.

## 2. Materials and methods

### 2.1 Materials and reagents

Commercial polypropylene fabric was kindly provided by Shijiazhuang Cigarette Industries Co. LTD. LA and BA purchased from Tianjiao Chemical Co., LTD, Tianjin, were used without further treatment. Other chemicals were analytical grade.

### 2.2 Grafting and modification procedure

Strips of PP films were immersed in monomer, cross-linking agents in glass ampoules. The reactant mixtures in glass ampoules were deaired by bubbling nitrogen gas for 10 min, sealed and then subjected to gamma ray irradiation from  $^{60}\text{Co}$ . The grafted films thus obtained were removed and washed thoroughly with distilled water and then soaked overnight in acetone to eliminate the residual monomer and homopolymer contained in the films. The films were then dried in an oven for 24 h at 50–60°C and then weighed. The degree of grafting  $G$  was calculated as follows:

$$G(\%) = [(W_g - W_0) / W_0] \times 100\%$$

where,  $W_0$  and  $W_g$  represent, the weights of the initial and grafted films, respectively.

### 2.3 FTIR measurement

A Vector-22 Fourier transform infrared (FTIR) spectrometer, which is a product of Bruker, Co. Ltd, Germany, was used for measuring and scanning the infrared absorption spectra at resolution of 4  $\text{cm}^{-1}$ . High signal-to-noise spectra were obtained by collection of hundred scans for each sample. The resultant digitized spectra were stored for further data processing.

### 2.4 SEM analysis

The phase morphological characteristics of the samples were observed by means of SEM (HITACHI, S-3500N) in the normal secondary electron imaging (SEI) mode and all the membrane samples were coated with gold-palladium and fixed by adhesive tape in the sample stage.

### 2.5 TG analysis

All samples were sheared to pieces and sputter-coated with Au. A NETZSCH STA409PC (Germany) thermogravimetry (TG) analyzer was used for thermal stability determinations of all samples under nitrogen atmosphere at a heating rate of 10°C/min from 0°C to 600°C.

### 2.6 DSC analysis

The thermal properties of PP composites were measured using a differential scanning calorimetry (Perkin-Elmer DSC-7, USA). Samples of about 10mg were heated from 0 to 200°C, and then cooled down to 60 °C at the heating rate of 10 °C/min under an atmosphere of dry nitrogen.

## 3. Results and discussion

### 3.1 Infrared spectroscopy measurement

The presence of grafting of LA and BA onto PP film was confirmed by FTIR analysis. The IR spectra of virginal PP and grafted polymers PP-g-LA and PP-g-BA are given in Fig. 1. The appearance of the new bands at about 2960~2915 and 2870~2840  $\text{cm}^{-1}$  on the pp matrix may be caused by the out-of-plane stretching vibrations and the symmetric stretching vibrations of the  $\text{CH}_3$ ,  $\text{CH}_2$ , respectively; The appearance of the new adsorption peaks at about 1455 and 1375  $\text{cm}^{-1}$  on the PP matrix may be caused by the  $\text{CH}_3$  out-of-plane bending vibrations and the symmetric bending vibrations of  $\text{CH}_2$ , respectively. Compared to the spectrum of the original fiber, a strong adsorption peak at 1730  $\text{cm}^{-1}$  can be observed, which characterizes the carbonyl group and caused by the stretching vibrations of carbonyl group of fatty acid esters, indicating that carbonyl has been grafted onto PP. The new characteristic absorption peak at 1150  $\text{cm}^{-1}$  was corresponded to the stretching vibrations of C—O and adsorption peaks at 1150  $\text{cm}^{-1}$ ~1180  $\text{cm}^{-1}$  and 1240  $\text{cm}^{-1}$ ~1270  $\text{cm}^{-1}$  was caused by the stretching vibrations of C—C—O—C. In combination with the vibration peak of carbonyl, it indicated that ester existed in the PP-g-LA and PP-g-BA matrix. A weak adsorption peak at about 720  $\text{cm}^{-1}$  in c was caused by the bending vibration of C—H in  $(\text{CH}_2)_n$  ( $n \geq 4$ ), which indicated that branch chains of LA had been grafted onto PP.

Grafted PP films seems quite complicated at the adsorption peak of 1000  $\text{cm}^{-1}$ ~1500  $\text{cm}^{-1}$ , due to the introduction of quaternary carbon ions after grafted, effects of carbonyl groups on the bending vibrations of methyl and the adsorption peak of C—O—C at 1000  $\text{cm}^{-1}$ ~1300  $\text{cm}^{-1}$ .

Taken together, we can speculate that both monomer LA and BA have been grafted onto the virginal PP fibers.

### 3.2 Scanning electron microscopy (SEM) study

The surfaces of the virginal PP and the grafted PP films were examined by SEM, and the results are shown in Figure 2.

The morphology of grafted PP is different significantly from that of virginal PP substrate. The grafted surface shows a markedly bumpy texture, while the virginal PP surface is very planar, which indicated that monomer LA and BA have been grafted onto the virginal PP fibers.

### 3.3 TG analysis of PP matrix fibers

Weight loss of virginal PP fiber and grafted fibers were measured at the heating rate of 10 °C /min under an atmosphere of dry nitrogen. According to the TGA curves of the original PP fiber and the grafted fiber PP-g-LA and PP-g-BA given in Figures 3 and 4, the grafted PP fibers showed an excellent thermal stability at a temperature up to 370 °C. As seen from the figure of TG and DTG, both PP-g-BA and PP-g-LA grafted fibers undergo two processes of thermal decomposition, corresponding to the decompositions of acrylic acid grafted chains and original PP fibers, respectively. Grafted chains experienced decomposition at a temperature from 371.6 to 425 °C, with a peak at 400.9°C; At a temperature from 455.6 to 649.3°C, original PP fibers experienced decomposition.

### 3.4 DSC analysis of PP matrix fibers

The melting temperature  $T_m$  and the apparent enthalpies of melting,  $\Delta H_f(\text{fiber})$ , were obtained from the maximum and the area of the melting peak, respectively. Similarly, the crystallization temperature ( $T_f$ ) and crystallization enthalpy,  $\Delta H_f(\text{cys})$  were obtained from the cooling DSC diagrams. The apparent crystallinity,  $W_c(\%)$ , of the PP and the grafted PP were calculated by the following equation:

$$W_c(\%) = \Delta H_f(\text{PP}) / \Delta H_f(\text{cys}) \times 100$$

where  $\Delta H_f(\text{cys})$  is the heat of fusion per gram of 100% crystalline PP, which was 209 J/g (Yin, 2001). Because crystallization of the grafted PP occurs in the PP portion, the crystallinity of PP portion in the grafted copolymer,  $\Delta H_f(\text{PP})$  can be expressed as the following:

$$\Delta H_f(\text{PP}) = \Delta H_f(\text{fiber}) / (1 - \alpha)$$

where  $\alpha$  is the weight fraction of grafts in the grafted copolymer.

The melting and crystallization behaviors of the samples are shown in Figure 5. The  $T_m$ ,  $\Delta H_f(\text{PP})$ ,  $\Delta H_f(\text{fiber})$  and  $W_c(\%)$  obtained from DSC curves in Figure 5 are listed in Table 1. It is known from these data that enthalpies of melting of grafted PP fibers decreased ascribed to “dilution effects” of grafts and “destructive effects” of radiation reaction on crystal zone (Huang, 2004, PP. 71-74, Zhu, 2004). Grafting of LA and BA onto PP film reduces the heat of melting and increases the melting enthalpy of PP. Influence of  $T_m$  is ascribed to two aspects. 1, grafting reaction was processed in the crazing zone of PP or main PP chains of crystal deficiency zone, regularity of crystal zone of PP got worse after grafted, destroyed the inherent crystal zone, which lead to the reduction of  $T_m$  of grafted PP fibers; 2, grafted PP polymers formed a new crystal which have a different  $T_m$  from virginal PP fibers. When the melting point of grafted chains is lower than virginal PP or grafted chains can't form crystal, melting point of grafted PP decreases compared to the virginal PP. On the contrary, it may increases. As seen from Table 1, the crystallinity and melting enthalpy of grafted PP fibers increased slightly compared to virginal PP.

### 3.5 Effects of monomer concentration on grafting level of PP

Figure 6 showed the effect of monomer (BA and LA) concentration on the grafting percentage. It can be seen that the grafting percentage increases initially with the concentration of the monomers when reaches a top value, and then decreases slightly. BA reached its top grafting level of 29.90% at the concentration of 7.5% while LA reached its top grafting level of 20.53% at the concentration of 10%. Grafting level is highly related to scavenging ability for the free radicals and diffusivity to PP substrate of monomers. It is easy to understand that more monomers will be impregnated into the matrix as the concentration of monomer is high. However, the amount of homopolymers increases with the monomer concentration, and the homopolymers have been removed in the extraction process. It can be deduced that all the active sites on the PP substrate can be grafted when the concentration of the monomer is high enough. The initial increase in the grafting level is caused by the increased availability of free radicals for the chain transfer to polymer backbone. But when the concentration of the monomer exceeds a value, the average molecular weight of the side chains is reduced as well as the diffusivity of monomers, and the degree of homopolymerization and viscosity of solutions are increased. Both of these result in the reduction of the grafting level.

### 3.6 Effects of cross linking reagent concentration on grafting level of PP

The influence of divinylbenzene (DVB) on the grafting degree is shown in Figure 7. The grafting degree increased initially and dramatically with the presence of DVB, reached a top value and then decreased. At the concentration of 2%, grafting levels of BA and LA reached a peak value of 20.53% and 21.64%, respectively. Cross linking reagent with two double bonds has higher activity compared to acrylate. With a low DVB concentration, the grafting chains to PP films may be mostly cross linking reagent but not acrylate, which leads to the reduction of grafting level; With a high enough DVB concentration, the degree of homopolymerization of monomer acrylates are dramatically increased, which

inhibited the diffusion of monomers to free radicals and thus interfered with the process of grafting reaction.

#### 4. Conclusions

(1) Virginal and grafted PP fibers was investigated by IR, TG and DSC, and SEM, which showed that both LA and BA have been grafted onto PP.

(2) The maximum degree of grafting BA was 20.53%, grafting percentage increased initially with the concentration of the monomer and cross linking reagent when reaching a top value, and then decreased, which indicated that excess higher or lower concentration of the monomer and cross linking reagent could lead to the reduction of grafting levels. The maximum degree of grafting LA was 29.90%, its grafting percentage was similar to BA, which indicated that whether excess higher or lower concentration of the monomer and cross linking reagent was unfavorable to grafting reaction.

#### References

- Bhuvanesh, G., Rachna, J., Nishat, A., et al. (2006). *Radiat. Phys. Chem.*, 75: 161~167.
- Chen, J., & Lu, Y.C. (1999). *Journal of Radiation Research and Radiation Processing*, 17(4):193~198.
- Chen, X.T., Tang, X.D., & Zhang, M.Z. (2005). *Ion Exchange and Adsorption*, 21(6): 536~54.
- Cho, J.D., Kim, S.G., & Hong, J.W. (2006) *J. Appl. Poly. Sci.*, 99: 1446~1461.
- Dong, Y., Lan, X.Z., & Li, J.X. (2006). *Applied Chemical Industry*, (8) :569~572.
- Huang, Z.Z., Lin, Z.D., & Cai, Z.W., et al. (2004). Preparation, structure and properties of polypropylene grafted with acrylic acid. *Engineering Plastics Application*, 32(2):71~74.
- Park, H.J., & Na, C.K. (2006) *J. Colloid. Interface. Sci.*, 301: 46~54.
- Ying, J.H., & Mo, Z.S. (2001). *Modern Polymer Physics*. Beijing: Science press.
- Zhang, Y.D., & Chen, D.T. (1999). *Polymer Materials Science & Engineering*, 15(5):79~82.
- Zhu, C.S. (2004). *Structure Analysis of Polymers*. Beijing: Science press.
- Vahdata, A., Bahramia. H., & Ansaria. N., et al. (2007). *Radiat. Phys. Chem.*, 76: 787~793.

Table 1. Related DSC parameters of virginal PP, PP-g-LA and PP-g-BA.

Samples and Grafting degree (%)	T <sub>m</sub> (°C)	ΔH <sub>f(fiber)</sub> (J/g)	ΔH <sub>f(PP)</sub> (J/g)	W <sub>c</sub> (%)
1 PP	163.8	88.36	88.36	42.28
2 PP-g-LA (15.75%)	162.7	79.27	94.08	45.01
3 PP-g-BA (15.88%)	163.4	77.79	90.14	43.13

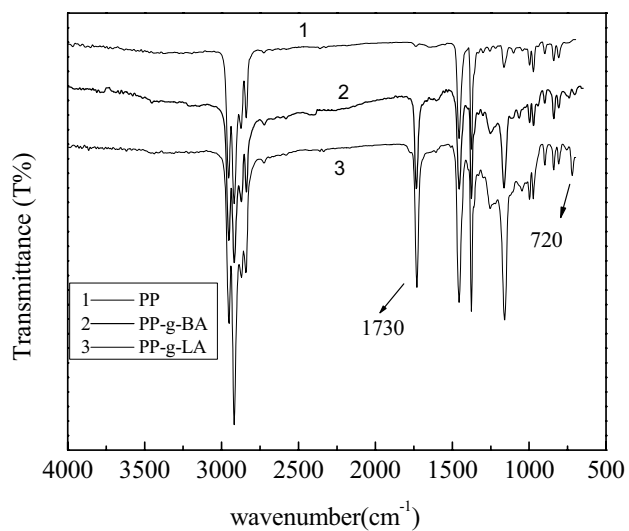


Figure 1. IR spectra of virgin PP (a), PP-g-LA (b), and PP-g-BA (c).

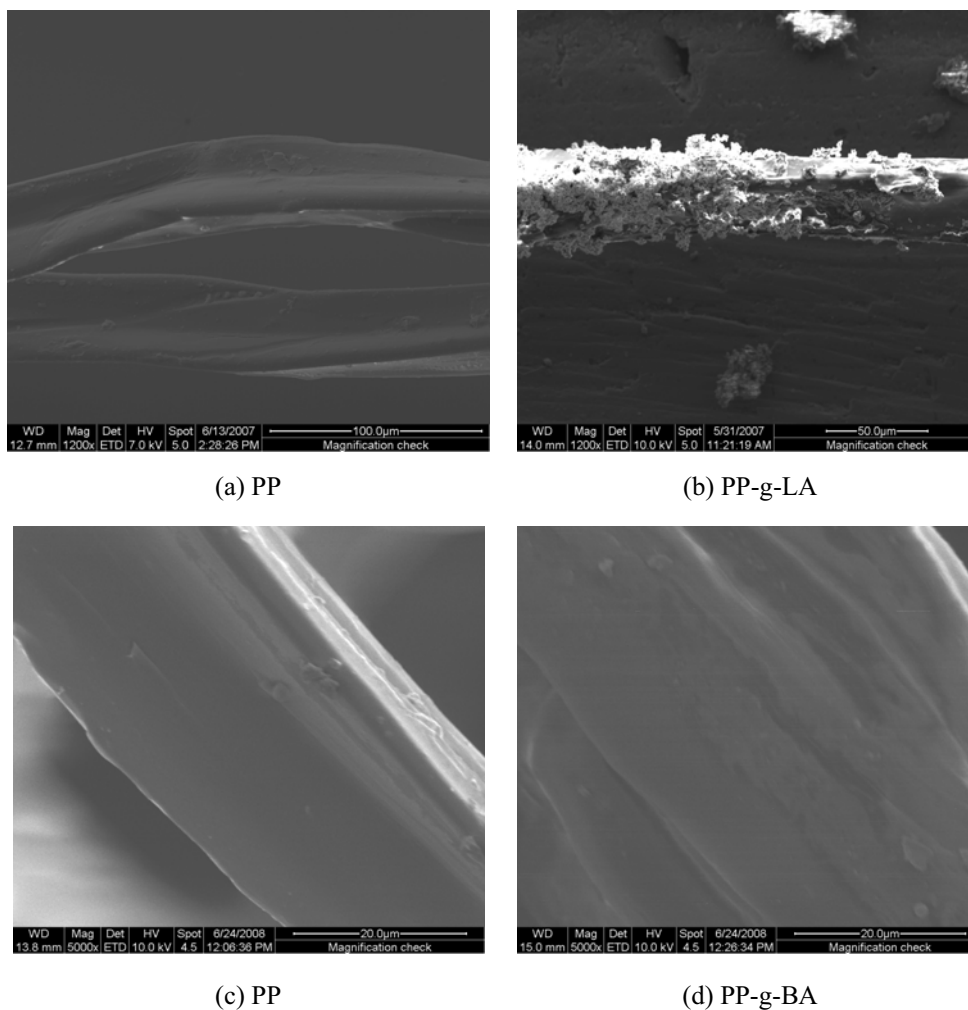


Figure 2. SEM images of virgin PP (a), PP-g-LA (b), and PP-g-BA (c)

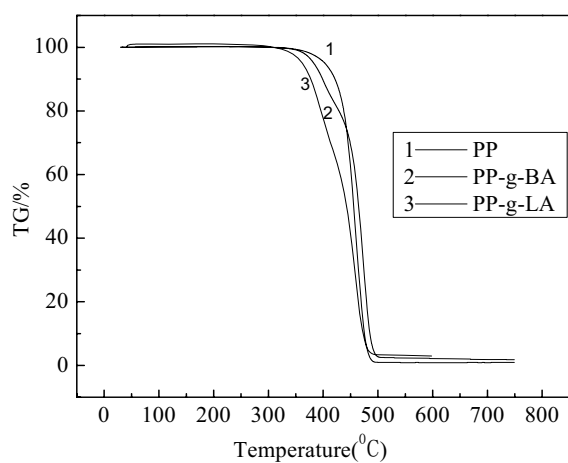


Figure 3. TG analysis of virgin PP (a), PP-g-LA (b), and PP-g-BA (c)

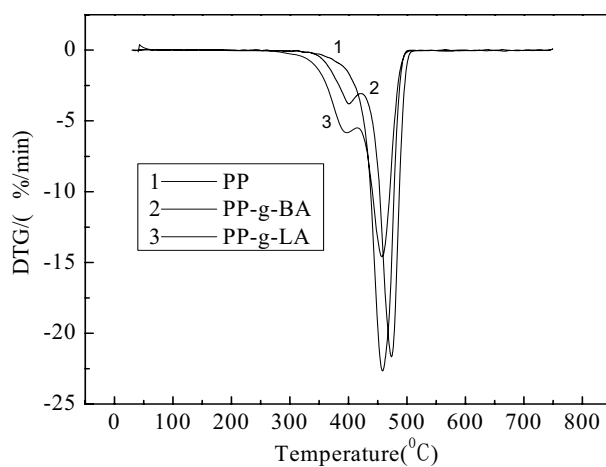


Figure 4. DTG analysis of virgin PP (a), PP-g-LA (b), and PP-g-BA (c)

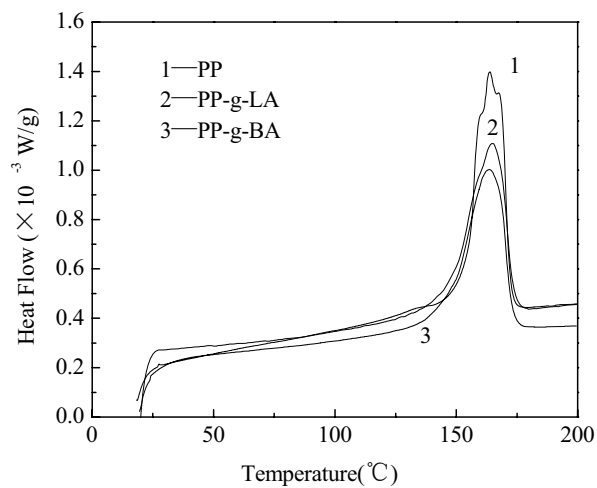


Figure 5. DSC thermographs of virgin PP (a), PP-g-LA (b), and PP-g-BA (c)

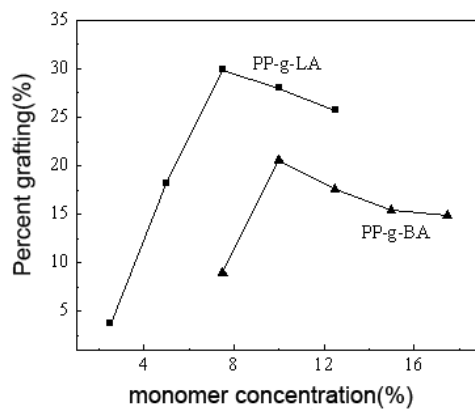


Figure 6. Relation between monomer concentration and grafting level

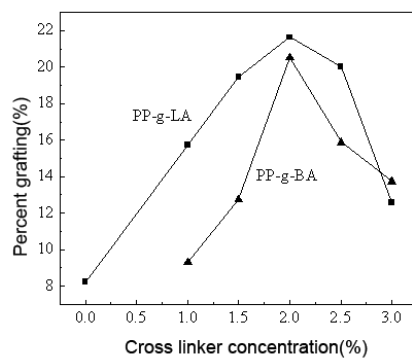


Figure 7. Relation between cross linking reagent concentration and grafting level



## Preparation and Properties of Polyester Based Nanocomposites with Good Air-tightness

Fusheng Luo

Department of Chemical Engineering, Huizhou University

Guangdong 516007, China

Tel: 86-752-252-7229 E-mail: lfs@hzu.edu.cn

*The research is financed by China National key fundamental Research Foundation (2004CB217808) and Scientific Research Foundation of Huizhou University (No505.0302).*

### Abstract

The permeability of polymer is determined by its chain configuration, phase morphology and the interaction with the penetrant. Based on these principles, the permeability of the polyester of poly (ethylene terephthalate)(PET) is enhanced through different modifiers in order to apply it to barrier packing bottle. In this paper, poly (m-xylylene adipamide-terephthalyl amide) (MXD6T) and nanometer silicon dioxide ( $\text{SiO}_2$ ) nanocomposite with  $\text{SiO}_2$  load from 5% to 20% (by mass) is prepared and used to improve the barrier property of polyester bottle materials. In preparing MXD6T- $\text{SiO}_2$  (NMXD6T), silica is in-situ polymerized with hexane diacid, terephthalic acid (TPA), alkyl and aromatic diamine. The different molar ratio of hexane diacid to terephthalic acid with the same molar diamine is designed to give the composites with different viscosity, thermal performance and the barrier properties. The 3-8 times of enhanced permeability of these polyester matrix nanocomposites with this NMXD6T to pure polyester resins are reported.

The relationship of NMXD6T's configuration and the permeability properties of polyester nanocomposites are characterized by techniques of the dynamic scanning calorimeter (DSC), FT Infrared, and Transmission Electronic Microscopy (TEM). DSC shows that NMXD6T is totally amorphous. FTIR shows the existence of silicon-oxygen bond formed in the nanocomposite, and TEM indicates an average size from 30nm to 100nm of  $\text{SiO}_2$  particles being phase separated from MXD6T matrix, while well bonded to the polyester chains. It is concluded that the NMXD6T-PET nanocomposites may be one of the best way to enhance the barrier properties of polyesters for their packing application.

**Keywords:** Nylon MXD6T, Silicon dioxide, PET, Nanocomposites

### 1. Introduction

In packing industry, the research of high barrier properties polymer materials is of increasing interest to prevent gases like oxygen, carbon dioxide or water vapor from permeating through the materials. In generally, the permeability of polymer is determined by penetrant, polymer's configuration and properties, the interaction of penetrant and polymer (Ding Yun-sheng, 2001, p.360-368. Soney C Georgy, 2000, p. 2136-2145 & Hongchul Seo, 2000, p. 2714-2720). Material's microcracks, pinholes and defects can increase the penetrability of micromolecules. Oxygen permeation, which is of great importance for packing purpose, is almost entirely defect-dominated (A. Gruniger, 2004, p. 308-315. A.P. Roberts, 2002, p. 75-82). Also, the free volume of polymer has important influence on the permeation of micromolecules through polymer matrix: the larger free volume is, the stronger penetrability is. Other important factors are polymer's surface polarity, chain rigidity and cohesion (He Zuoyun, 1996, p. 17-23). Temperature and humidity are exterior effect factors. For most polymers, the contributions of microcracks, pinholes and defects to permeation increase with increasing temperature and humidity. However, the penetrability of amorphous nylon decreases with increasing humidity. U. S. Pat. NO. 637, 659,1 describes the combination of at least two of the diacids with the diamine effectively disrupts the crystallization tendency of these macromolecules to allow clear transparent amorphous structures to be maintained throughout the processing steps (Lan, Tie, 1999).

Poly (m-xylylene adipamide) (MXD6), a semicrystalline polymer, is prepared by m-xylylenediamine and hexane diacid. It is one of the high barrier property materials with good properties: high gas barrier (even in the high humidity surrounding, it also has outstanding barrier property (CHEN Yan, 1997, p. 73-78)); high heat stability; good preserving verdure property; proper crystallization speed; and good moulding machining property, which make it possible to be applied to several fields in packing industry (especially for multilayer containers), automobiles and magnetism materials.

Several reports showed that the oxygen penetrate rate of MXD6 biaxially oriented film is one tenth to one twentieth of that of nylon 6 biaxially oriented film and one twentieth to one twenty fifth of that of PET biaxially oriented film (WANG Yunqiu, 1997, p. 43-49). Also, for carbon dioxide, the penetrate rate of MXD6 is one fifth of that of PET. Moreover, when the amount of MXD6 is about 10% weight in PET, the barrier properties of PET can be improved nearly two times.

Nanocomposites technology has been described as the next great frontier of material science. The principle that uses a nanometer material to enhance or improve the properties of a polymer matrix is researched by many people. Employing minimal addition levels (< 10 wt %) nanoclays enhance mechanical, thermal, dimensional and barrier performance properties significantly (Maxfield, MacRae, 1992). The use of dispersed clay in matrix such as MXD6 of the inner layer a multilayer container may reduce the haze of multilayer structures and improve the appearance of oriented films and molded articles, including bottles. But clay particles in a nylon-6 nanocomposite induce crystallization and lead to void and holes formation in the polymer films, which decrease the barrier properties of these composites (FANG Sheng xing, 2001, p. 24-28). For MXD6 has higher dispersity in PET, terephthalic acid was added to get poly (m-xylylene adipamide-terephthalyl amide) (MXD6T).

In this paper, MXD6T-SiO<sub>2</sub> (NMXD6T) nanocomposites with SiO<sub>2</sub> load from 5% to 20% (wt) is prepared, and the influences of its properties and morphology on barrier properties are investigated. The structure and properties of NMXD6T are investigated by TEM, DSC and FITR, etc. The NMXD6T was added in PET to prepare NMXD6T-PET(NPET). The measurement of the air permeability of PET and NPET showed that the barrier properties of NPET were enhanced obviously 3-8 times.

## 2. Materials and methods

### 2.1 Materials

Monomer of m-xylylenediamine (analytical reagent) was purchased from Mitsubishi Gas Chemical (MGC), while hexane diacid (chemical reagent) from Beijing Xingjin Chemical Company, terephthalic acid (TPA) (Tianjin-Yiheng Technology Co. Ltd). Ethyl silicate hydrolyzed to prepare nanometer SiO<sub>2</sub> particles was chemical reagent from Beijing Yili Fine Chemical Co. Ltd.

### 2.2 Preparation of MXD6T-SiO<sub>2</sub> and NPET nanocomposites

The MXD6T-SiO<sub>2</sub> nanocomposite was prepared by a two-step method. First, ethyl silicate was hydrolyzed to prepare SiO<sub>2</sub> particles, in which liquid ethyl silicate was added dropwise to a solution mixture of m-xylylenediamine, hexane diacid, terephthalic acid and distilled water. The molar ratio of acid to diamine was maintained at 1.0. The liquid-solid mixture was stirred for at least 30min at room temperature to form a homogenate system. Then, the obtained homogenate was heated up to 98°C gradually under the protection of nitrogen gas and started dewatering about 1 h until this liquid system became a solid one. After that, dewatering process was kept on and temperature was increased from 100°C to 220°C for 1-1.5h. At last, the second step polymerization reaction began and lasted for 1.5-2 h under 240°C to 260°C. The final product was obtained at the protection of nitrogen gas.

The MXD6T-SiO<sub>2</sub> nanocomposites (wt-10%) were sufficiently mixed with PET powder by ball mill to obtain the new composite materials (NPET). NPET were pressed into film with 0.1mm thickness by tablet at 275°C.

### 2.3 Preparation of samples

NMXD6T was smashed in disintegrator and vacuum-dried at 60°C for 4 h. Then NMXD6T small particles were sealed in self-given bags and saved in desiccators.

### Characterization

DSC: DSC patterns were measured by a differential scanning calorimeter (NETZSCH STA 409 PC) from room temperature to 360 °C at a heating rate of 10 °C/min with error of ±1°C.

FITR: The FTIR spectra of the MXD6T and NMXD6T were determined by a MAGNA-AR560E.S.P FTIR spectrometer. TEM: TEM observation operated under Hitachi 800.

Intrinsic Viscosity: MXD6T and NMXD6T samples were dissolved in mixed solvents of 50/50 (by mass) of 1, 1, 2, 2-tetrachloro ethane and phenol, and then measured with U II-man viscometer with a concentration of 0.001g·ml<sup>-1</sup> at temperature of (25±0.1) °C.

Gas permeation properties: Gas permeation Tester, Jinan blue light Electrical and Mechanical Technology Co., Ltd.

## 3. Results and discussion

### 3.1 The influences of acid ratio and SiO<sub>2</sub> content on nanocomposites viscosity

The influences of TPA content and SiO<sub>2</sub> content on polymer viscosity are shown in Fig.1. In Fig.1A, it can be found that the viscosity of nanocomposites decreases with decreasing TPA. It is well known that increase of aliphatic acid can

improve the flexibility of the polymer. While the increase of the aromatic acid can increase the rigidity of the polymer chain which also means the improvement of polymer barrier properties. Hence, perfect acid ratio and SiO<sub>2</sub> content are important for betterment of barrier property and polymerization degree. So, to balance barrier property and polymerization degree, the content of TPA is from 20% to 50% (by mole) and SiO<sub>2</sub> content is from 5% to 20% (by mass).

### 3.2 Bonds of MXD6T and NMXD6T

The FTIR spectrum figures of MXD6T and NMXD6T are shown in Fig2. The appearance of the absorption bands at 1643 cm<sup>-1</sup>(C=O bond stretch of amido group), 1546 cm<sup>-1</sup>(C-N bond stretch of amido group) (part A) and 1643 cm<sup>-1</sup>, 1547 cm<sup>-1</sup>(part B) confirmed the formation of amido group. The amido group is strong polarity bond so it has good barrier properties to nonpolarity gas, such as oxygen gas and carbon dioxide. Comparing (Fig.1A) with (Fig.1B), 1030 cm<sup>-1</sup> and 868 cm<sup>-1</sup> (Si-O bond absorption) confirm the formation of composite system which has strong interaction between inorganic phase SiO<sub>2</sub> and organic phase polymer matrix.

### 3.3 Glass transition temperature of oligomers

The increase of glass transition temperature (T<sub>g</sub>) reflects the rigidity increase of polymer chain; meanwhile, the increase of rigidity enhances the polymer barrier properties. The glass transition temperatures of the oligomers can be obtained from the DSC curves showed in Fig.3. In Fig.3A, it can be found that the T<sub>g</sub> values shift to higher temperatures with the increase of SiO<sub>2</sub> content. While in Fig.3B, the T<sub>g</sub> values decrease with the increasing ratio of hexane diacid to TPA. The dependence of T<sub>g</sub> values on SiO<sub>2</sub> and TPA indicated that the incorporation of nanoparticles and TPA into polymer matrix have direct effects on its chain rigidity.

### 3.4 Dispersion of SiO<sub>2</sub> nanoparticles in polymer matrix

The interspace of polymer matrix macromolecules can be filled by nanometer particles dispersed homogeneously. Figure 4 shows the TEM morphology of NPET. In figure 4A, it can be found that most of particles are dispersed homogeneously. But there are black agglomerations in some areas. Fig4B is the enlargement of these agglomerations. The enlarged TEM graph showed that the particles also exist in nanometer dimension.

### 3.5 The air permeability of the polyester

Table 1 shows the gas permeability of PET and NPET. It can be found that the permeability can be enhanced by the addition of nanometer particles SiO<sub>2</sub> and the increase of TPA. The results indicated that the NMXD6T-PET nanocomposites can be a potential material in packing application for their enhanced air-tightness property.

## 4. Conclusions

In conclusion, a new nanocomposites system with different TPA content and SiO<sub>2</sub> content were prepared and used as a modifier to improve barrier property of PET. The measurement of the viscosity and T<sub>g</sub> values showed the influence of TPA and SiO<sub>2</sub> content. The investigation of TEM indicated that SiO<sub>2</sub> particles exist in nanometer dimension in the polymer matrix. The enhanced the air-tightness properties of polyesters revealed that the NMXD6T-PET nanocomposites can be a potential material in packing application.

## References

- Ding, Yunsheng, Zhang, Zhicheng, Shi, Tiejun. Progress and Research of Impermeable Polymer Materials. (2001). *Jounral of Functional Polymers*. 14, 360-368.
- Soney C Georgy, G Groeninckx, K N Ninan, et al.. Molecular transport of aromatic hydrocarbons through nylon- 6/ ethylene propylene rubber blends. (2000 ). *J Polym S CI: Part B: Polym Physics*. 38, 2136-2145.
- Hongchul Seo, Jongho Jeon, Yong Gun Shul, et al. Water sorption and activation energy in polyimide thin films. (2000). *J Polym S CI: Part B: Polym Physics*. 38, 2714-2720.
- A. Gruniger, Ph. Rudolf von Rohr. Influence of defects in SiO<sub>2</sub> thin films on their barrier properties. (2004). *Thin Solid Films*. 308-315.
- A.P. Roberts, B.M. Henry, A.P. Sutton, et al.. The minute development direction of high barrier properties resins and materials. (2002). *J. Membr Sci*. 208, 75-82.
- He, Zuoyun, Xion Yuanfan, Yang Yuehui. The development of preparation of barrier nylon resins. (1996). *China Plastics*. 10. 17-23.
- Lan, Tie, *Psihogios*. (1999 ). US6376591.
- Chen, Yan, Wan, Xinyu, et al. Study on polyimide/ silica nanocomposite films. (1997). *Acta polymeica sinica*. 11, 73-78.

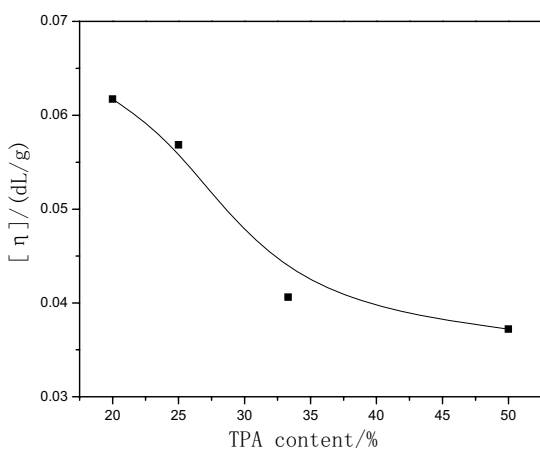
Wang, Yunqiu. A new ultra-high functional nylon MXD6 resin. (1997). *Modern plastics processing and applications*. 9, 43-49.

Maxfield, MacRae, Christiani, et.al.. 1992. US5385776.

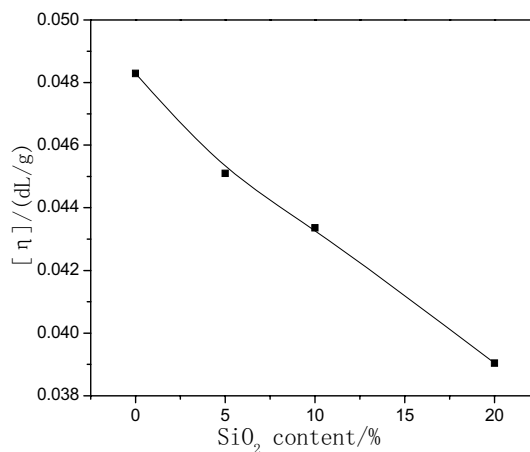
Fang, Shengxing & Hu, Yingmei. Manufacturing Scheme of Plastic Beer Bottles. (2001). *Plastics*. 30, 24-28.

Table 1. The comparison of gas permeation properties for PET and NPET

Sample	SiO <sub>2</sub>	air permeability	O <sub>2</sub>	CO <sub>2</sub>
T(25°C)	(%)	/ [cm <sup>3</sup> . m <sup>-2</sup> . (24h . atm) <sup>-1</sup> ]		
PET			153	576
SNPET -1	SiO <sub>2</sub> ( 10 %)	A/TPA=3	62	195
SNPET -2	SiO <sub>2</sub> ( 10 %)	A/TPA=2	45	154
SNPET -3	SiO <sub>2</sub> ( 10 %)	A/TPA=1	37	112
SNPET -4	SiO <sub>2</sub> ( 20 %)	A/TPA=1	19	72

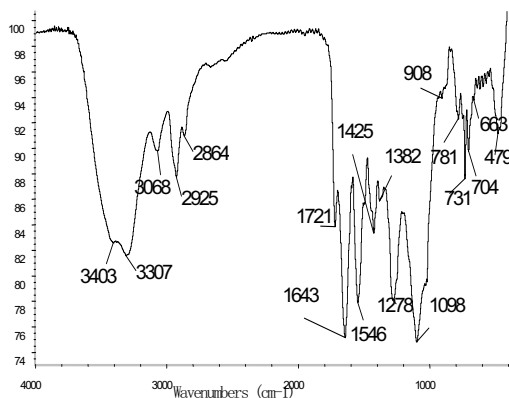


A: Different TPA content

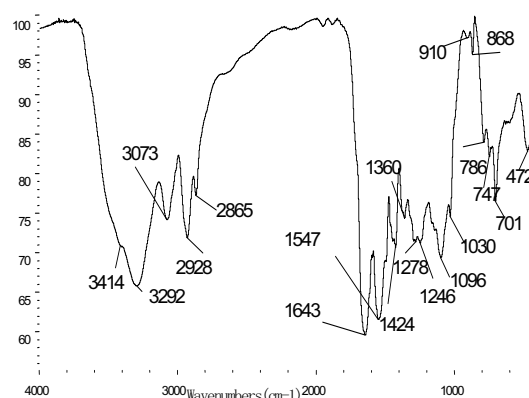


B: Different SiO<sub>2</sub> content

Figure 1. The influences of TPA content and SiO<sub>2</sub> content on polymer viscosity



A:MXD6T



B: NMXD6T

Figure 2. The FTIR spectrum of MXD6T and NMXD6T

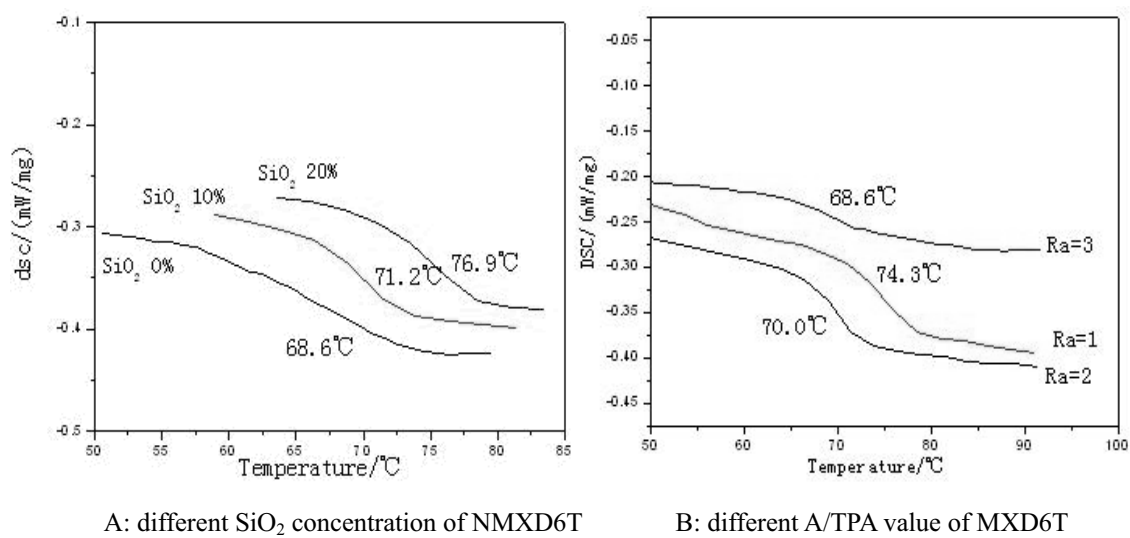


Figure 3. The glass transition temperatures of oligomers

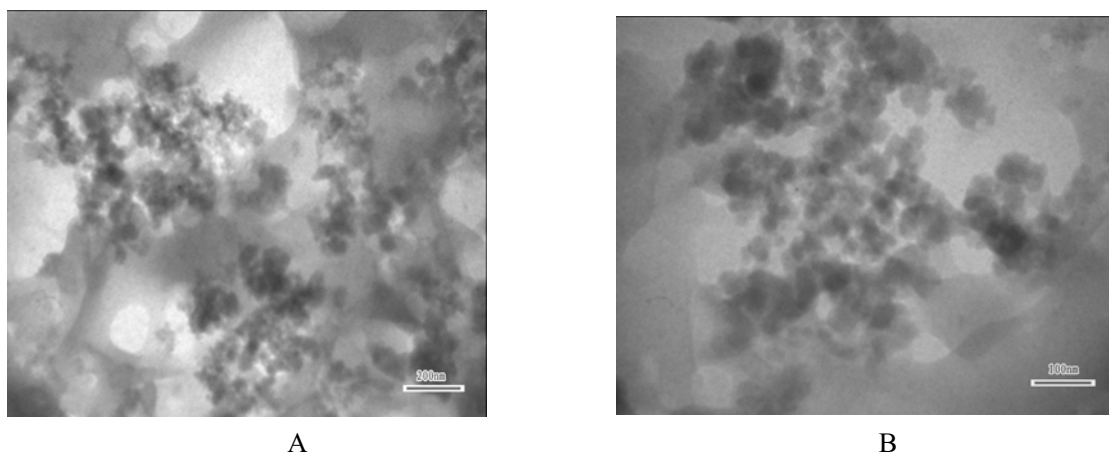


Figure 4. The dispersion of nanometer particles in NPET



## Preparation of Cation Exchange Resin Filled EVAL Hollow Fiber Membrane Adsorbent

Fengli Zhang (Corresponding author)

Key laboratory of Hollow Fiber Membrane Process of Ministry of Education

Tianjin Polytechnic University, Tianjin 300160, China

E-mail: Zhangfengli2008@126.com

### Abstract

This paper presents a generic technology allowing the incorporation of functional entities into a porous substrate. Ion exchange particles were incorporated into an ethylene vinyl alcohol (EVAL) copolymer porous matrix by a dry-wet spinning process and a heterogeneous matrix, composed of solid particles surrounded by a polymeric film, was formed. Hydrophilic ethylene vinyl alcohol copolymer (EVAL) and cation exchange resin D061 powder used as matrix material for hollow fiber membrane and functional particles, respectively, resins with different loading were prepared to fill EVAL hollow fiber membrane adsorbents. The membrane adsorbents were characterized with respect to their morphology, porosity, pure water flux (PWF), and rejection rate. Micro morphology was observed by the scanning electron microscope method. Effects of resin load on the performance of membrane adsorbents were mainly discussed. The experimental results showed that PWF and porosity increased and retention coefficient decreased with higher resin loading.

**Keywords:** EVAL, Hollow fiber membrane adsorbent, Cation exchange resin

### 1. Introduction

In order to prepare a kind of hollow fiber membrane with large adsorption of protein, hydrophobic membrane matrix materials and ion exchange resin with good function of adsorption. Polymeric membrane materials with hydrophilic groups have been increasingly developed in recent years, especially in biological and biomedical applications. Incorporation of hydrophilic groups reduces the hydrophobic interaction between the biological compound and the membrane surface and increases the water-wettability of the membranes. Especially in protein separation, hydrophobic interactions between proteins and hydrophobic surfaces are generally responsible for non-selective (irreversible) adsorption and membrane fouling (Avramescu, 2003, PP. 155-173). In order to avoid the fouling of membrane adsorbents due to solute adsorption, hydrophilic polymer membranes was applied in the present study. Ethylene vinyl alcohol (EVAL), a semi-crystalline random copolymer consisting of hydrophobic ethylene and hydrophilic vinyl alcohol segments, has become a promising biomedical material, since it is water insoluble and can prevent membrane fouling in the membrane separation application. EVAL also displays a good mechanical strength, has high thermal stability, good chemical and biological resistance, and is easy to sterilize using (Matsuyama, 2001, PP. 2583-2589, Young, 1998, 717-724). Moreover, cation exchange resins (CER) D061 were incorporated as particulate material into an EVAL porous structure to prepare heterogeneous membranes with high protein adsorption capacity.

Avramescu (2003, PP. 171-183, 2003, PP. 219-233, 2003, PP. 177-193) have reported that EVAL panel membrane and fiber adsorbents filled by ion exchange resins were prepared by the phase inversion process and modified to separate and purify protein mixtures. The mixed-matrix adsorber membranes developed in the study feature high protein adsorption and desorption capacities of model protein, BSA. Zhang Yuzhong (2005, PP. 224-232) reported that incorporated with resin powder in fiber matrix, the resin CNP80ws filled EVAL fibrous adsorbents with some extent of open pore on its surface were prepared by the method of controlled phase transition with some external liquids. The more open structure on its surface was obtained with higher resin loading and the resin filled EVAL fibrous adsorbents had good adsorption capacity and desorption. EVAL hollow fiber membrane adsorbents filled by resins were prepared by a dry-jet wet spinning process, Hydrophilic EVAL and cation exchange resin D061 powder used as matrix material for hollow fiber membrane and functional particles, respectively. In this method, most suitable particles have, in combination with the porous matrix morphology, rapid adsorption kinetics, a capacity and selectivity commensurate with the application and allows for desorption of the molecule with an appropriate agent. The affinity of suitable adsorptive particles for specific molecules can be defined in terms of hydrophobic, hydrophilic or charged functionalities, in particular ion exchange functionalities, molecular (imprinted) recognition, or other specific interactions.

## 2. Materials and methods

### 2.1 Materials

EVAL (a random copolymer of ethylene and vinyl alcohol) with an average ethylene content of 44 % was purchased from Kuraray, Japan and used as membrane material without further modification. Dimethylsulfoxide (DMSO, Tianjin) was employed as solvent and 1-octanol (Tianjin) as non-solvent-additive in the casting solution. Water was used as non-solvent in the coagulation bath. Cation exchange resins D061 kindly supplied by Nankai University, China, were used as adsorbent particles. Buffer solutions were freshly prepared in ultrapure water. BSA was used as a model protein in the adsorption/desorption experiments. Ultrapure water was prepared using a Millipore purification unit Milli-Q plus. All other chemicals were of chemical reagent grade and used as received.

### 2.2 Adsorbent preparation

Due to large size of the resins purchased, the spinning solution obtained was unstable and declined to deposit with lower absorption capacity, and therefore the resins should be further processed.

#### 2.2.1 Drying

The resin beads with high water content and impurity were washed with demiwater in a stirred vessel until neutral pH and dried at 80 °C in a conventional oven until constant weight.

#### 2.2.1 Grinding

Cation exchange resin particles are crushed mainly by the apparatus of Super Fine Pulverizer HMB-701 (Beijing Huanya Tianyuan Machinery technology Co., Ltd, China). It has a dynamic plate and static plate. The material is pulverized with the impact, friction and cutting forces on the static plate by the high-speed rotation of the dynamic plate. Due to the impact, if the particles were too large to control the biotechnology conditions, and thus fail to obtain the expected effects, all the resins were primarily crushed from large size to lower size (above 325 mesh). At the influence of negative pressure, the qualified powder (10 $\mu$ m) enters into classifying zone and gathers in the collector while the coarse material returns for further pulverizing. Through above resin processing, micron resin particle sample was prepared for study.

### 2.3 Analysis of resin particle size distribution

The particle size distribution of different particle fractions was measured using LA-300 Laser Scattering Particle Size Distribution Analyzer. Using a concentric multiple photo-diode array detectors, which act as receptors for light refracting off of particles suspended in the flow cell, the analyzer measures particles ranging anywhere between 0.1 and 1000  $\mu$ m in diameter with unprecedented precision. Electrical signals corresponding to the intensity of the scattered light are used to calculate the size distribution of the particles. Based on the Mie scattering theory and Fraunhofer diffraction theory patterns, this measurement method consistently yields superior repeatability with astounding precision. Before performance, the analyzer was first filled with solvents (usually water), then resin samples were scattered in the solvents, and immediately transferred to evaluating pool to measure, in order to avoid the formation of agglomerates and swellings.

### 2.4 EVAL hollow fiber membrane preparation

Cation exchange particles D061 were successively added to a solution containing EVAL polymer in DMSO in order to obtain membranes with different adsorptive properties. Ten percent 1-octanol was added to the casting solution in order to improve the membrane morphology. The mixtures were stirred over night to break the clusters of particles. The blend hollow fiber membranes were fabricated through a wet spinning process, as schematically represented in Figure 1. The clear and homogeneous blend dope solution was then forced through a stainless steel spinneret comprising an annular ring and extruded into an external coagulation bath. A bore liquid coagulant was simultaneously delivered through the inner core of the spinneret by a high pressure syringe pump. The hollow fiber membranes were collected by a drum from the external coagulation tank. All prepared membranes were washed by water, followed by rinsed with ethanol to remove the additives and solvents and immersed in 30% glycerin solution for 24 hours, and afterwards dried in air.

### 2.5 EVAL hollow fiber membrane characterization

#### 2.5.1 Scanning electron microscopy

The structure and morphology of membranes were observed by scanning electron microscopy (SEM), cross-sections of the membranes freeze-fracturing under liquid nitrogen, and the membrane samples were coated with gold-palladium. A QUANTA200 SEM (FEI, Netherlands) with an accelerating voltage set to 20 kV was used to examine the membrane cross-section.

#### 2.5.2 PWF measurement

The pure water flux was determined using a dead-end ultrafiltration cell connected to a gas cylinder of compressed

nitrogen to apply the feed pressure (Tianjin, China). The filtration experiments were carried out at room temperature and a applied pressure of 0.1MPa. The pure water flux was determined after steady state conditions were reached. Average values were obtained from several different samples. PWF Q was calculated according to the formula:

$$Q = \frac{V}{At} \quad (2-1)$$

Where V is volume flow (L), A is membrane area (m<sup>2</sup>), and t is tested time (s).

### 2.5.3 Porosity measurement

The porosities of the blend hollow fibers were measured by the dry-wet weighing method. The dried hollow fibers were equilibrated with pure water for 24 h. The porosity was then determined by dividing the amount of water adsorbed (mL) with the amount of the wet hollow fibers (mL). The experiment was done for several samples and the average porosity was used for each type of the blend hollow fibers. The porosity was calculated according to the formula:

$$P_r = \frac{W_w - W_d}{S \cdot d \cdot \rho} \times 100\% \quad (2-2)$$

Where W<sub>w</sub> is membrane weight with water adsorbed(g), W<sub>d</sub> is membrane weight without water(g), S is membrane area(cm<sup>2</sup>), d is average membrane thickness(cm), and ρ is solvent density (pure water density, 1.0g/cm<sup>3</sup>).

### 2.5.4 Rejection rate measurement

For the rejection rate measurements, a freshly prepared BSA (67,000Da) solution (0.1% acetate buffer at pH 7.4) was permeated through the membrane. The BSA concentration in the feed and the permeate samples was determined by measuring the absorbance at 280 nm with a spectrophotometer UV2450. All the filtration experiments were carried out at room temperature. The retention coefficient R was calculated according to the formula:

$$R = \frac{E_i - E_s}{E_i} \times 100\% \quad (2-3)$$

Where, R is the rejection rate (%),  $E_i$  is the absorbency of the initial liquid (mg/ml) and  $E_s$  is the absorbency of the filtered liquid (mg/ml).

## 3. Results and discussion

### 3.1 Configuration and particle size distribution of D061

Milling is a simple way to reduce the size of sorbent particles and potentially a method to increase the surface area. As seen from Figure 2, resin D061 showed an irregular configuration with coarse surface and equal particle distribution. Data on particle size distribution and total surface area are presented in Figure 3. According to particle size distribution of D061 (Figure 1), the size of the ion exchange resins was reduced from an average particle diameter of 100 μm to less than 0.5 μm, mostly ranged from 10 to 30μm. The mean size of resin particle was 17.17μm in diameter.

As seen from Figure 4, there was no difference in resins with or without grinding, which indicated that after grinding, functional groups of resins haven't changed. Moreover, specific surface area of resins increased, and thus adsorption capacity increased.

### 3.2 Structure and morphology of hollow fiber membrane adsorbent

An important parameter for the preparation of adsorber membranes is the amount of resins incorporated into the polymeric matrix. By increasing of the resin loading, the amount of adsorptive-sites increases and a higher protein adsorption capacity is expected. The morphologies of the adsorber membranes prepared in the solid fiber geometry with different loading capacities of D061 cation exchange resins are shown in Figure 5. Both surfaces became coarser and the pores of outer surface became wider and increased with increasing the resin loading. Meanwhile, finger-like pores of cross-section decreased and became denser and denser. We interpret the solid particles to act as a nucleus in the casting solution limiting the grow size of the macrovoids. The solid particles also increase the viscosity of the polymer solution and therefore decrease the macrovoid formation. Moreover, outer surface possessed an open, interconnected porous structure which allowed the protein to permeate free in favor of protein adsorption.

### 3.3 Effects of resin loading on PWF and porosity of membrane adsorbents

As seen from Figure 6 and Table 1, with increasing resin loading, PWF and porosities of EVAL hollow fiber membrane adsorbents increased. The ion-exchange particles are tightly held together within the porous polymeric matrix. The solid particles also increase the viscosity of the polymer solution and therefore decrease the macrovoid formation. The

presence of resin inhibited the processing of solvent to coagulating bath, decreased the speed of membrane separation and formed a dense membrane. However, a further increase in the resin content leads to an increase of viscosity, formation of a stack of resins. Membrane became looser with more and more pores inside, so porosity increased with increasing PWF.

### 3.4 Effects of resin loading on retention coefficient of membrane adsorbents

As seen from Figure 7, with increasing resin loading, retention coefficient of BSA decreased. Retention function of membrane was ascribed to pore size of surface, which was interfered by adsorption when ion exchange resin was involved. Proteins constitute in amino acid groups which possess amino and carboxyl groups, and thus belong to ampholyte with isoelectric point ( $pI$ ). When amino acid become zwitterions and have no net charge, the  $pH$  of solvents is its isoelectric point. When  $pH$  is lower than  $pI$ , amino acids in the presence of cations and could be adsorbed by cation exchange resins; when  $pH$  is higher than  $pI$ , amino acids in the presence of anion could be adsorbed by anion exchange resins. Therefore buffer solution ( $pH$  7.4) higher than  $pI$  was applied and resin have a lower adsorption capacity of proteins, mainly due to the function of pore size of surface. With increasing resin load, configuration of EVAL hollow fiber membrane adsorbents filled with resins have changed, large voids of cross section appeared, and thus retention coefficient decreased.

## 4. Conclusions

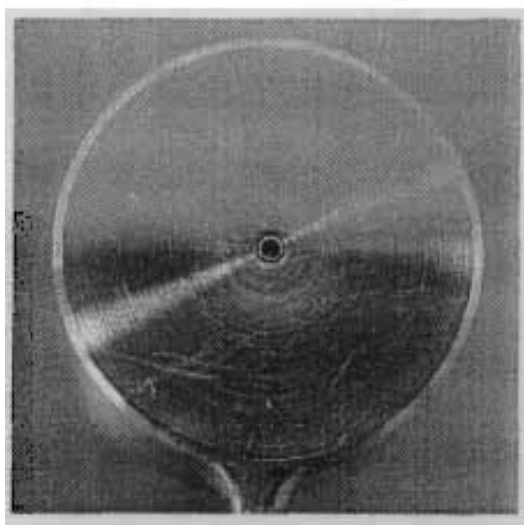
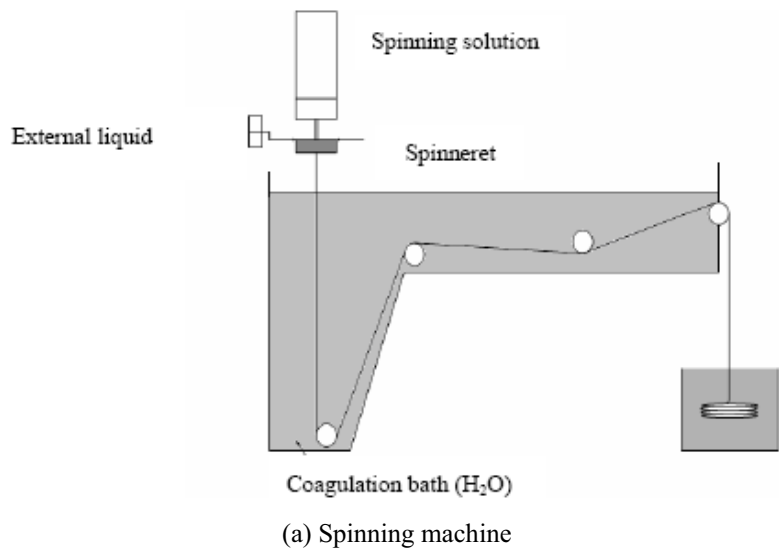
In the present paper, cation exchange resins D061 were incorporated into EVAL copolymer porous matrix by a dry-wet spinning process and a heterogeneous matrix, composed of solid particles surrounded by a polymeric film, was formed. When the content of EVAL and 1-octanol was stable, by increasing the resin loading, configuration of EVAL hollow fiber membrane adsorbents filled with resins have changed, and its PWF and porosity increased while retention coefficient decreased.

## References

- Avramescu, M. E., Gironès, M., & Borneman, Z., et al. (2003). Mixed-matrix membrane adsorbents for protein separation. *Journal of Chromatography A*. 1006: 171-183.
- Avramescu, M.E., Sager, W.F.C., Wessling, M. (2003). Functionalised ethylene vinyl alcohol copolymer (EVAL) membranes for affinity protein separation. *Journal of Membrane Science*. 216:177-193.
- Avramescu, M. E., Sager, W. F. C., & Mulder, M. H. V., et al. (2002). Preparation of ethylene vinylalcohol copolymer membranes suitable for ligand coupling in affinity separation. *Journal of Membrane Science*. 210:155-173.
- Avramescu, M. E., & Wessling, M., et al. (2003). Preparation of mixed matrix adsorber membranes for protein recovery. *Journal of Membrane Science*. 218: 219-233.
- Matsuyama, H., Kobayashi, K., & Maki, T., et al. (2001). Effect of the ethylene content of poly (ethylene-co-vinyl alcohol) on the formation of microporous membranes via thermally induced phase separation. *J App Polym Sci*, 82:2583-2589.
- Young, T. H., Yao, C. H., & Sun J. S., et al. (1998). The effect of morphology variety of EVAL membranes on the behavior of myoblasts in vitro. *Biomaterials*. 19(7-9): 717-724.
- Zhang, Y.Z., & Li, R., et al. (2005). Preparation of resin filled EVAL fibrous adsorbents and characteristics of their adsorption. *Ion exchange and adsorption*. 21(3): 224-232.

Table 1. Effects of resin loading on porosities of membrane adsorbents

Resin loading(%)	Porosity(%)
50	65
55	70
60	73
65	77



(b) Spinneret

Figure 1. Spinning machine and spinneret

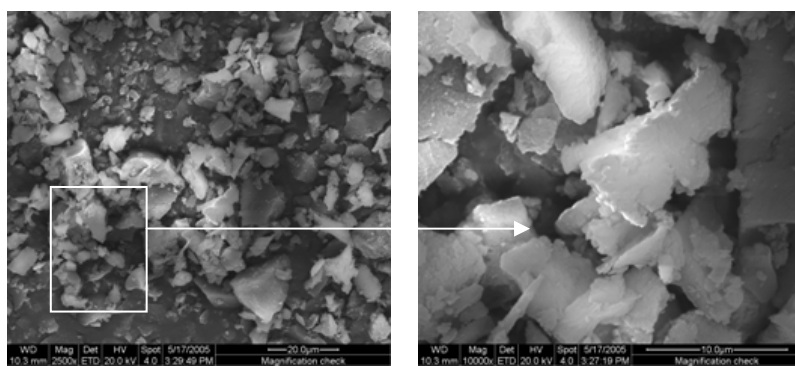


Figure 2. The surface morphological structure of D061

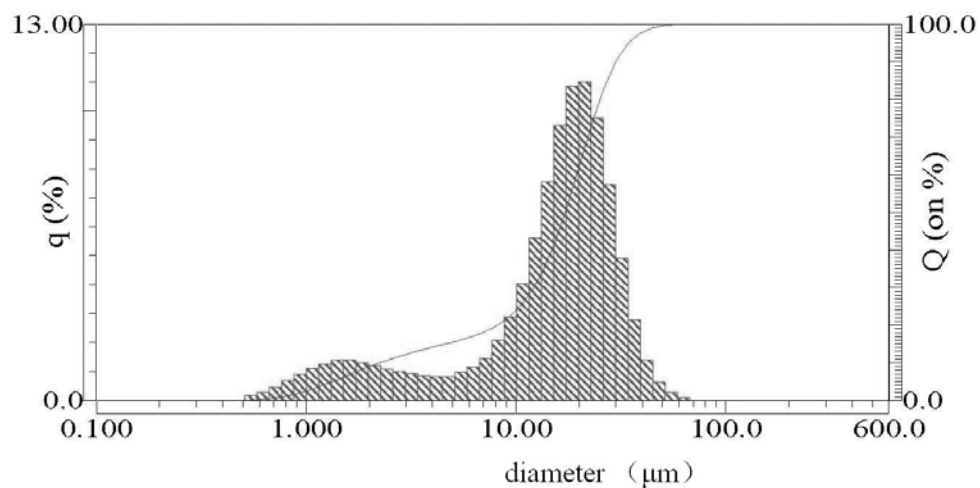


Figure 3. Particle size distribution of D061

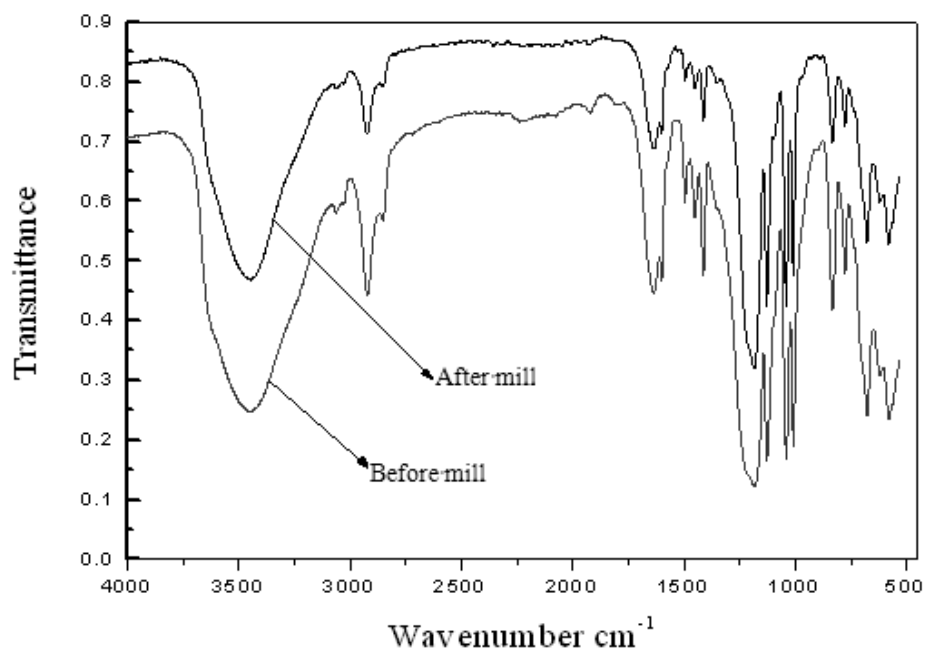


Figure 4. Infrared spectrum of D061 before or after grinding

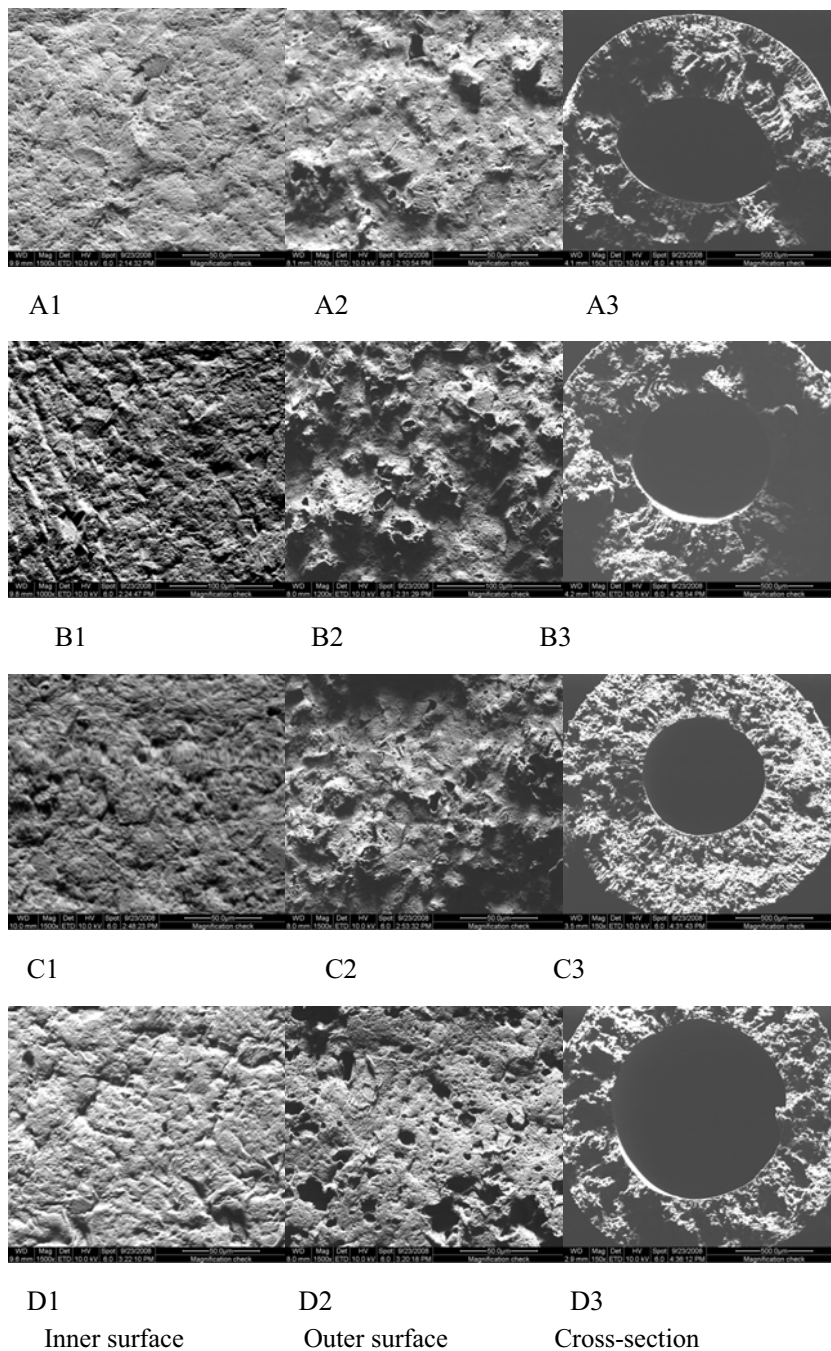


Figure 5. SEM images of resin D061 mixed EVAL-based fibrous adsorbents (A<sub>1</sub>~A<sub>3</sub> resin loading 50%, B<sub>1</sub>~B<sub>3</sub> resin loading 55%, C<sub>1</sub>~C<sub>3</sub> resin loading 60%, D<sub>1</sub> ~D<sub>3</sub> resin loading 65%)

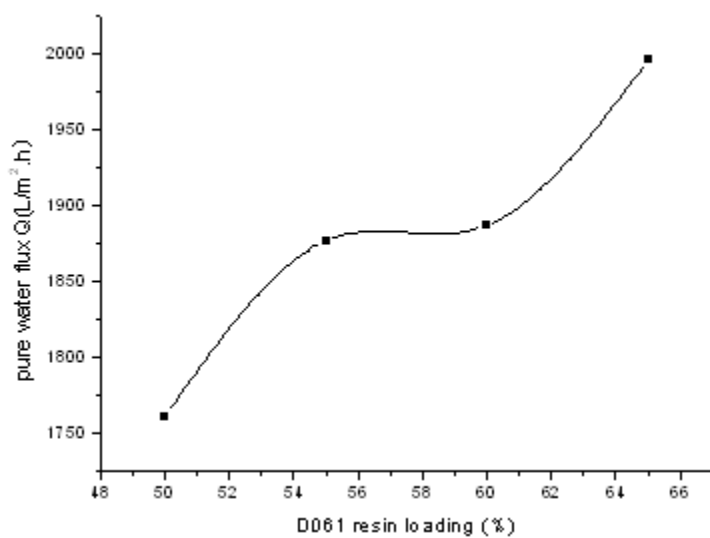


Figure 6. Effects of resin loading on PWF of membrane adsorbents

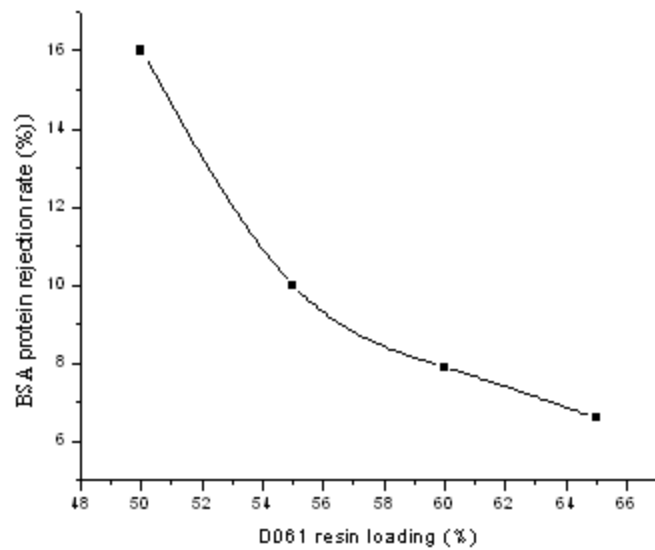


Figure 7. Effects of resin loading on retention coefficient of BSA

# Editorial Board

Anne Brown	Canadian Center of Science and Education, Canada
Dilip Venkatrao Jarikote	University College Dublin, Ireland
Guy L. Plourde	University of Northern British Columbia, Canada
K. Girish Kumar	Cochin University of Science and Technology, India
Konstantinos Kasiotis	Benaki Phytopathological Institute, Greece
Mehta Jignasu P	Bhavnagar University, India
Pankaj Das	Dibrugarh University, India
Patrick Marcel Schaeffer	James Cook University, Australia
Prathapan Sreedharan	Cochin University of Science and Technology, India
R. K. Dey	Birla Institute of Technology, India
Sagar Pal	Birla Institute of Technology, India
Shyamal Kumar Chattopadhyay	Bengal Engineering and Science University, India
Sirshendu De	Indian Institute of Technology, India
Sujatha. C.H	Cochin University of Science and Technology, India
Sushil Kumar Kansal	Panjab University, India
Wenwu Zhao	Macrothink Institute, USA

**A journal archived in Library and Archives Canada**  
**A journal indexed in Canadiana (The National Bibliography)**  
**A journal indexed in AMICUS**  
**A peer-reviewed journal in chemistry**

# **International Journal of Chemistry**

**Semiannual**

**Publisher Canadian Center of Science and Education**

**Address 4915 Bathurst St. Unit # 209-309, Toronto, ON. M2R 1X9**

**Telephone 1-416-208-4027**

**Fax 1-416-208-4028**

**E-mail [ijc@ccsenet.org](mailto:ijc@ccsenet.org)**

**Website [www.ccsenet.org](http://www.ccsenet.org)**

**Printer William Printing Inc.**

**Price CAD.\$ 20.00**

